The role of the NLRP3 inflammasome in microglial senescence in tauopathies

Doctoral thesis

to obtain a doctorate (PhD)

from the Faculty of Medicine

of the University of Bonn

Deniz Sükrü Bernard Karabag

from Maastricht, The Netherlands

2024

Written with authorization of
the Faculty of Medicine of the University of Bonn

First reviewer: Prof. Dr. Michael Heneka
Second reviewer: Prof. Dr. Martin Korte

Day of oral examination: 04.03.2024

From the Department of Neurodegenerative Diseases and Geriatric Psychiatry/Neurology, University Hospital Bonn
Director: Prof. Dr. Michael Heneka

From the Institute of Innate Immunity
Director: Prof. Dr. Eicke Latz

Table of Contents

List of abbreviations

ANPC	Adult neural progenitor cell
AHN	Adult hippocampal neurogenesis
ALS	Amyotrophic lateral sclerosis
AEC	Airway endothelial cells
AD	Alzheimer’s disease
APCs	Antigen-presenting cells
ALRs	Aim-like receptors
AIM2	Absent-in-melanoma 2
ASC	Apoptosis-associated speck-like protein
ATP	Adenosine triphosphate
Aβ	Amyloid beta
ATM	Ataxia-telangiectasia mutated
ATR	Ataxia-Rad3 related
ATV	Atazanavir
BSA	Bovine Serum Albumin
CD11b	Cluster of differentiation molecule
CM	Conditioned medium
CNS	Central nervous system
CXCL-1	Chemokine (C-X-C motif) ligand 1
CLRs	C-type lectin receptors
CDKI	Cyclin-dependent kinase inhibitor
CBD	Corticobasal degeneration
COPD	Chronic obstructive pulmonary disease
DAPI	4’,6-diamidino-2-phenylindole
DDR	DNA damage response
DG	Dentate gyrus
DMEM	Dulbecco's modified eagle's medium
DAMPs	Danger-associated molecular patterns
DM	Diabetes Mellitus

DSBs	Double-stranded breaks
ECM	Extracellular matric
ETC	Electron transport chain
ER	Endoplasmic reticulum
FCS	Fetal Calf Serum
FTD	Frontotemporal dementia
GSDMD	Gasdermin D
GRP75	Glucose-regulated protein 75
HGPS	Hutchinson-Gilford Progeria Syndrome
H3K9me3	Lysine 9 trimethylation on histone 3
IBA1	Ionized calcium-binding adapter molecule 1
Ils	Interleukins
IR	Irradiation
IP3R	Inositol 1,4,5-trisphosphate receptor
JAK	Janus kinase
Lamin B1	Nuclear lamina type B1
LSM	Laser scanning microscope
LTP	Long term potentiation
MAMs	Mitochondria-associated endoplasmic reticulum membranes
MCI	Mild cognitive impairment
MMPs	Matrix metalloproteinases
MiDAS	Mitochondrial dysfunction-associated senescence
MTs	Microtubules
MAPT	Microtubule associated-protein tau
MAEC	Mice aortic endothelial cells
NOD	Nucleotide-binding oligomerization domain
NLRs	Nod-like receptors
NGS	Normal Goat Serum
NF-κB	Nuclear factor kappa-light-chain-enhancer of activated B cells
OMM	Outer membrane of mitochondria
PD	Parkinson’s Disease
PFA	Paraformaldehyde

PAMPs	Pathogen associated molecular patterns
PRRs	Pattern recognition receptors
PIIPS	Proteasome inhibition-induced premature senescence
RIPA	Radioimmunoprecipitation assay lysis buffer
RRID	Research Resource Identifier
RS	Replicative senescence
ROS	Reactive oxygen species
RLRs	RIG-like receptors
SAH	Subarachnoid haemorrhage
SASP	Senescence-associated secretory phenotype
SISP	Stress-induced premature senescence
SGZ	Subgranular zone
STAT	Signal transducer and activator of transcription
TNF-α	Tumor necrosis factor-alpha
VDAC1	Voltage-dependent anion channel 1
VSMCs	Vascular smooth muscle cells
yH2AX	Phosphorylated histone H2AX

1 Introduction

1.1 The microtubule-associated protein tau (MAPT)

1.1.1 The physiological role of microtubule-associated protein tau (MAPT)

From birth to adulthood, the development of the CNS heavily depends on the neuronal cytoskeleton (Lasser et al., 2018). The neuronal cytoskeleton consists of dense bundles in axons, also known as microtubules (MT), that have the ability to polymerize (grow) or depolymerize (shrink). This allows the neurons to rapidly reorganize and adapt spatially and temporally depending on the microenvironment. One of the major proteins involved in microtubule assembly, organization and stabilization is the microtubule-associated protein tau (MAPT), which is highly abundant in the axonal compartment of neurons and to a lesser extent present in the cell soma (Bachmann et al., 2021; Barbier et al., 2019). The human MAPT gene is located on chromosome 17q21, which is predominantly expressed in the brain and alternative splicing of the mRNA at exons 2, 3 and 10 results in 6 tau isoforms. The composition of the six isoforms is dependent on the presence of none (0N), one (1N) or two (2N) N-terminal acidic inserts and three (3R) or four (4R) C-terminal repeat domains (Goedert, 2004; Avila et al., 2004). Although the isoforms are differentially expressed during development, the 3R and 4R tau isoforms are equally expressed in the cerebral cortex of the healthy adult brain (Goedert et al., 1989). In the adult mouse brain, however, the 4R isoforms are exclusively expressed (Kosik et al., 1989).

1.1.2 The pathophysiological role of MAPT

Tau is considered a natively unfolded soluble protein (Jeganathan et al., 2006). However, complex posttranslational modifications like phosphorylation, acetylation, oxidation, deamidation, nitration, sumoylation and ubiquitylation, affect its biochemical properties and interaction with microtubules (Avila et al., 2004; Didonna, 2020). To some degree, posttranslational modifications are necessary for regulating the physiological function of tau. However, abnormal posttranslational modifications, like hyperphosphorylation, have been shown to weaken the affinity of tau to microtubules, resulting in disassembled microtubules and self-aggregation of tau (Gong and Iqbal, 2008; Gao et al., 2018), a

phenomenon that has been observed in many neurological diseases, including tauopathies (Avila et al., 2004; Didonna, 2020; Guo et al., 2017). To be more specific, hyperphosphorylation of tau results in the dissociation of tau from microtubules, disrupting microtubule function and stability (Qiang et al., 2018). The dissociated form of tau is prone to seeding, meaning that it is able to serve as templates to recruit native tau into growing assemblies (e.g., self-replicate) and misfold, resulting in the formation of tau oligomers (Congdon et al., 2008; DeVos et al., 2018; Friedhoff et al., 1998; Lathuiliere and Hyman, 2021; Mirbaha et al., 2018). Tau oligomers are aggregation- competent and eventually form into fibrils and then into neurofibrillary tangles (NFTs) (Fig. 1) (Avila et al., 2006; Maeda et al., 2006).

1.1.3 Tauopathies

The term “tauopathies” represents an umbrella term for a group of heterogenous neurodegenerative diseases that are clinically and pathologically characterized by the abnormal accumulation and deposition of tau in the brain (Kovacs, 2017) (Fig. 1). There are over 20 forms of tauopathies, each presenting with a unique clinical phenotype ranging from cognitive and behavioral deficits, including memory loss and apathy, to motor deficits like postural instability and asymmetrical limb apraxia (Zhang et al., 2022). Tauopathies are subdivided in primary and secondary tauopathies. Primary tauopathies, like Progressive Supranuclear Palsy (PSP), Corticobasal Degeneration (CBD), and certain forms of Frontotemporal Dementia (FTD) are predominantly characterized by the abnormal deposition of tau. Secondary tauopathies, on the other hand, involve a shared co-pathology such as the formation of amyloid beta (Aβ) plaques in Alzheimer’s Disease (AD) (Kovacs, 2017; Olfati et al., 2022; Saha and Sen, 2019). Both classifications are characterized by abnormal hyperphosphorylation of tau, resulting in its intracellular deposition and aggregation into neurofibrillary tangles (NFTs) (Lee et al., 2001; Avila et al., 2004; Kovacs, 2017). This results in axonal transport deficits, disruption in neuronal communication and subsequently neurodegeneration (Wang and Mandelkow, 2016).

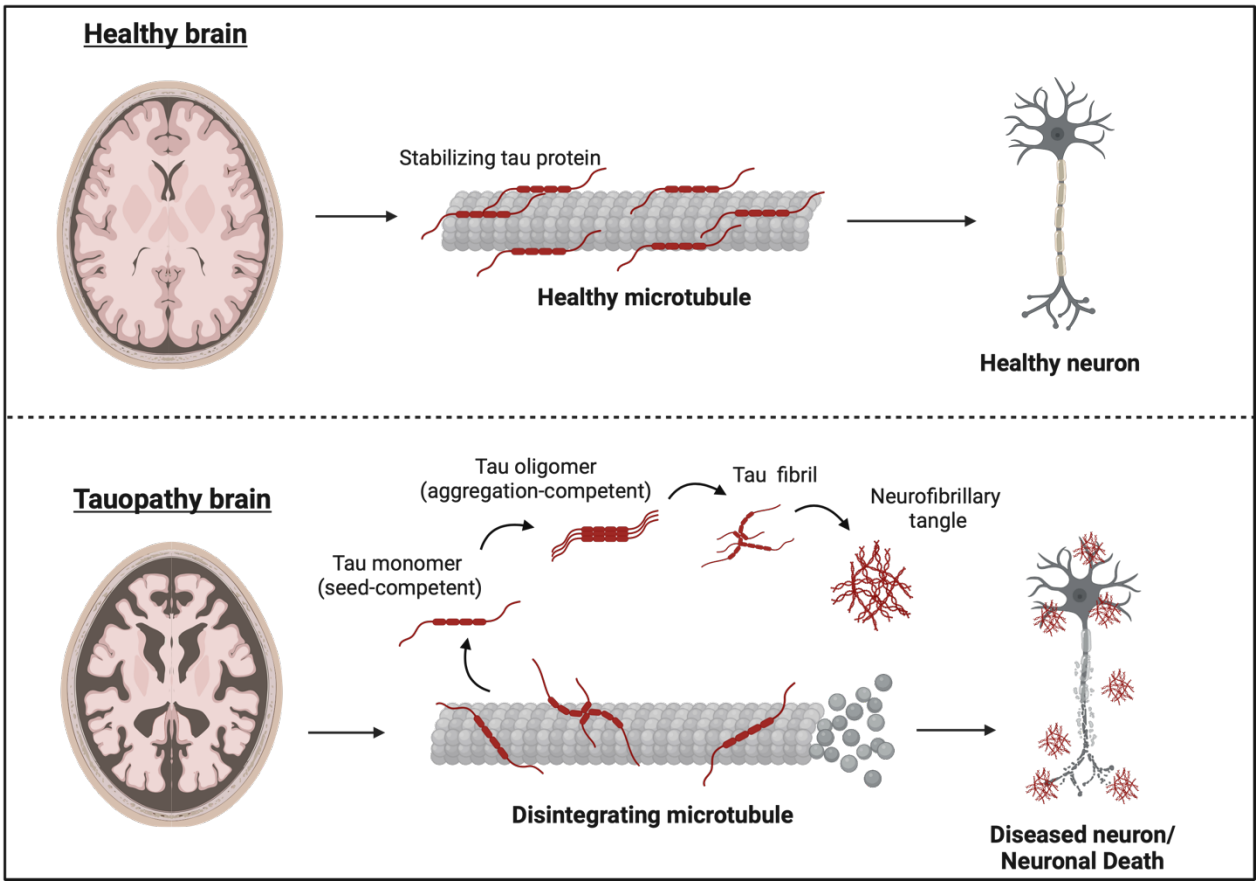

Fig. 1: The pathological deposition of tau protein during tauopathies.The tau protein is essential for the stabilization, spatial organization and assembly of neuronal microtubules. In pathological conditions, however, various post-translational modifications result in the detachment of tau monomers from microtubules. This marks the beginning of pathology, where seed-competent monomeric tau transforms into aggregation-competent tau oligomers, fibrils and eventually neurofibrillary tangles. This cascade contributes to disintegrating microtubules and eventually leads to a diseased neuron (e.g., neuronal death). Created with BioRender.com.

1.2 Immunity and Inflammation in the Central Nervous System (CNS)

1.2.1 Immune system in the CNS

The immune system is comprised of specialized cells that serve to protect our body from hostile environments induced by microbes, viruses, toxins and other pathogens (Mapunda et al., 2022; Marshall et al., 2018). The central nervous system (CNS) is characterized by its own unique immune system that is separated from the periphery (Norris and Kipnis, 2018). For example, the CNS lacks traditional lymphatics and major histocompatibility complex (MHC) class II-expressing antigen-presenting cells (APCs) (Forrester et al.,

2018). However, the CNS is comprised of its own lymphatic-like structure, the so called glymphatic system which serves as a waste clearance system (Jessen et al., 2015). In addition, the CNS comprises several barriers that allow segregation between the CNS parenchyma and periphery such as the blood-brain-barrier to prevent the spread of pathogens into the brain (Ampie and McGavern, 2022; Forrester et al., 2018).

In vertebrates, the immune system is subdivided into the innate and adaptive immune systems (Waisman et al., 2015). In response to any threat that disrupts CNS homeostasis, the first line of defence comes from the innate immune system which primarily consists of brain-resident macrophages, called microglia, that become activated and trigger an inflammatory response in the brain, known as neuroinflammation (Ransohoff and Brown, 2012; Waisman et al., 2015). On the contrary, and only in few cases, the adaptive immune system consisting of T cells and B cells might infiltrate into the CNS parenchyma where it might potentialy result in brain inflammation contributing to autoimmune diseases (Norris and Kipnis, 2018).

1.2.2 Microglia: guardians of the CNS

Microglia were first discovered by Santiago Ramón y Cajal (Río-Hortega, 1939), account for 10 % of the cells in the entire brain and are derived from embryonic hematopoietic precursors, the yolk sac (YS) macrophages (Augusto-Oliveira et al., 2019; Ginhoux and Prinz, 2015; Li and Barres, 2018). Nowadays, it has become clear that microglia significantly contribute to the development of a healthy brain and maintenance of tissue integrity through tissue repair, modulation and shaping of neuronal synapses and maintenance of CNS homeostasis through phagocytosis (Colonna and Butovsky, 2017; Frost and Schafer, 2016; Galloway et al., 2019). Phagocytosis is the clearance process that eliminates microbes, protein aggregates, cellular debris, dead cells and other pathogens that endanger the CNS (Colonna and Butovsky, 2017; Galloway et al., 2019).

Microglia detect various danger signals through pattern recognition receptors (PRRs) (Janeway, 1992). As the name indicates, PRRs detect patterns and structures on the surface of potential pathogens (e.g., bacteria, fungi and viruses) or danger signals (e.g., infection or tissue damage signals), called pathogen associated molecular patterns

(PAMPs) and danger-associated molecular patterns (DAMPs) (Gong et al., 2020; Li and Wu, 2021). The PRR family consists of Toll-like receptors (TLRs), Nod-like receptors (NLRs), C-type lectin receptors (CLRs), RIG-like receptors (RLRs) and aim-like receptors (ALRs) that all can contribute to an inflammatory response (Augusto-Oliveira et al., 2019; Kigerl et al., 2014).

1.2.3 The NLRP3 inflammasome

Inflammasomes were discovered in 2002 as intracellular multiprotein complexes (Martinon et al., 2002) present in macrophages, dendritic cells and non-immune cells (Erlich et al., 2019; Schroder and Tschopp, 2010). Inflammasome complexes are made up of sensors and effectors linked by an optional adaptors and they detect and respond to PAMPs and DAMPs by stimulating the release of IL-1β and IL-18 as a consequence of caspase-1 activation (de Zoete et al., 2014). The four key inflammasome sensors include the nucleotide-binding oligomerization domain (NOD) and leucine-rich repeat (LRR)-containing proteins (NLR) family members NLRP1, NLRP3, and NLRC4, as well as absent-in-melanoma 2 (AIM2) (Kelley et al., 2019; Pretre et al., 2022). Among these, the NLRP3 inflammasome has received most attention due to its role in various diseases, including cancer (Pretre et al., 2022), metabolic syndromes (Jiang et al., 2018; Wani et al., 2021), liver diseases (Csak et al., 2011; Zhu et al., 2011), cardiovascular diseases (Elhage et al., 2003; Sandanger et al., 2013) and neurodegenerative diseases (Codolo et al., 2013; Halle et al., 2008; Ising et al., 2019; Yan et al., 2015; Heneka et al., 2013, 2014).

The NLRP3 inflammasome is composed of a sensor (NLRP3), adaptor (apoptosis-associated speck-like protein; ASC) and effector (caspase-1) protein (Swanson et al., 2019). Activation of the NLRP3 inflammasome is a two-step process (Fig. 2). First, a priming signal is required, where the recognition of PAMPs and DAMPs induces nuclear factor kappa-light-chain-enhancer of activated B cells (NF-κB)-mediated transcription of NLRP3 pathway components, such as the genes coding for NLRP3, pro-IL-1β and pro-IL-18. A second intra- or extracellular stressor such as ionic flux (K^+/Cl^- efflux and Ca^{2+} flux), toxins, bacteria, extracellular adenosine triphosphate (ATP), reactive oxygen species (ROS), viruses and pathological protein aggregates (e.g., amyloid-beta (Aβ) and tau) mediate the assembly and activation of the NLRP3-inflammasome (Duez and

Pourcet, 2021; Ising et al., 2019; Jung et al., 2022; McKee and Coll, 2020; Pike et al., 2021; Stancu et al., 2019; Trudler et al., 2021). Activation of the NLRP3 inflammasome induces cleavage of gasdermin D (GSDMD), which creates pores in the plasma membrane, resulting in the release of caspase-1-cleaved, mature IL-1β and IL-18 (Liu et al., 2016; Shi et al., 2015).

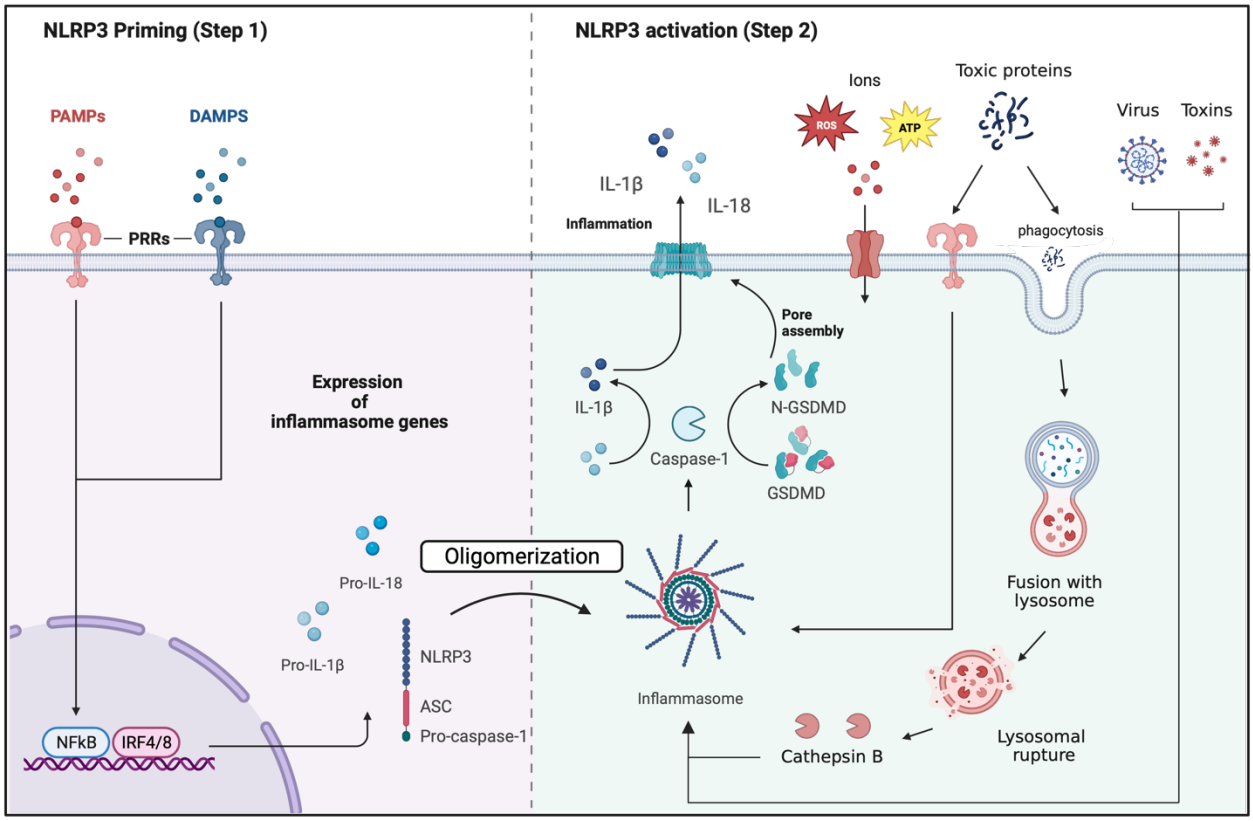

Fig. 2: NLRP3 inflammasome assembly and activation. Priming of the NLRP3 inflammasome is induced by the binding of PAMPs and DAMPs to PPRs, subsequently resulting in NF-kB-dependent transcriptional upregulation of NLRP3, pro-IL-1β and pro-IL-18 (Step 1). Secondary intra- and extracellular stressors, including ion flux (e.g., K^+ and Ca^{2+}), reactive oxygen species (ROS), ATP, toxins (e.g., nigericin), pathological proteins (e.g., tau) and viruses are necessary to induce full formation and activation of the NLRP3 inflammasome, which results in the release of mature IL-1β and IL-18 (Step 2). Created with BioRender.com.

1.2.4 The role of microglia in the pathophysiology of tauopathies

As described earlier, microglia represent the innate immune cells of the CNS that survey the microenvironment and remove harmful proteins, bacteria, cells and pathogens that endanger the CNS. The first evidence for the involvement of microglia in tauopathies was demonstrated as a result of the interaction between microglia and NFTs (Cras et al.,

1991). Later, it was demonstrated that microglial activation occurred simultaneously with hippocampal synaptic pathology and astrogliosis and preceded the formation of NFTs in a mouse model of tauopathy expressing human tau with a P301S mutation (PS19 mice) (Yoshiyama et al., 2007). Strikingly, immunosuppressant treatment with FK506 (Tacrolimus) inhibited microglial activation and ameliorated tau pathology in these mice, suggesting that early microglial activation drives tau pathology (Yoshiyama et al., 2007). This raises questions about the driving factor of early microglial activation. As such, it became clear that neuronal phosphorylated tau (pTau) aggregation in early stages of disease onset contribute to microglia activation (van Olst et al., 2020). In addition, it was demonstrated that microglia are able to phagocytose tau aggregates and facilitate the spreading of tau from neuron to neuron (= cell to cell), a process called propagation, via phagocytosis and exocytosis (Asai et al., 2015). In line with this, it was reported that microglia internalize insoluble tau (derived from human AD brain) *in vitro* as well as *in vivo* (Bolós et al., 2016). Lastly, it was observed that cultured adult isolated microglia from rTg4510 mice contained more seed-capable tau aggregates and released significantly more tau seeds in the conditioned medium compared to adult isolated microglia from WT mice (Hopp et al., 2018).

Interestingly, genome-wide association studies (GWAS) have identified various risk variants present in microglia that contribute to the development of AD including triggering receptor expressed on myeloid cells 2 (TREM2) and cluster of differentiation 33 (CD33) (McQuade and Blurton-Jones, 2019). TREM2 is a transmembrane glycoprotein expressed on myeloid cells (e.g., microglia), which is known to be involved in immune modulation (Colonna, 2003). Interestingly, PS19 mice being deficient in *Trem2* (PS19/*Trem2*$^{-/-}$) showed a significant reduction in microglial-mediated inflammation and neurodegeneration (Leyns et al., 2017). Moreover, mutations in CD33, another transmembrane receptor on myeloid cells, have been widely associated with the development of AD (Hollingworth et al., 2011; Jiang et al., 2014). Interestingly, AD patients show increased expression of CD33 which correlates with disease progression and amyloid plaque deposition in the brain (Linnartz and Neumann, 2013). Moreover, mouse models of AD lacking CD33 expression showed an increased ability in Aβ phagocytosis and less amyloid plaque burden (Griciuc et al., 2013). However, the contribution of CD33

to the spreading of tau remains elusive. Another genetic risk factor highly involved in the development of late-onset AD is apolipoprotein E (APOE) (Corder et al., 1993), which is known to be an immune modulator as well (Krasemann et al., 2017; Zhu et al., 2012). As such, it was demonstrated that APOE regulates microglia-mediated tau pathology and neurodegeneration in PS19 mice (Shi et al., 2019). In addition to genetic risk factors, recent studies have revealed an important contribution of other components present in microglia, in particular the NLRP3 inflammasome, to inflammation-mediated tau phosphorylation and aggregation in neurons and subsequent cognitive decline in various models of tauopathies (Ising et al., 2019; Stancu et al., 2019).

1.3 Cellular Senescence

1.3.1 Overview of cellular senescence and aging

Cellular senescence was discovered by Hayflick and Moorhead (Hayflick and Moorhead, 1961) and imposes a permanent state of cell cycle arrest as a consequence of progressive aging (Hayflick and Moorhead, 1961; Hernandez-Segura et al., 2018; Van Deursen, 2014). Despite its association with aging, senescence has become a field of interest in cancer biology as it can provide an opportunity to prevent cancer growth by limiting the replication of tumor cells through cell cycle arrest (Herranz and Gil, 2018). Additionally, cellular senescence has been regarded as beneficial in various biological processes, ranging from tissue repair and wound healing after injury to embryonic development (Van Deursen, 2014). For instance, senescent hepatic stellate cells were shown to accumulate in fibrotic tissue in a mouse model of liver fibrosis (Krizhanovsky et al., 2008). Strikingly, mice being deficient in $p16^{INK4A}$, a protein involved in cell cycle arrest in senescence, showed increased liver fibrosis, indicating that the accumulation of senescent cells in fibrotic tissue is a protective mechanism to halt liver fibrosis (Krizhanovsky et al., 2008). In addition, a study investigating cellular senescence in chick and mouse embryo's showed that the occurrence of senescent cells in particular regions, such as the neural tube and limbs, contributes to the development of these areas (Storer et al., 2013). Furthermore, senescent cells were shown to assist placental, fetal and fetal membrane development during reproduction (Velarde and Menon, 2016). Despite its beneficial role in many physiological processes, cellular senescence can also have adverse

consequences by contributing to age-related pathologies, including atherosclerosis, osteoarthritis, diabetis and neurodegenerative diseases like Alzheimer's Disease (AD) (Childs et al., 2015; He and Sharpless, 2017; Kritsilis et al., 2018; Bussian et al., 2018).

1.3.2 The induction of cellular senescence

Senescence can be categorized into replicative senescence (RS), stress-induced premature senescence (SIPS) and oncogene-induced senescence (OIS) (Kuilman et al., 2010). RS occurs in response to shortening of telomeres after a finite number of cell divisions over time (Hayflick and Moorhead, 1961; Kritsilis et al., 2018). In contrast to RS, SISP occurs in response to chemical or physical cellular insult, such as oxidative stress (ROS), DNA damage, ultraviolet radiation (UV), chemotherapeutic agents (e.g., bleomycin or doxorubicin) and hydrogen peroxide (Chen et al., 1995; Suzuki and Boothman, 2008). OIS, a hallmark of cell transformation and cancer, is induced upon abnormal oncogenic signaling, such as activation of an oncogene (e.g., BRAF, AKT, E2F1 and cyclin E) or inactivation of a tumor-suppressor gene (e.g., PTEN and NF1) (Chen et al., 1995; Liu et al., 2018). More recently, studies have identified other 'subtypes' of senescence, including mitochondrial dysfunction-associated senescence (MiDAS), epigenetically induced senescence and paracrine senescence (Hernandez-Segura et al., 2018). Despite the various subtypes, a persistent DNA damage response (DDR) is triggered in any senescent cell irrespective of the initiating factor (Herranz and Gil, 2018).

Upon initiation of a DDR, several DNA damage kinases, including ataxia-telangiectasia mutated (ATM) and Rad3-related (ATR) are recruited to the site of insult. This leads to the phosphorylation of the histone variant H2AX as a result of DNA double-stranded breaks (DSBs) (Ben-Porath and Weinberg, 2005; Campisi and Di Fagagna, 2007). As a consequence, cell cycle arrest is mediated via activation of the cyclin-dependent kinase inhibitor (CDKI) pathways p53/$p21^{WAF1}$ and/or $p16^{INK4a}$ (Ben-Porath and Weinberg, 2005; Childs et al., 2015; Herranz and Gil, 2018; Muñoz-Espín and Serrano, 2014) (Fig. 3).

Despite the contribution of p53/$p21^{WAF1}$ and $p16^{INK4a}$ to cell cycle arrest, it is noteworthy to state that cell cycle arrest is not equal to senescence . For example, quiescence, which is known as a stable, yet temporary state of cell cycle arrest, is also $p21^{WAF1}$ (Overton et

al., 2014; Perucca et al., 2009) and $p16^{INK4a}$ dependent (Agarwal et al., 2013, 2018). Quiescence is likely the result of exposure to short-term stress from which the cells are likely to recover. However, upon continuous exposure to stress, quiescence can passage to senescence (Alessio et al., 2021). This is in line with the observation that chronic exposure to various stressors induces a continuous DNA-damage response (DDR), subsequently inducing a senescent state (Garwood et al., 2014; Giunta et al., 2008; Rodier et al., 2009).

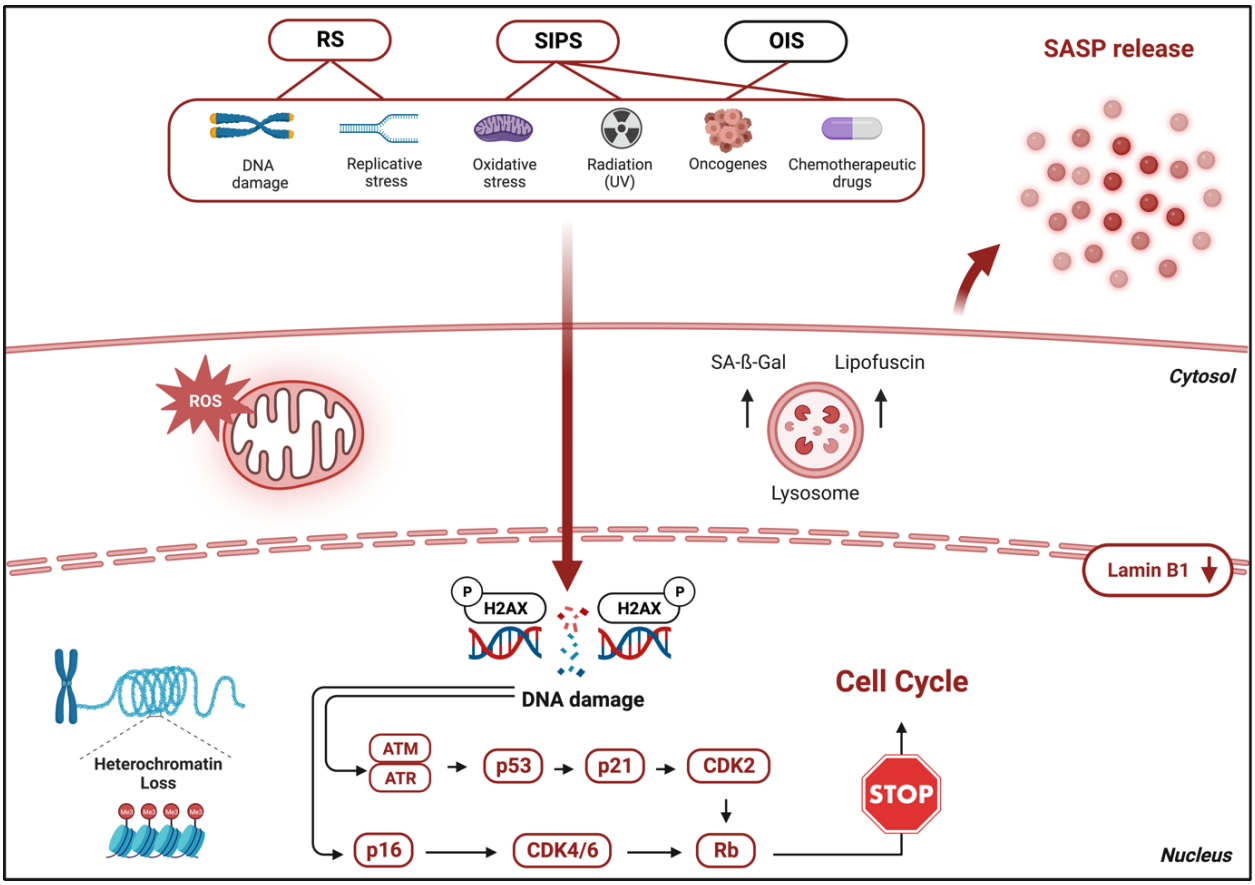

Fig. 3: Molecular pathways regulating cell cycle arrest: a path to cellular senescence. Intra- and extracellular stressors can activate the two most important signaling pathways involved in cellular senescence. Upon exposure to stressors, double-stranded breaks trigger a DNA damage response is triggered, resulting in the activation of DDR kinases ataxia-telangiectasia mutated (ATM) and Rad3-related (ATR). This eventually results in the phosphorylation of the histone variant H2AX, causing transcription of the cyclin-dependent kinase inhibitors (CDKIs) $p21^{WAF1}$ and $p16^{INK4a}$. As a consequence, inhibition of CDK2 and CDK4/6 causes hypophosphorylation of Retinoblastoma (Rb), inducing cell cycle arrest. In addition to DNA damage and cell cycle arrest, senescent cells present with loss of heterochromatin H3K9me3 and lamin B1, increase in lysosomal content of senescence-associated β-Galactosidase (SA-β-Gal) and lipofuscin, mitochondrial

dysfunction and release of a senescence-associated secretory phenotype (SASP). Created with BioRender.com.

1.3.3 The Senescent Phenotype

Senescent cells present with a unique phenotype, including a senescence-associated secretory phenotype (SASP) (Fig. 3). The SASP is a proinflammatory secretome consisting of various signaling factors (e.g. cytokines, chemokines and growth factors), proteases (e.g. matrix metalloproteinases -MMPs), lipids and extracellular matrix (ECM) components (Chinta et al., 2015; Coppé et al., 2010; Lopes-Paciencia et al., 2019). The main proinflammatory factors upregulated during senescence are IL-1α, IL-1β, IL-6 and IL-8 (Kiecolt-Glaser et al., 2003), whereas anti-inflammatory cytokines like IL-2, IL-4, IL-11 and IL-18 remain unaffected (Coppé et al., 2010). The existence of distinct SASP profiles is recognized and depends on the origin of the tissue, the mechanism behind senescence induction and the biophysical properties (Schafer et al., 2020). As an illustration, irradiated human senescent epithelial cells and myoblasts express a different SASP in comparison to irradiated preadipocytes, endothelial cells and fibroblasts (Kyjacova et al., 2021; Saker et al., 2016).

Not only the origin of the cell but also the type of senescent inducer determines the expression of the SASP. It was reported that the SASP of primary human lung fibroblasts and renal cortical epithelial cells after X-irradiation (IR), inducible RAS overexpression (RAS) and atazanavir (ATV) treatment was different. For example, *Cxcl1* and *Hmgb1* gene expression levels were upregulated in IR-induced senescent fibroblasts, but downregulated or even absent in IR-induced senescent epithelial cells (Basisty et al., 2020). In addition, mice lung fibroblasts that were exposed to stress-induced premature senescence (SIPS), replicative senescence (RS) or proteasome inhibition-induced premature senescence (PIIPS) all expressed several of the most commonly reported SASP components, including IL-6, IL-10, IL-12, MIP-2 and IFN-y (Maciel-Barón et al., 2016). However, despite similarities in their SASP expression, the magnitude of release significantly depends on the senescent stimulus. For instance, IL-10, IL-12 and MIP-2 secretion was significantly higher during RS compared to SISP and PIIPS, whereas IL-6 secretion was higher in PIIPS compared to RS and SISP (Maciel-Barón et al., 2016).

Next to alterations of their secretory phenotype, senescent cells show differences in morphology, lysosomal content, mitochondrial function and nuclear structure (Herranz and Gil, 2018; Kritsilis et al., 2018). Senescent cells present with a larger, flatter, vacuolized and irregular shape compared to non-senescent cells (Herranz and Gil, 2018; Kritsilis et al., 2018). In addition, increased activity of the enzyme senescence-associated beta-galactosidase (SA-β-gal) is often used to detect increased lysosomal content in senescent cells (Hernandez-Segura et al., 2018; Kritsilis et al., 2018). However, contradictory results in the specificity of this assay suggests it should not be used as the only method to detect senescence. In fact, it has been shown that SA-β-gal activity is not only specific to senescent cells but is also detectable in non cell-aging conditions and quiescent cells (Terzi et al., 2016; Yang and Hu, 2005). Next, senescent cells are characterized by alterations in mitochondrial function, including imbalanced NAD^+/NADH ratios, electron transport chain (ETC) disruptions, mitochondrial calcium (Ca^{2+}) overload, impaired mitophagy and increased mitochondrial mass (Chapman et al., 2019; Dodig et al., 2019; Kritsilis et al., 2018; Miwa et al., 2022). Dysfunctional mitochondria are associated with the release of various DAMPs like cardiolipin, mitochondrial DNA (mtDNA), extracellular ATP and reactive oxygen species (ROS) (Chu et al., 2013; Dela et al., 2018; Nakahira et al., 2015), which could contribute to DNA damage (Chapman et al., 2019; Nadalutti et al., 2020; Srinivas et al., 2019). In the context of senescence, mitochondrial-derived DAMPs can leak into the cytoplasm and act on various innate immune signaling pathways, such as the NLRP3 inflammasome (Pereira et al., 2019; Rimessi et al., 2015; Zhou et al., 2011). Depletion of mitochondria is known to suppress the pro-inflammatory and pro-oxidant phenotype of senescent cells in vivo (Correia-Melo et al., 2016).

Next to mitochondrial alterations, senescent cells present with irregular changes in the nuclear envelope and chromosome distribution. Nuclear lamina type B1 (lamin B1) is involved in many nuclear functions, including nuclear stabilization and chromatin organization (Saito et al., 2019). Loss of lamin B1 is a common characteristic of senescent cells (Hernandez-Segura et al., 2018) and has been observed in mouse and human cells undergoing senescence (Chapman et al., 2019). Reduction of lamin B1 is accompanied by changes in the senescence-associated heterochromatin foci (SAHFs) which are

responsible for nuclear stabilization and chromatin organization (Hernandez-Segura et al., 2018). Accompanied is also a loss of lysine 9 dimethylation on histone 3 (H3K9me3), a heterochromatin that has been associated with cellular senescence (Sidler et al., 2017; Tsurumi and Li, 2012; Zhang et al., 2021). Lastly, phosphorylation of histone variant H2AX as a consequence of the DDR leads to alterations in gene expression levels of p53, $p16^{INK4A}$ and $p21^{WAF1}$ in senescent cells and is therefore another widely accepted marker for the detection of senescence (Chinta et al., 2015; Muñoz-Espín and Serrano, 2014).

1.3.4 Cellular Senescence in Tauopathies

Aging represents the greatest risk factor for dementia, in particular AD, which is the most prevalent form tauopathy, as well as other neurodegenerative disorders (Muñoz-Espín and Serrano, 2014). The cellular and molecular hallmarks underlying the gradual loss of function during aging remain poorly understood. Research on cellular senescence has helped to conceptualize the mechanisms behind aging (Hayflick and Moorhead, 1961; McHugh and Gil, 2018; Muñoz-Espín and Serrano, 2014). Although senescence is an essential process during development, tissue repair and wound healing (Hayflick and Moorhead, 1961; van Deursen, 2014), it has also been implicated in tau pathophysiology and neurodegeneration (Bussian et al., 2018; Martínez-Cué and Rueda, 2020; Mendelsohn and Larrick 2018; Musi et al., 2018).

1.3.4.1 The SASP

During ageing, the brain suffers from a low-grade chronic inflammation, also known as inflammaging (Bauer et al., 1991; Kiecolt-Glaser et al., 2003), which is mainly the result of IL-1α, IL-1β, IL-6, IL-8, interferon gamma (IFN-y) and tumor necrosis factor α (TNF-α) signaling. These signaling molecules have been associated with the SASP during senescence (Coppé et al., 2010; Kiecolt-Glaser et al., 2003; Lasry and Ben-Neriah 2015; von Bernhardi et al., 2015) and are mainly regulated by the transcription factors nuclear factor-κB (NF-κB) (Chien et al., 2011; Mongi-Bragato et al., 2020; Salminen et al., 2012), CCAAT/enhancer binding protein β (C/EBPβ) (Kuilman et al., 2008; Salotti and Johnson, 2019) and the janus kinase 2 (JAK2) / signal transducer and activator of transcription 3 (STAT3) pathway (Bai et al., 2020; Toso et al., 2014; Wu et al., 2020). A SASP has also been detected during neurodegenerative conditions. For instance, research on post-

mortem brains, cerebrospinal fluid (CSF) and serum of AD patients revealed increased levels of IL-1β, IL-6 and TNF-α (Lai et al., 2017; Rea et al., 2018; Streit, 2006; Wood et al., 1993). Furthermore, the expression of IL-1α, IL-1β, IL-6 and TNF-α was positively correlated with the phosphorylation of tau (Griffin et al., 2006; Ising et al., 2019). In line with this, gene expression analysis of human and mouse NFT-bearing neurons indicated an upregulation of the SASP, in particular IL-1β and TNF-α, which correlated with NFT formation and density (Musi et al., 2018). Genetic ablation of endogenous murine tau from human mutated tau-expressing mice reduced NFT formation and was accompanied by a significant reduction in the gene expression levels of the SASP (Musi et al., 2018). In addition, elevated levels of mature IL-1β in cortex samples of patients with frontotemporal dementia (FTD) were found (Ising et al., 2019).

1.3.4.2 Nuclear and gene expression changes

Senescent cells show increased DNA damage, increased expression of cell cycle arrest markers (Ben-Porath and Weinberg, 2005; Campisi and Di Fagagna, 2007), loss of H3K9me3 (Lee et al., 2020; Paluvai et al., 2020) and lamin B1 (Freund et al., 2012; Saito et al., 2019) and increased formation of yH2AX foci (Campisi and Di Fagagna, 2007). These features have also been demonstrated during the pathogenesis of neurodegenerative disorders belonging to the spectrum of tauopathies. For instance, astrocytes and lymphocytes in hippocampal sections of human AD patients showed signs of DNA damage. Moreover, astrocytes (Baker and Petersen, 2018; Bhat et al., 2012), hippocampal neurons (McShea et al., 1997) and microglia (Hu et al., 2021) in the brains of AD patients expressed increased levels of $p16^{INK4a}$ and $p21^{WAF1}$. Furthermore, the rapid proliferation and activation of microglia prior to the development of pathological conditions in AD promotes replicative microglial senescence, characterized by increased levels of $p16^{INK4a}$, $p21^{WAF1}$ and SA-β-gal staining (Hu et al., 2021).

Not only humans, but also mice overexpressing mutated human tau (rTg(tauP301L)4510 transgenic mice) presented with increased gene expression levels of *Cdkn1a* (Protein name: $p21^{WAF1}$) and *Cdkn2a* (Protein name: $p16^{INK4a}$) and showed increased formation of yH2AX foci, which correlated with brain atrophy and NFT formation (Musi et al., 2018). In the same study, deletion of the endogenous tau gene in tau-transgenic mice, resulting

in reduced NFT pathology as mentioned already before, led to more than 50% reduction of *Cdkn2a* gene expression levels, suggesting that the formation of NFTs is associated with cell cycle arrest (Musi et al., 2018). To confirm the association between senescence and tau pathology in humans, the same study showed that *Cdkn2a* gene expression levels were increased in post-mortem brains of PSP patients in comparison to age-matched controls (Musi et al., 2018).

Shortly after, another study reported increased gene expression levels of *Cdkn1a* and *Cdkn2a* in the hippocampus and cortex of another mouse model of tauopathy expressing human tau with a P301S mutation, namely PS19 (Bussian et al., 2018). Interestingly, increased *Cdkn2a* gene expression levels were observed at 4 months of age, whereas cognitive impairments are noticeable at 6 months of age (Gosselin & Rivest, 2018). More importantly, crossing of PS19 mice with the so-called INK-ATTAC transgene (hereafter called PS19/ATTAC), was used to investigate the contribution of senescent cells to the progression of tau pathology (Bussian et al., 2018). The INK-ATTAC model was designed by Darren Baker (Baker et al., 2011) to investigate the mechanism(s) underlying age-related dysfunction by elimination of $p16^{INK4a}$-expressing cells. Weekly administration of AP20187, a compound specifically targeting the $p16^{INK4a}$-expressing cells in PS19/ATTAC mice, has been proven to normalize $p16^{INK4a}$ and $p21^{WAF1}$ levels (Bussian et al., 2018). Remarkably, genetic and pharmacological deletion of $p16^{INK4a}$-expressing cells attenuated tau hyperphosphorylation, ameliorated neurodegeneration and improved cognitive function (Bussian et al., 2018).

Lastly, neurons in a Drosophila model of tauopathy are characterized by loss of heterochromatin as a result of tau-mediated neurodegeneration (Frost et al., 2014). In addition, their study showed that DNA damage, as a consequence of increased oxidative stress, is involved in heterochromatin relaxation (Frost et al., 2014). Later, the authors reported that loss of lamin B1 preceded heterochromatin relaxation, DNA damage and cell cycle arrest in neurons which subsequently resulted in neuronal death in tau-transgenic *Drosophila* (Frostet et al., 2016). In line with this, disortions as well as loss of neuronal lamin B1 levels were observed in post-mortem human brain tissue of AD (Frost et al., 2016) as well as FTD patients (Paonessa et al., 2019).

In light of these observations, it could be hypothesized that the formation and accumulation of senescent cells potentially contribute to neuronal tau pathologies and that elimination of these cells could present a promising therapeutic approach for tauopathies (Gosselin and Rivest, 2018).

1.4 Linking NLRP3 inflammasome activation to senescence in tauopathies

Aging is accompanied by a decline in immune efficacy, contributing to age-related inflammatory diseases (Aiello et al., 2019). The term inflammaging has been previously described and is closely linked to immunosenescence, a phenomenon that describes the progressive deterioration of the immune system with age (Aiello et al., 2019; Aw et al., 2007; Sebastian-Valverde and Pasinetti, 2020). Microglia are susceptible to a senescent state during aging and neuropathological conditions, such as AD (Streit, 2006). For instance, aged microglia display features that resemble the SASP, including elevated secretion of IL-1β, IL-6 and TNF-α (Norden and Godbout, 2013; Greenwood and Brown, 2021). The release of these proinflammatory molecules has been shown to induce paracrine senescence (Beyne-Rauzy et al., 2004; Kojima et al., 2013; Shang et al., 2020). As an illustration, exposure to IL-1β has been shown to be sufficient to drive cellular senescence in rat astrocytes (Shang et al., 2020), vascular smooth muscle cells (VSMC) (Han et al., 2020; Zhao et al., 2021) and chondrocytes (Huang et al., 2021).

Since activation of the NLRP3 inflammasome mediates the release of IL-1β and contributes to tau mediated neurodegeneration (Heneka et al., 2013; Ising et al., 2019; Mangan et al., 2018), it could be speculated that the NLRP3 inflammasome acts as an essential component in the mediation of the SASP (Bussian et al., 2018; Maphis et al., 2015). Indeed, it was elegantly proven that activation of the NLRP3 inflammasome controls the SASP in vitro as well as in mouse models of OIS in vivo (Acosta et al., 2013). Later studies aiming to decipher the link between aging and immunosenescence confirm activation of the NLRP3 inflammasome as a potential mediator (Sebastian-Valverde and Pasinetti, 2020; Spadaro et al., 2016). More specifically, these studies reported that NLRP3 inflammasome activation resulted in telomere shortening in mouse cardiomyocytes (Marín-Aguilar et al., 2020), modulated the SASP in human IRM-90 cells

(Wiggins and Clarke, 2019) and induced premature senescence in aortic endothelial cells (MAECs) and VSMCs in a mouse model of diabetic vasculopathy (Tai et al., 2022). Since activation of the NLRP3 inflammasome significantly contributed to tau pathology and cognitive deficits in tau transgenic mice (Ising et al., 2019), it could be speculated that the NLRP3 inflammasome plays an important role in microglial senescence and potentially underlies inflammation-mediated tau pathology (Heneka et al., 2013, 2015; Ising et al., 2019).

1.5 Aim(s) of the Study

Worldwide, more than 50 million people suffer from dementia and by 2050, approximately 140 million people will be affected (Xu et al., 2014). Clinically, tauopathy patients may present with cognitive dysfunction, behavioral symptoms like aggression and apathy and disturbance of movement and language (Höglinger et al., 2018). Aging represents the greatest risk factor for dementia, in particular AD, which is the most prevalent form of tauopathies (Zhang et al., 2022). In addition, other forms of tauopathies, including primary tauopathies such as FTD, account for 2.6% of all forms of dementia and the incidence is known to peak in elderly around the age of 70 (Zhang et al., 2022). Given this, it might be speculated that ageing is potentially associated with the development of primary tauopathies as well. Therefore, a better understanding of the contribution of aging to the pathophysiology of tauopathies is essential. Cellular senescence is a hallmark of aging. Interestingly, senescent microglia have been identified in the brains of tauopathy patients as well as animal models of tauopathy. However, the contribution of the NLRP3 inflammasome to microglial senescence in the context of tauopathies and the role of tau on the induction of microglial senescence remains unclear. Therefore, the aims of this study are as follows:

1. To identify microglial senescence in a mouse model of tauopathy.
2. To decipher the contribution of the NLRP3 inflammasome to the development of microglial senescence in this model.
3. To explore the effect of monomeric tau on the induction of microglial senescence in a primary microglia culture, focusing on the contribution of the NLRP3 inflammasome to the induction of microglial senescence.

2 Material and Methods

2.1 Material

2.1.1 Instruments

Equipment	Supplier
Eppendorf ThermoMixer®	Eppendorf
Trans-Blot® Turbo™ Transfer System	Bio-Rad
Trans-Blot® Turbo™ Cassette	Bio-Rad
Power Supply EV3020	Carl Roth
Eppendorf™ Mastercycler X50s 96-Well Silver Block Thermal Cycler	Thermo Fisher Scientific
RT-PCR System StepOnePlus™	Thermo Fisher Scientific
Leica CM3050 S Research Cryostat	Leica
Zeiss Laser Scanning Microscope 900 (LSM900)	Zeiss
LI-COR ODYSSEY® CLx	LI-COR® Biosciences
gentleMACS™ Octo Dissociator	Milteny Biotec
Infinite® M200 PRO	Tecan
Nanodrop 2000c	Thermo Fisher Scientific
Bandelin Sonorex	Bandelin
Meso quickplex sq 120	Meso Scale Discovery
OctoMACS™ Separator	Milteny Biotec
Nikon ECLIPSE Ti	Nikon
FACSCanto II	Becton Dickinson
Speedvac	Thermo Fisher Scientific

2.1.2 Software

Software	Supplier

ImageStudio™ software version 5.2.5	LI-COR® Biosciences
ImageJ/Fiji software version 2.0	ImageJ
FACSCanto™ II and FACSDiva™ software	Becton Dickinson
FlowJo™ (v3.05470)	Ashland
Graph Pad Prism version 8.0	GraphPad
CellProfiler software version v3.1.8	Broad Institute of Harvard and MIT
StepOne™ software	Applied Biosystems™

2.1.3 General lab equipment

Name	Supplier	Cat #
15 ml tubes	CELLSTAR®	188261-N
50 ml tubes	CELLSTAR®	227261
6-well plates	CELLSTAR®	657160
12-well plates	CELLSTAR®	665180
24-well plates	CELLSTAR®	662160
Eppendorf Tubes® 1.5 ml	Gibco™	0030121872
Eppendorf Tubes® 2.0 ml	Gibco™	0030120094
Eppendorf Tubes® 5.0 ml	Sigma-Aldrich®	0030119401
Pipette tip 2.5 µl	Sarstedt	703010365
Pipette tip 10 µl	Sarstedt	703010100
Pipette tip 200 µl	Sarstedt	703030100
Pipette tip 1000 µl	Sarstedt	703050100
Aspiration pipet (2 ml)	Sarstedt	861252011
Serological pipet with tip (5 ml)	Sarstedt	861253025
Serological pipet with tip (10 ml)	Sarstedt	861254025

Serological pipet with tip (25 ml)	Sarstedt	861685020
Eppendorf Research® Plus pipet (0.5 – 10 µl)	Eppendorf	3123000020
Eppendorf Research® Plus pipet (2 – 20 µl)	Eppendorf	3123000098
Eppendorf Research® Plus pipet (20 – 200 µl)	Eppendorf	3123000055
Eppendorf Research® Plus pipet (100 – 1000 µl)	Eppendorf	3123000063

2.1.4 Kits, substances and chemicals for tissue processing, immunohistochemistry and immunocytochemistry

Name	Composition	Supplier	Cat #
Dulbecco's PBS (10x)	-	Applichem	2004367
Cryoprotectant solution	1x PBS	Applichem	2004367
	30% (w/v) sucrose	Sigma-Aldrich®	57-50-1
	30 % (v/v) Ethylenglycol	Sigma-Aldrich®	324558
Paraformaldehyde (PFA, 4%)	-	Merck Millipore	P6148
PBS-T (pH = 7.4)	1x Dulbecco's PBS	Applichem	2004367
	0.1% Triton® X-100 (v/v)	Carl Roth	3051.3
Citrate Buffer (pH 6.0)	0.1 M	Carl Roth	3580.3
ProLong™ Gold with DAPI	-	Invitrogen™	P36931
DAPI (0.1 µg/mL)	-	Thermo Fisher Scientific	62247
SuperFrost® microscope slides	-	Thermo Fisher Scientific	12372098
Sucrose Solution	30% (w/v) sucrose	Sigma-Aldrich®	57-50-1

	1x PBS	Applichem	2004367
Immuno-Mount mounting medium	-	Thermo Fisher Scientific	9990402
Coverslips (24 x 60 mm)	-	Menzel-Gläser	15628
Coverslips (13 mm^2)	-	Paul Marienfeld	0111530
Counting chamber	-	Paul Marienfeld	0642110
Normal Goat Serum (NGS)	-	Abcam	Ab7481
Bovine Serum Albumin (BSA)	-	Rockland	BSA-1000

Primary Antibodies					
Antigen	**Host**	**Dilution**	**Supplier**	**Cat #**	**RRID**
Lamin B1	Mouse	1:500	Proteintech	66095-1-Ig	AB_11232208
Caspase-1	Mouse	1:1000	Adipogen	AG-20B-0042-C100	AB_2755041
p21	Rabbit	1:1000	Abcam	218311	AB_2890611
p16	Rabbit	1:1000	Abcam	211542	AB_2891084
Total STAT3	Mouse	1:1000	Abcam	119352	AB_10901752
p-STAT3	Rabbit	1:1000	Abcam	76315	AB_1658549
Parkin	Mouse	1:500	BioLegend	808501	AB_2564744
GAPDH	Rabbit	1:5000	Sigma-Aldrich®	G9594	AB_796208
IBA1	Rabbit	1:1000	FUJIFILM Wako	019-19741	AB_839504
yH2AX	Mouse	1:100	Merck Millipore	05-636	AB_309864
H3K9me3	Rabbit	1:200	Abcam	8898	AB_306848
CD11b	Rat	1:250	Bio-Rad	MCA711	AB_321292

Secondary antibodies					
Antigen	**Host**	**Dilution**	**Supplier**	**Cat #**	**RRID**
AlexaFluor488 Mouse	Goat	1:500	Invitrogen™	A-11001	AB_2534069
AlexaFluor594 Rabbit	Goat	1:500	Invitrogen™	A-11012	AB_2534079
AlexaFluor594 Rat	Goat	1:500	Invitrogen™	A-11007	AB_10561522
IRDye® 800CW Goat anti-Rabbit IgG (H + L)	Goat	1:20,000	LI-COR® Biosciences	926-32211	
IRDye® 800CW Goat anti-Mouse IgG (H + L)	Goat	1:20,000	LI-COR® Biosciences	926-32210	
IRDye® 680CW Goat anti-Rabbit IgG (H + L)	Goat	1:20,000	LI-COR® Biosciences	926-68071	
IRDye® 680CW Goat anti-Mouse IgG (H + L)	Goat	1:20,000	LI-COR® Biosciences	926-68070	

2.1.5 Kits, substances and chemicals for Primary Microglia Culture

Name	Supplier	Cat #
DPBS	Gibco™	14190169
DMEM	Gibco™	31966047
Fetal Calf Serum (FCS)	Gibco™	26140079
DNase I	Roche	11284932001
Trypsin	Life Technologies	15400054
HBSS	Gibco™	24020091
penicillin–streptomycin	Gibco™	15070063

L929 cell line	Sigma-Aldrich®	85011425
N-2 supplement (100x)	Gibco™	17502048
poly-L-lysine (PLL)	Merck Millipore	P1524
T75 flasks	Greiner	658175

Pharmacological compound	**Supplier**	**Cat #**
CRID3 sodium salt	Tocris	5479
Selective STAT3 inhibitor (Stattic)	Tocris	2798
phorbol 12-myristate 13-acetate (PMA)	Sigma-Aldrich®	16561-29-8

2.1.6 Kits, substances and chemicals for Western Blotting

Name	**Supplier**	**Cat#**
BCA Protein Assay Kit	Thermo Fisher Scientific	23225
4-12% NuPAGE™ Novex gel (10 wells)	Thermo Fisher Scientific	NP0321BOX
4-12% NuPAGE™ Novex gel (15 wells)	Thermo Fisher Scientific	NP0323BOX
4-12% NuPAGE™ Novex gel (20 wells)	Thermo Fisher Scientific	WG1402BOX
Protease and Phosphatase Inhibitor Cocktail (100X)	Thermo Fisher Scientific	78441
Bovine Serum Albumin (BSA)	Rockland	BSA-1000
PageRuler™ Prestained Protein Ladder	Thermo Scientific	26616
Trans-Blot® Turbo™ mini 0.2 µm nitrocellulose transfer packs	Bio-Rad	170-4158
Trans-Blot® Turbo™ midi 0.2 µm nitrocellulose transfer packs	Bio-Rad	170-4159

Name	Composition	Supplier	Cat#
TBS-T (pH 8.0)	150 mM NaCl	Applichem	7647-14-5
	10 mM Tris-HCL	Carl Roth	77-86-1
	0.05% Tween 20	Carl Roth	9005-64-5
RIPA buffer	Triton® X-100 (1%)	Carl Roth	9036-19-5
	50 mM Tris-HCl	Sigma-Aldrich®	1185-53-1
	Sodium deoxycholate (0.5 %)	Sigma-Aldrich®	145224-92-6
	Sodium dodecyl sulfate (SDS) (0.1%)	Carl Roth	151-2-3
NuPAGE™ MES SDS running buffer		Invitrogen™	NP0002
Selfmade (4x) LDS Sample Buffer Based on the NuPAGE™ LDS Sample Buffer (Thermo Fisher Scientific, Cat # R1381)	Tris-HCl (0.666 g)	Sigma-Aldrich®	1185-53-1
	Tris Base (0.682 g)		
	SDS (0.800 g)	Carl Roth	151-2-3
	EDTA (0.006 g)	Carl Roth	6381-92-6
	Glycerol (4 g)	Applichem	56-81-5
	DTT (555.3 g)	Carl Roth	3483-12-3
	Ultrapure water (10 ml)	-	-
	Orange G (final concentration 0.2%)	Sigma-Aldrich®	03756-25G

2.1.7 Kits, substances and chemicals for ELISA and Mesoscale

Name	Supplier	Cat#
Mouse IL-1 beta/IL-1F2 DuoSet ELISA	R&D Systems	DY401
Mouse IL-6 DuoSet ELISA	R&D Systems	DY406
Mouse TNF-α DuoSet ELISA	R&D Systems	DY410

V-PLEX Plus Proinflammatory Panel 1 Mouse Kit	Meso Scale Diagnostics	K15048G-1
V-PLEX Cytokine Panel 1 Mouse Kit	Meso Scale Diagnostics	K15245D
V-PLEX Mouse Cytokine 19-Plex Kit	Meso Scale Diagnostics	K15255D-1

Name	**Composition**	**Supplier**	**Cat#**
PBS-T	PBS Dulbecco	Applichem	A0965 and A0750
	1% Tween 20	Carl Roth	9005-64-5

2.1.8 Kits, substances and chemicals for qRT-PCR

Name	**Supplier**	**Cat #**
Triton® X-100	Carl Roth	9036-19-5
QIAzol™ Lysis Reagent	Qiagen	79306
miRNeasy Micro Kit	Qiagen	217084
High-Capacity cDNA Reverse Transcription Kit	Applied Biosystems™	4368814
TaqMan™ gene expression master mix	Applied Biosystems™	4369016
Chloroform	Carl Roth	3313.1
cyclin-dependent kinase inhibitor 1A (Cdkn1a) TaqMan™ assay	Applied Biosystems™	Mm00432448_m1
cyclin-dependent kinase inhibitor 2A (Cdkn2a) TaqMan™ assay	Applied Biosystems™	Mm00494449_m1
lamin B1 (Lmnb1) TaqMan™ assay	Applied Biosystems™	Mm00521949_m1
18S rRNA TaqMan™ assay	Applied Biosystems™	4319413E
Interleukin-6 (Il-6) TaqMan™ assay	Applied Biosystems™	Mm00446190_m1

Interleukin-1 beta (IL-1β) TaqMan™ assay	Applied Biosystems™	Mm00434228_m1
chemokine (C-X-C motif) ligand 1 (Cxcl1) TaqMan™ assay	Applied Biosystems™	Mm04207460_m1

2.1.9 Kits, substances and chemicals for Isolation of Adult Mouse Microglia

Name	Supplier	Cat #
gentleMACS™ C tubes	Miltenyi Biotec	130-093-237
Adult Brain Dissociation Kit	Miltenyi Biotec	130-107-677
gentleMACS™ Octo Dissociator	Miltenyi Biotec	130-096-427
MACS® SmartStrainer (70 µM)	Miltenyi Biotec	130-098-462
CD11b MicroBeads	Miltenyi Biotec	130-126-725
MACS® Separator with LS columns	Miltenyi Biotec	130-042-401
QIAzol™ Lysis Reagent	Qiagen	79306

2.1.10 Kits, substances and chemicals for the preparation of recombinant human tau

Name	Supplier	Cat #
BL21(DE3) E. coli	Agilent	230245
IPTG	Merck Millipore	I6758
2-mercapthoethanol	Sigma-Aldrich®	M3148
PMSF	Merck Millipore	10837091001
Sepharose fast flow beads	Merck Millipore	GE17-0729-01
Amicon ultra centrifugal units	Merck Millipore	UFC9010
Endotoxin quantification kit	Thermo Fisher Scientific	A39552S
LB-agar plate	Thermo Fisher Scientific	J61525-EQF
LB-medium	Carl Roth	X968.1

Ampicillin		Thermo Fisher Scientific	J60977.06
SOC medium		Thermo Fisher Scientific	15544034
Chemical	**Composition**	**Supplier**	**Ca t#**
BRB-8 (pH 6.8)	80 mM PIPES	Sigma-Aldrich®	P6757
	1 mM magnesium sulfate	Merck Millipore	7487-88-9
	1 mM EGTA	Carl Roth	67-42-5

2.1.11 Kits, substances and chemicals for fluorescent labeling of tau and tau clearance

Name	**Supplier**	**Cat #**
Alexa Fluor™ 405 NHS ester	Thermo Fisher Scientific	A30000
Glycine	Merck Millipore	104201
PBS	Applichem	2004367
Slide-A-Lyzer™ dialysis cassette, 10 K MWCO	Thermo Fisher Scientific	66383
Protein low-binding tubes	Eppendorf™	0030108116
Trypsin	Thermo Fisher Scientific	15400054
PBS	Gibco™	2004367
Fetal Bovine Serum (FBS)	Gibco™	10500064
Allophycocyanin anti-mouse/human CD11b	BioLegend	101212

Name	**Composition**	**Supplier**	**Cat #**
FACS buffer	1x PBS	Applichem	2004367
	2% FBS	Gibco™	10500064

2.1.12 Kits, substances and chemicals for Morphology Analysis

Name	Composition	Supplier	Cat #
Paraformaldehyde (PFA, 4%)	-	Merck Millipore	P6148
PBS-T (pH = 7.4)	1x Dulbecco's PBS	Applichem	2004367
	0.1% Triton® X-100 (v/v)	Carl Roth	3051.3
DAPI (0.1 µg/mL)	-	Thermo Fisher Scientific	62247
Alexa Fluor™ 647 Phalloidin	-	Invitrogen™	A22287
SuperFrost® microscope slides	-	Thermo Fisher Scientific	12372098
Epredia™ Immu-Mount™	-	Thermo Fisher Scientific	9990402
Coverslips (13 mm^2)	-	Paul Marienfeld	0111530

2.1.13 Kits, substances and chemicals for protein precipitation

Name	Supplier	Cat #
Methanol	Merck Millipore	107018
Chloroform	Carl Roth	3313.1
NuPAGE™ Sample Buffer (2x)	Thermo Fisher Scientific	R1381

2.1.14 Kits, substances and chemicals for cytotoxicity measurements

Name	Supplier	Cat #
Cytotoxicity detection kit (LDH)	Roche	11644793001
HCl	Carl Roth	9277.1

2.2 Methods

2.2.1 Mouse strains and sample collection

All mice were on a C57BL/6N genetic background. THY–Tau22 transgenic mice (named Tau22) express a four-repeat isoform of human tau (1N4R) with a G272V and P301S mutation under control of the Thy1.2 promoter (Schindowski et al., 2006a). These mice, together with *Cias1*-knockout mice (named *Nlrp3*$^{-/-}$; Millennium Pharmaceuticals), were previously generated and characterized (Kanneganti et al., 2006). Crossing between Tau22 and *Nlrp3*$^{-/-}$ mice took place to generate Tau22/*Nlrp3*$^{-/-}$ mice. Non-tau-transgenic littermates were used as controls throughout the study. Mice were housed according to the standardized conditions in the University Hospital of Bonn animal facility. All mouse studies complied with relevant ethical regulations and were performed as approved by the local ethical committee (81-02.04.202.A104 and 81-02.04.202.A221). As no overt difference in tau pathology between aged male and female Tau22 mice is reported, mixed genders were used throughout the study. Mice were grouped according to genotype before random assignment to the experimental conduct. Researchers performing animal experiments were blinded to the genotype.

2.2.2 Tissue processing and histology

Aged animals (11 months old) were transcardially perfused with cold 1x phosphate-buffered saline (1x PBS, Applichem, Cat #2004367). The brains were dissected and fixed in 4% paraformaldehyde (PFA, Merck Millipore, Cat #P6148) for 24 hours at 4 °C. Afterwards, brains were put in a 30% sucrose (Sigma-Aldrich®, Cat #57-50-1) solution until the brains sank. Mouse brains were cut into 40 µM thick sections using a Leica CM3050S Cryostat and emerged in a cryoprotectant solution before storage at -20 °C. Immunohistochemistry on three serial sections per anatomical region per mouse brain was performed using a free-floating technique. Prior to the incubation with primary antibodies, sections were washed for three times five minutes in 1x PBS (Applichem, Cat #2004367) to wash out the cryoprotective solution. Epitope retrieval was performed using 10 mM citrate buffer (pH 6.0) (Carl Roth, Cat #3580.3) at 95 °C for 15 minutes without shaking. Sections were allowed to cool down at RT for 20 minutes before washing in PBS-

T (0.1 % Triton® X-100/PBS) for three times five minutes at RT. Blocking and permeabilization was performed by incubation with a blocking solution (10 % goat serum (Abcam, Cat#7841) in PBS-T) for one hour at RT. Sections were then incubated in primary rabbit anti-Iba1 (FUJIFILM Wako Shibayagi Cat #019-19741, RRID:AB_839504) (1:1000), rat anti-yH2AX (Millipore Cat# 05-636, RRID:AB_309864) (1:100) and mouse anti-lamin B1 (Proteintech Cat # 66095-1-Ig, RRID:AB_11232208) (1:500) antibodies in blocking solution at 4 °C overnight (ON). Sections incubated in blocking solution without primary antibody were used as a negative control. After washing, incubation in secondary antibodies goat anti-mouse AlexaFluor-488 (Thermo Fisher Scientific Cat# A-11001, RRID:AB_2534069) (1:500) and goat anti-rabbit AlexaFluor-594 (Thermo Fisher Scientific Cat# A-11012, RRID:AB_2534079) (1:500) was done for 90 minutes at RT. After the final washing step, ProLong™ Gold with 4′,6-diamidino-2-phenylindole (DAPI) (Invitrogen™, Cat #P36931) or DAPI (0.1 µg/mL) (Thermo Scientific, Cat #62247) was used as a mounting medium on SuperFrost® microscope slides (Thermo Fisher Scientific, Cat #12372098) with coverslips (24 x 60 mm, Menzel-Gläser, Cat #15628). Images were acquired using a Zeiss LSM900 microscope with a 40x oil objective and analyzed with ImageJ software version 2.0. A manual threshold was set and applied to all images. The nucleus was set as a region of interest (ROI). Intensity of lamin B1 and yH2AX inside the nucleus (ROI) was calculated by area * IntDen. Three images per section were captured close to the CA1 region by going from the posterior side (dentate gyrus) towards the anterior side (CA3). No other inclusion or exclusion criteria were applied.

2.2.3 Immunocytochemistry

After senescence induction, cells were washed with 1x PBS once and subsequently fixed in 4 % paraformaldehyde (PFA, Merck Millipore , Cat #P6148) dissolved in 1x PBS (PBS, Applichem, Cat #2004367) for 10 minutes at RT. After fixation, cells were washed three times for five minutes each with 1x PBS, before permeabilization with 1x PBS containing 0.1 % Triton® X-100 (Carl Roth, Cat #9036-19-5) (PBS-T) for 10 minutes at RT. Blocking was performed using PBS-T supplemented with 3 % bovine serum albumin (BSA, Rockland, Fraction V, Cat #BSA-1000) and 5 % goat serum (Abcam, Cat #ab7481) for 30 minutes at RT. The cells were incubated in primary antibodies rabbit anti-IBA1 (FUJIFILM Wako Shibayagi, Cat #019-19741, RRID:AB_839504) (1:1000), rat anti-CD11b (Bio-Rad,

Cat #MCA711, RRID:AB_321292) (1:250), mouse anti-yH2AX (Millipore, Cat #05-636, RRID:AB_309864) (1:100), rabbit anti-H3K9me3 (Abcam, Cat #ab8898, RRID:AB_306848) (1:200) and mouse anti-Parkin (BioLegend Cat# 808501, RRID:AB_2564744) (1:500) dissolved in blocking solution overnight at 4 °C. The following day, cells were washed in 1x PBS for three times five minutes followed by incubation in secondary antibodies goat anti-rabbit-AlexaFluor594 (Invitrogen™, Cat #A-11012, RRID:AB_2534079) (1:500), goat anti-mouse-AlexaFluor488 (Invitrogen™, Cat #A-11001, RRID:AB_2534069) (1:500) and goat anti-rat-AlexaFluor594 (Invitrogen™, Cat #A-11007, RRID:AB_10561522) (1:500) dissolved in blocking solution for one hour at RT.. After the last washing step (three times five minutes with 1x PBS), the cells were mounted using ProLong™ Gold with 4′,6-diamidino-2-phenylindole (DAPI) (Invitrogen™, Cat #P36931). A Zeiss Laser Scanning Microscope 900 (LSM 900) with a 40x oil objective was used to obtain Z-stack images. ImageJ/Fiji software version 2.0 was used to process acquired images. A manual threshold was set and applied to all images. Each complete nucleus within a field-of-view was defined as a region of interest (ROI). Intensity of yH2AX and H3K9me3 inside the nucleus (ROI) was calculated by area * IntDen. For measurements of Parkin intensity, the cell body as defined by a CD11b staining was set as ROI. Three to four images were captured in the mid-centre of the coverslip, which contained optimal cell density. No other inclusion or exclusion criteria were applied.

2.2.4 Primary microglia culture

Mixed glial cultures were prepared from the brains of P0-P3 wild-type (WT) and *Nlrp3*-knockout (*Nlrp3*$^{-/-}$) pups. Pups were sacrificed by decapitation before brains were taken out. After removing the meninges, the brains from the same genotypes were combined in a 50 ml tube and washed three times with Hanks' Balanced Salt Solution (HBSS; Gibco™, Cat #24020091) followed by incubation with 0.25 % trypsin (LIFE Technologies, Cat #15400054) for 10 minutes at 37 °C. After incubation, DNase I (Roche, Cat #11284932001) was added and a single cell suspension was generated by mechanical shearing using a 10 ml pipet before the cells were pelleted at 300 *xg* for five minutes. The supernatant was discarded and the cells were resuspended in an appropriate amount of Dulbecco's Modified Eagle Medium (DMEM; Gibco™, Cat #31966047) with 10 % Fetal Bovine Serum (FBS, Gibco™, Cat #26140079) and 5 U/ml penicillin–streptomycin

(Gibco™, Cat #15070063) (5 ml per two brains). Cells were then added to pre-coated T75 flasks containing 10 ml of DMEM with 10 % FBS and 5 U/ml penicillin-streptomycin per flask. Pre-coating of the T75 flasks was done using 8 ml of a 0.1% poly-L-lysine solution in 1x PBS (PLL, Merck Millipore, Cat #P1524) for at least 30 minutes at 37 °C to stimulate anchoring of cells in culture. The pre-coated T75 flasks were washed three times with Dulbecco‘s Phosphate-Buffered Saline (DPBS; Gibco™, Cat #14190169) before the cells were added to the flasks. The following day, the cells were gently washed with DPBS to get rid of cellular debris and supplemented with 10 ml DMEM containing 10 % FBS, 10 % L929 conditioned medium and 5 U/ml penicillin-streptomycin. Seven to ten days after cultivation, microglia were shaken at RT by tapping against the flasks multiple times by hand and confirming floating of the cells under the microscope, followed by counting and plating in DMEM (Gibco™, Cat #31966047) supplemented with 1x N2-Supplement (Gibco™, Cat #17502048) and 5 U/ml penicillin–streptomycin (Gibco™, Cat #15070063) overnight before treatment. Microglia were shaken off up to three times.

2.2.5 Primary microglia treatment

Plating of primary mouse microglia was done overnight in 6-well plates (1.3 x 10^6 cells/well) for immunoblotting and collection of conditioned medium (CM), in 12-well plates (5 × 10^5 cells/well) for RNA isolation, in 24-well plates for phagocytosis (3.5 × 10^5 cells/well) or migration assays (5 x 10^5 cells/well) and on 13 mm^2 coverslips in 24-well plates (1-1.5 x 10^5 cells/well) for immunocytochemistry and morphology analysis. The next day, cells were gently washed with DPBS (Gibco™, Cat #14190169) and treated with 5 or 15 nM of recombinant human wildtype (2N4R) tau for 18 hours. After treatment with tau, the cells were washed with DPBS again and cultured for another 48 hours in 500 µl (12- and 24-well plates) or 1 ml (6-well plates) of medium. As the dried tau proteins (see 2.2.10 for tau preparation) were directly dissolved in medium, the control treatment was performed using only medium. Cells were treated for one hour with 1 µM of CRID3 sodium salt (Tocris, Cat #5479) and/or 1 µM of the selective STAT3 inhibitor stattic (Tocris, Cat #2798) prior to senescence induction to block NLRP3 inflammasome and STAT3 activation. The cells received an additional stimulation with 1 µM CRID3 and/or stattic after withdrawal of tau (18 hours). Furthermore, a 72 hours treatment with 50 ng/ml of phorbol 12-myristate 13-acetate (PMA; Sigma-Aldrich®, Cat #16561-29-8) (diluted from stock in

medium) was included as a positive control. Overnight plating and treatments were performed in DMEM (Gibco™, Cat #31966047) supplemented with 1x N2-Supplement (Gibco™, Cat #17502048) and 5 U/ml penicillin–streptomycin (Gibco™, Cat #15070063). For each experiment, three (n=3) to four (n=4) biologically independent experiments were performed using three to four independently prepared mixed glia cultures for shaking off microglia. Individual wells were assessed in each independent experiment. No samples were pooled.

2.2.6 Western blotting

At the end of the experimental procedure, the microglia were washed with ice cold 1x PBS and lysed in appropriate volumes of 1x Radio-Immunoprecipitation Assay Lysis Buffer (RIPA) buffer (50 mM Tris-HCl, 1% Triton® X-100, 0.5% sodium deoxycholate, 0.1% sodium dodecyl sulfate (SDS) with protease/phosphatase inhibitor (Thermo Scientific™, Cat #78441). Cells were scraped off and transferred to a 1.5 ml tube on ice for 30 minutes and vortexed a few times in between. Afterwards, samples were centrifuged at 20,000 *xg* for 15 minutes at 4 °C. Protein quantification was performed using a BCA Protein Assay Kit (Thermo Scientific™, Cat #23225) according to the manufacturer's instructions on the supernatants containing the soluble proteins. For immunoblotting, samples were supplemented with a selfmade 1x LDS Sample Buffer (see *section 2.1.6* for composition) that is based on the NuPAGE™ sample buffer (Thermo Scientific™, Cat #R1381) and heated for five minutes at 95 °C. A total of 25 µg protein per sample were loaded on 4–12 % NuPAGE™ gels with ten wells (Thermo Scientific™, Cat # NP0321BOX), 15 wells (Thermo Scientific™, Cat #NP0323BOX) or 20 wells (Thermo Scientific™, Cat #WG1402BOX). Running of the gels was performed using 1x MES SDS running buffer (Invitrogen™, Cat #NP0002) with 150V and 300 mA for 90 minutes using the Power Supply EV3020 (Carl Roth). Transfer of proteins was done using a Trans-Blot® Turbo™ transfer pack (BIO-RAD, Cat #1704158 and Cat #1704159) according to the manufacturer's instructions. After protein transfer, the membranes were blocked for one hour in 3 % Bovine Serum Albumin (BSA) (Rockland, Fraction V, Cat #BSA-1000) in Tris-buffered saline supplemented with Tween-20 (TBS-T; 10 mM Tris-HCl, 150 mM NaCl, 0.05 % Tween-20, pH 8.0), followed by incubation in primary antibodies rabbit anti-p21 (Abcam, Cat #ab218311, RRID:AB_2890611) (1;1000), rabbit anti-p16 (Abcam, Cat

#ab211542, RRID:AB_2891084) (1:1000), mouse anti-lamin B1 (Proteintech, Cat #66095-1-Ig, RRID:AB_11232208) (1:1000), mouse anti-caspase-1 (AdipoGen Cat #AG-20B-0042, RRID:AB_2490248), mouse anti-STAT3 (Abcam Cat #ab119352, RRID:AB_10901752) and rabbit anti-pSTAT3 (Abcam Cat #ab76315, RRID:AB_1658549) in blocking solution at 4 °C overnight. Incubation in primary rabbit anti-GAPDH antibody (Sigma-Aldrich®, Cat #G9545, RRID:AB_796208) (1:5000) was done in blocking solution for one hour at RT. After incubation in primary antibodies, the membranes were washed three times five minutes in TBS-T, before incubation in fluorescently-tagged secondary antibodies (LI-COR® Biosciences). Protein expression was visualized using a LI-COR ODYSSEY® CLx (LI-COR® Biosciences). ImageStudio™ software version 5.2.5 (LI-COR® Biosciences) was used to analyze the data. The intensity of GAPDH per condition per experiment was used as a reference to normalize the protein levels of the respective conditions. Next, the normalized protein value obtained per condition per experiment was then normalized to the averaged value obtained for control-treated microglia or WT mice. PageRuler™ Prestained Protein Ladder (Thermo Fisher Scientific, Cat #26616) was used as a molecular weight marker.

2.2.7 ELISA and mesoscale

Conditioned medium (CM) was collected from the cells that were plated in 6-well plates and subsequently used for western blot analysis. The CM was centrifuged at 300 *xg* for five minutes at 4 °C to remove cellular debris. The undiluted CM was used to determine the concentration of pro-inflammatory factors using the Mouse IL-1 beta/IL-1F2 DuoSet ELISA (R&D Systems, Cat #DY401), Mouse IL-6 DuoSet ELISA (R&D Systems, Cat #DY406), V-PLEX Plus Proinflammatory Panel 1 Kit (Meso Scale Diagnostics, Cat #K15048G-1), V-PLEX Cytokine Panel 1 Mouse Kit (Meso Scale Diagnostics, Cat #K15245D-1) and V-PLEX Mouse Cytokine 19-Plex Kit (Meso Scale Diagnostics, Cat #K15255D-1) according to the manufacturer's recommendations. CM of at least three (n=3) biologically independent experiments (e.g., at least three independent cell culture preparations were run on the same plate.

2.2.8 RNA isolation, cDNA synthesis and real time qRT-PCR

To isolate RNA of primary cultured microglia, the conditioned medium (CM) was discarded and cells were washed with 1x PBS before adding 700 µl QIAzol™ Lysis Reagent (Qiagen, Cat# 79306) to the cells. Cells were scraped off and transferred to a 1.5 ml tube. The homogenate was incubated for five minutes at RT, followed by addition of 125 µl chloroform (Carl Roth, Cat #3313.1). Samples were shaken vigorously and centrifuged for 15 minutes at 12,000 *xg* at 4 °C. The aqueous phase was collected for RNA isolation using a miRNeasy Micro Kit (Qiagen, Cat #217084) according to the manufacturer's instructions. RNA concentration and purity were quantified spectrophotometrically using the Nanodrop 2000c (Thermo Fisher Scientific). 400 nanograms (ng) of total RNA were reverse transcribed in a total volume of 20 µl using the High-Capacity cDNA Reverse Transcription Kit (Applied Biosystems™, Cat #4368814). The cDNA was amplified in TaqMan gene expression master mix (Applied Biosystems™, Cat #4369016) with predeveloped TaqMan assays and reagents in a 96-well plate according to the manufacturer's instructions. Reactions were carried out using primer sets for *Cdkn1a* (Applied Biosystems™, Mm00432448_m1), *Cdkn2a* (Applied Biosystems™, Mm00494449_m1), *Lmnb1* (Applied Biosystems™, Mm00521949_m1), *Il-1b* (Applied Biosystems™, Mm00434228_m1), *Il-6* (Applied Biosystems™, Mm00446190_m1), *Cxcl1* (Applied Biosystems™, Mm04207460_m1) and 18S rRNA (Applied Biosystems™, Cat #4310893E), which was used as a loading control for all reactions. The qPCR run as well as the subsequent analyses were performed using the RT-PCR System StepOnePlus™ together with the StepOne™ software (both from Applied Biosystems™). Transcript levels were quantified by the comparative $\Delta\Delta C_T$ method.

2.2.9 Isolation of adult mouse microglia

Adult mouse hippocampi were removed from transcardially perfused mice (see section 3.2.2) and transferred to gentleMACS C tubes (Miltenyi Biotec, Cat #130-093-237) with enzymes supplied by the MACS Adult Brain Dissociation Kit (Miltenyi Biotec, Cat #130-107-677). The gentleMACS C were attached to the gentleMACS Octo Dissociator (Miltenyi Biotec, Cat #130-096-427) for dissociation. Samples were applied to a MACS SmartStrainer (70 µM) (Miltenyi Biotec, Cat #130-098-462) to obtain uniform single-cell suspensions. Debris and Red Blood Cell Removal Solutions (supplied) were added to the

cell suspension and microglia were extracted using magnetically labeled CD11b MicroBeads (Miltenyi Biotec, Cat #130-126-725) and a MACS Separator with LS columns (Miltenyi Biotec, Cat #130-042-401) to elute the negative fraction and collect the CD11b positive cells. 700 µl QIAzol Lysis Reagent (Qiagen, Cat #79306) was added to the isolated adult microglia and kept in -20 °C before RNA was extracted as described under 2.2.8.

2.2.10 Preparation of recombinant human tau

Recombinant human wildtype tau (2N4R) was cloned into pRK172 and the purification was performed as described previously (Ising et al., 2019). Tau-expressing inducible plasmids were transformed into BL21(DE3) *E. coli* (Agilent, Cat #230245). First, 10 ng plasmid was mixed with 50 µl bacteria and incubated on ice for 30 minutes. Afterwards, heatschock at 42 °C for 45 seconds was applied to the mixture, followed by two minutes incubation on ice. Next, 900 µl SOC medium was added and the bacteria were incubated at 37 °C while shaking at 250 rpm for one hour. Bacteria were resuspended and spread on a pre-warmed (37 °C) LB-agar plate with 0.1 mg/ml ampicillin. The LB-agar plate containing bacteria was then incubated upside down at 37 °C overnight to grow single colonies. The following day, a single colony was picked and grown in 5 ml LB medium supplemented with 0.1 mg/ml ampicillin overnight on a shaker at 37 °C. The next day, the bacteria were equally divided into 500 ml baffeled beakers with 250 ml LB supplemented with 0.1 mg/ml ampicilin and incubated for apprixmately two to three hours at 37 °C to grow larger cultures. Optical density 600 (OD600) was measured in between until the desired level was reached (OD 0.5-0.6). Tau expression was induced by adding 0.6 mM IPTG (Merck Millipore, Cat# I6758) to each 500 ml flask for three hours at 37 °C. Bacteria containing tau were centrifuged at 3810 *xg* for ten minutes at 4 °C using an Avanti centrigure, followed by resuspension of the pellet in 15 ml BRB-80 (80 mM PIPES, 1 mM magnesium sulfate, 1 mM EGTA, pH 6.8) supplemented with 0.1 % 2-mercapthoethanol and 1 mM PMSF. The resuspended pellet was transferred to a 50 ml tube and sonicated at 80 % power (four cycles of one minute with two minutes on ice in between). Bacterial debris were removed by centrifugation for 20 minutes at 3810 *xg* at 4°C. The tau-containing supernatant was boiled for 10 minutes and centrifuged again for 15 minutes at 3810 *xg*. Enrichment of the tau protein was done by cation exchange chromatography

using sepharose fast flow beads (Merck Millipore, Cat #GE17-0729-01). Afterwards, different concentrations of sodium chloride dissolved in BRB-80 supplemented with 0.1 % 2-mercaptoethanol were used to elute tau. A Coomassie gel stain was used to test the presence of tau and tau-containing fractions were combined and concentrated in 10 mM ammonium bicarbonate buffer using Amicon ultra centrifugal units (10-kDa molecular weight cut-off, Merck Millipore, Cat #UFC9010). The prepared tau preparation was tested for the presence of endotoxins using an endotoxin quantification kit (Thermo Fisher Scientific, Cat #A39552S). The concentration of tau was assessed by a BCA assay (Thermo Fisher Scientific, Cat #23225) according to the manufacturer's instructions before aliquoting. Tau samples were dried in a speed vac before storage at -80 °C. Tau proteins were resuspended in DMEM supplemented with 1x N2-Supplement and 5 U/ml penicillin–streptomycin right before use.

2.2.11 Fluorescent labeling of recombinant human tau

Purified recombinant tau was reconstituted in DPBS (Gibco™, Cat #14190169) to a final concentration of 8 µM. Afterwards, the reconstituted recombinant tau was incubated with 0.025 mg Alexa Fluor™ 405 NHS ester (Thermo Fisher Scientific, Cat #A30000) for one hour at RT followed by shaking at 4 °C overnight. The following day, glycine was added to the solution to a final concentration of 100 mM and incubated for one hour at RT. The solution was dialyzed for two times two hours in 1x PBS at RT using a 10 K MWCO Slide-A-Lyzer™ dialysis cassette (Thermo Fisher Scientific, Cat #66383). Labeled tau was aliquoted in protein low-binding tubes (Eppendorf™, Cat #0030108116) and stored at -80 °C before use.

2.2.12 Tau clearance assay

After senescence induction (e.g., tau exposure and recovery), microglia were treated with 200 nM AlexaFluor-405-labeled tau monomers dissolved in DMEM (Gibco™, Cat #31966047) supplemented with 1x N2-Supplement (Gibco™, Cat #17502048) and 5 U/ml penicillin–streptomycin (Gibco™, Cat #15070063) and incubated for 30 or 60 minutes. Tau uptake was stopped by washing the cells with 1x PBS to remove free tau and cells were collected using 0.5 % trypsin (Thermo Fisher Scientific, Cat #15400054). Afterwards, the cells were incubated in a blocking solution containing 1x PBS and FCS (Gibco™, Cat

#10500064) (1:1 ratio) for 10 minutes on ice, followed by incubation in allophycocyanin anti-mouse/human CD11b antibody (BioLegend Cat #101212, RRID: AB_312795) (1:100) for 30 minutes in FACS buffer (1x PBS supplemented with 2 % FCS) on ice. After incubation, cells were collected and resuspended in 300 µl ice-cold FACS buffer before measurement by flow cytometry using the FACSCanto™ II and the FACSDiva™ software (Becton Dickinson, Heidelberg, Germany). FlowJo™ software (v3.05470; Ashland, OR) was used to analyze tau uptake and clearance in CD11b-positive cells. Experiments were performed with support from Dr. Hannah Scheiblich, Institute of Innate Immunity, Bonn.

2.2.13 Morphology analysis

After senescence induction, the cells were washed with 1x PBS, followed by fixation in 4 % PFA. Afterwards, cells were washed in in PBS-T for three times five minutes and stained with Alexa Fluor™ 647 Phalloidin (Invitrogen™, Cat #A22287, RRID: AB_2620155) (1:100) and DAPI (Thermo Scientific™, Cat #62247) (0.1 µg/mL) for 30 minutes in PBS-T. Mounting of the cells was done using Epredia™ Immu-Mount™ mounting medium (Thermo Fisher Scientific, Cat #9990402) and images were taken using a Nikon ECLIPSE Ti fluorescence microscope equipped with a 20x objective. A total of five images per condition were taken, with an estimate of 20 cells per image per condition. A total of three independent cell culture preparations (n=3) were used for this experiment. CellProfiler (v3.1.8, Broad Institute of Harvard and MIT, MA, USA) was used to analyze the images (Kamentsky et al., 2011). The final analysis was performed by Dr. Hannah Scheiblich, Institute of Innate Immunity, Bonn .

2.2.14 Migration assay

The migration assay was based on the method of Liang and colleagues (Liang et al., 2007). After senescence induction, a pipet tip was used to create a scratch in the confluent cell monolayer. This was followed by a washing step in 1x PBS and subsequent incubation in 500 µl DMEM (Gibco™, Cat #31966047) supplemented with 1x N2-Supplement (Gibco™, Cat #17502048) and 5 U/ml penicillin–streptomycin (Gibco™, Cat #15070063) for 8 hours before images were acquired using a Nikon ECLIPSE Ti brightfield microscope (10x) at desired times in a marked sector as reference area. Migration was calculated by dividing scratch widths measured before and after incubation, quantified at 20 distinct

locations within the reference area. ImageJ/Fiji software version 2.0 was used to analyze the images. Imaging and analysis was performed by Dr. Hannah Scheiblich, Institute of Innate Immunity, Bonn.

2.2.15 Protein precipitation

To measure cleavage of caspase-1 in the supernatants, 500 µl ice-cold methanol (Merck Millipore, Cat #107018) and 125 µl ice-cold chloroform (Carl Roth, Cat #3313.1) was added to 500 µl conditioned medium. Samples were vortexed and centrifuged at 13,000 *xg* for five min at 4°C. The aqueous phase was discarded and 500 µl Methanol (Merck Millipore, Cat #107018) was added to the protein phase and vortexed vigorously. Another centrifugation was performed and the supernatant removed. The pellet was dried and resuspended in 20 µl (2x) Western Blot loading buffer. Denaturing of samples was done at 95°C for five minutes using a ThermoShaker.

2.2.16 Cytotoxicity assay (LDH)

Cellular cytotoxicity was measured in a 96-well plate containing 50 µl supernatants using the cytotoxicity detection kit (LDH) (Roche, Cat #11644793001) according to the manufacturer's protocol. To stop the reaction, 25 µl 1 M HCl (Carl Roth, Cat #9277.1) was added to the wells and absorbance was measured at 490 and 680 nm using a microplate reader (Infinite M200; Tecan).

2.2.17 Statistical analysis

At least three independent primary cell culture preparations (n) were used for each experiment. Data were analyzed with Graph Pad Prism (version: 9.4.1 (681)) and are shown as mean + SD for parametric data or median ± 95% CI for non-parametric data of at least three biologically independent cell culture preparations (*n*). Normal distribution of the data sets was evaluated using Shapiro-Wilk test and outliers were identified using the ROUT (Q = 1%) method. Statistical significance for parametric data was analyzed by one-way ANOVA with post hoc Tukey’s test and for non-parametric data, Kruskal-Wallis test with post hoc Dunn’s test or unpaired t-test (two-tailed) with Mann-Whitney test was applied. Statistical significance was assumed for $p<0.05$. Statistical details for all figures can be found at the end of the dissertation (see section *11. Statistical details*)

3 Results

3.1 Microglial senescence in the hippocampus of aged Tau22 mice

3.1.1 Reduced expression of lamin B1 in microglia in the stratum radiatum close to the CA1 region of Tau22 mice

Histopathological findings in the brain of AD patients revealed features of senescent rather than activated microglia, which colocalized with tau-positive structures and preceded the spread of tau (Streit et al., 2009). A decade later, research demonstrated that the formation of senescent microglial precedes the onset of neurofibrillary tangle (NFT) deposition in the brains of PS19 mice (Bussian et al., 2018). Here, we aimed to investigate the presence of senescent microglia in another tauopathy mouse model, called Tau22. Tau22 mice show progressive accumulation of pathological tau species including but not restriced to the CA1 region of the hippocampus, which starts at 6 months (middle-aged) and reaches a full tau pathology spectrum at 12 months of age (aged) (Schindowski et al., 2006b). Within the CA1 region, many microglia can be found within the stratum radiatum, from where they are extending their processes also towards the neuronal, tau aggregate-containing cell bodies in the stratum pyramidale of the CA1 (Ising et al., 2019). Hence, we postulated an increased number of senescent microglia in the stratum radiatum of the CA1 region of aged Tau22 mice in comparison to age-matched wildtype mice (WT).

Downregulation of nuclear lamin B1 is a hallmark of cellular senescence (Freund et al., 2012; Saito et al., 2019). Remarkably, a decline in neuronal lamin B1 levels was observed in post-mortem human brain tissue of AD and frontotemporal dementia (FTD) patients (Frost et al., 2016; Paonessa et al., 2019). In addition, a downregulation of lamin B1 was found in senescent astrocytes in the context of PD (Chinta et al., 2018). However, it remains to be elucidated whether lamin B1 levels are altered in microglia in the context of tauopathies. To this end, we first investigated the expression of lamin B1 in microglia in the stratum radiatium close to the CA1 cell body region of aged (11 months) Tau22 mice using immunofluorescent stainings. Our findings demonstrate a decline in the immunoreactivity of nuclear lamin B1 in microglia in the stratum radiatum close to the CA1 cell body region of Tau22 mice in comparison to WT mice (Fig. 4).

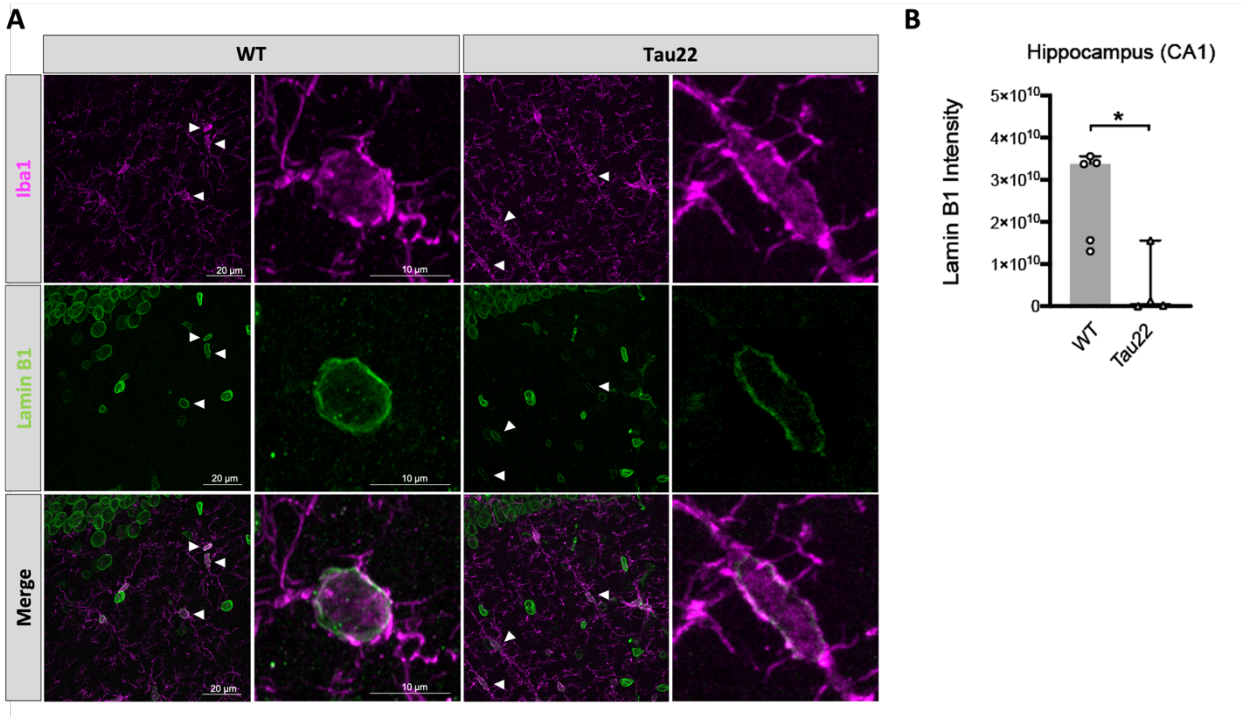

Fig. 4: Loss of microglial lamin B1 in the stratum radiatum close to the CA1 cell body region of Tau22 mice. **A.** Representative immunohistochemical staining for lamin B1 (green) and ionized calcium-binding adapter molecule 1 (Iba1; magenta) in WT and Tau22 mice at 11 months of age. **B**. Quantification of lamin B1 in microglia of WT (n=5) and Tau22 (n=4) mice shown in A. Graph is presented as median + 95% confidence interval (CI) and analyzed by non-parametric unpaired (two-tailed) Mann-Whitney test (**P*=0.0317). ROUT test (Q = 1%) showed no outliers. Shapiro-Wilk normality test was violated. No exclusion criteria were pre-determined and no samples were excluded from the analysis. Arrow heads indicate the expression of lamin B1 in microglia.

3.1.2 Microglia in the stratum radiatum close to the CA1 cell body region of Tau22 mice showed accumulation of yH2AX foci

Phosphorylation of H2AX (yH2AX) is another widely accepted marker of senescence. Prolonged exposure to stress might result in the formation of yH2AX in response to double-strand breaks (DSBs) that promote a DNA damage response (DDR). This mechanism is initiated in order to avoid the propagation of damaged DNA into daughter cells by promoting cell cycle arrest. Upon proper repairment of DSB, however, the cells resume normal proliferation. But, when the cells are unable to initiate proper repairment, for example during chronic activation of the DDR, it might result in a permanent cell cycle arrest and subsequently cellular senescence (Kumari and Jat, 2021; Mah et al., 2010). Interestingly, increased yH2AX has been observed in post-mortem brains of AD patients as well as tau transgenic mice (Farmer et al., 2020; Musi et al., 2018). In addition,

expression of yH2AX in the brains of PS19 mice correlated with increased cell cycle arrest, brain atrophy and NFT formation (Musi et al., 2018). Given this finding and our previous observation on the loss of lamin B1 in Tau22 mice (Fig. 4), we sought to address whether microglia in the stratum radiatum close to the CA1 cell body region of Tau22 mice also present with double-strand breaks, characterized by yH2AX. Here, we found that microglia in this particular region of Tau22 mice showed a significant increase in yH2AX in comparison to WT mice (Fig. 5).

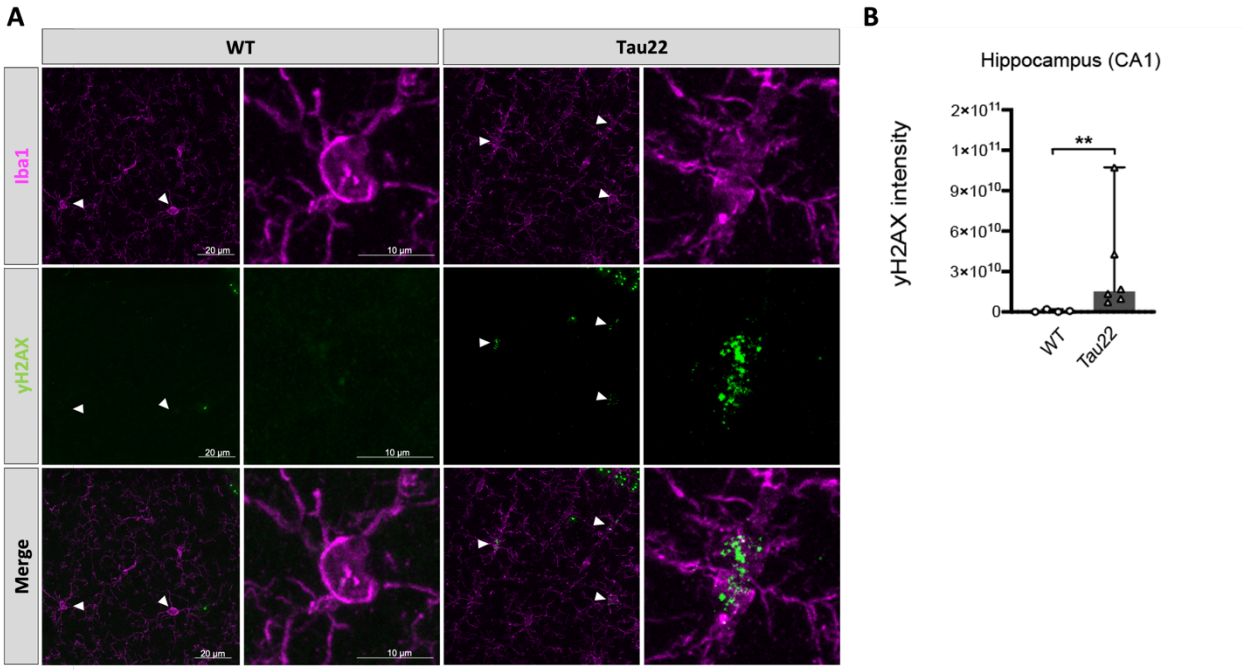

Fig. 5: Increased expression of phosphorylated H2AX (yH2AX) in microglia in the stratum radiatum close to the CA1 cell body region of Tau22 mice. **A**. Representative immunohistochemical staining for yH2AX (green) and Iba1 (magenta) in WT and Tau22 at 11 months of age. **B**. Quantification of yH2AX in microglia of WT (n=4) and Tau22 (n=6) mice shown in A. Graph is presented as mean + 95% CI and analyzed by non-parametric unpaired (two-tailed) Mann-Whitney test (***P*=0.0095). **C**. ROUT test (Q = 1%) showed no outliers. Shapiro-Wilk normality test was violated. No exclusion criteria were pre-determined and no samples were excluded from the analysis. Arrow heads indicate the expression of yH2AX in microglia.

3.1.3 NLRP3 deficiency in Tau22 mice normalized the levels of lamin B1 in microglia in the stratum radiatum close to the CA1 cell body region

Aging is accompanied by a decline in immune efficacy, contributing to age-related inflammatory diseases (Aiello et al., 2019). The term inflammaging has been described previously and is closely linked to immunosenescence, a phenomenon that describes the

progressive deterioration of the immune system with age (Aiello et al., 2019; Aw et al., 2007; Sebastian-Valverde and Pasinetti, 2020). Studies trying to decipher the link between aging and immunosenescence point towards the NLRP3 inflammasome as a potential mediator (Sebastian-Valverde and Pasinetti, 2020; Spadaro et al., 2016). While activation of the NLRP3 inflammasome has been implicated in tauopathies (Ising et al., 2019), its role in (immuno)senescence in tauopathies is unknown. To monitor the effect of the NLRP3 on microglial senescence *in vivo*, we first performed an immunostaining against lamin B1 in Tau22 mice crossed to *Nlrp3*-knockout mice (Tau22/*Nlrp3*$^{-/-}$). In line with our previous results, we observed a significant decrease in lamin B1 in microglia close to the CA1 cell body region of Tau22 compared to WT mice (Fig. 6 A, B). Strikingly, Tau22 mice with a deficiency in the NLRP3 inflammasome showed normalization of lamin B1 levels in microglia close to the CA1 cell body region (Fig. 6 A, B).

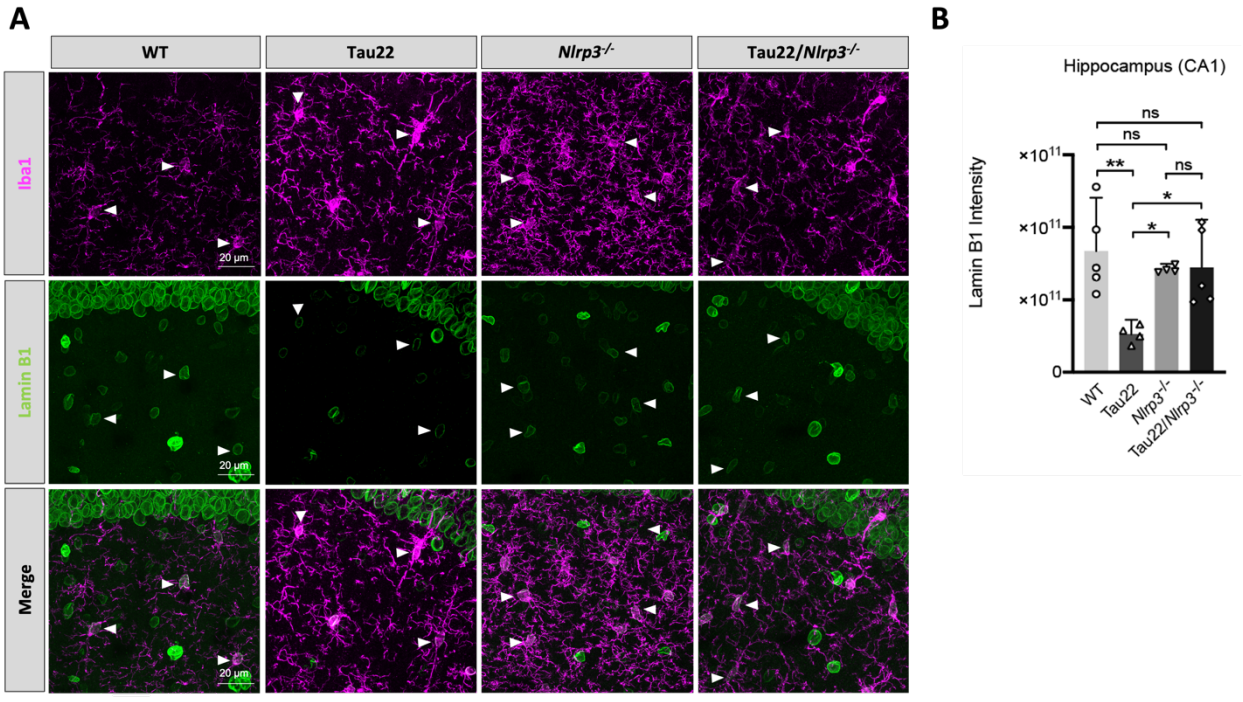

Fig. 6: NLRP3 deficiency prevented loss of lamin B1 in microglia in the stratum radiatum close to the CA1 cell body region of Tau22 mice. **A.** Representative immunohistochemical staining for lamin B1 (green) and Iba1 (magenta) in 11 months old WT, Tau22, *Nlrp3*$^{-/-}$ and Tau22/*Nlrp3*$^{-/-}$ mice. **B**. Quantification of lamin B1 in microglia (WT, n=5; Tau22, n=4, *Nlrp3*$^{-/-}$, n=4; Tau22/*Nlrp3*$^{-/-}$, n=5). Graph is represented as mean + SD and analyzed by one-way ANOVA with Tukey's test **F**: F (3,14) = 5.830, *P* = 0.0084. Statistical significance is presented as **P*<0.05 and ***P*<0.01. ns = not significant, exact *P* values are shown in *section 11, table 6 B*. Arrow heads indicate the expression of lamin B1 in microglia. ROUT

test (Q = 1%) showed no outliers. Shapiro-Wilk normality test was not violated. No exclusion criteria were pre-determined and no samples were excluded from the analysis.

3.1.4 Isolated adult hippocampal microglia from NLRP3 deficient mice exhibit a non-senescent gene expression profile

Microglia in the temporal cortex of AD patients demonstrated a significant increase in the mRNA expression of markers associated with senescence, including *Cdkn2a*, *Il-1b* and *Il-6* (Hu et al., 2021). Similarly, an elevation of these markers was observed in the cortices and hippocampi of PS19 mice and both regions were marked by substantial tau pathology at the analyzed age (Bussian et al., 2018). Given these findings, we wanted to confirm increased mRNA expression of markers associated with senescence in isolated adult hippocampal microglia from Tau22 mice, the region mainly affected by tau pathology in this tauopathy model. In addition, we aimed to explore the contribution of the NLRP3 inflammasome to the senescent gene expression profile in isolated adult hippocampal microglia. Surprisingly, isolated adult hippocampal microglia from 11-month-old Tau22 mice showed no increase in *Cdkn1a* gene expression levels compared to isolated adult hippocampal microglia from age-matched WT mice (Fig. 7 B). However, our data demonstrated that isolated adult hippocampal microglia from 11-month-old Tau22 mice (Fig. 7 A) showed a significant increase in *Cdkn2a* (Fig. 7 C), *Il-1b* (Fig. 7 D) and *Il-6* (Fig. 7 E) gene expression levels compared to isolated adult hippocampal microglia from age-matched WT mice. In addition, we observed an increased gene expression of *Cxcl1* (Fig. 7 F), which is one of the well-documented factors of the SASP (Rodier et al., 2009). Strikingly, Tau22 mice with a NLRP3 deficiency showed a significant reduction in *Cdkn2a* (Fig. 7 C), *Il-1b* (Fig. 7 D), *Il-6* (Fig. 7 E) and *Cxcl1* (Fig. 7 F) gene expression levels as compared to Tau22 mice. Deficiency in NLRP3 did not affect the gene expression levels of *Cdkn1a* (Fig. 7 B).

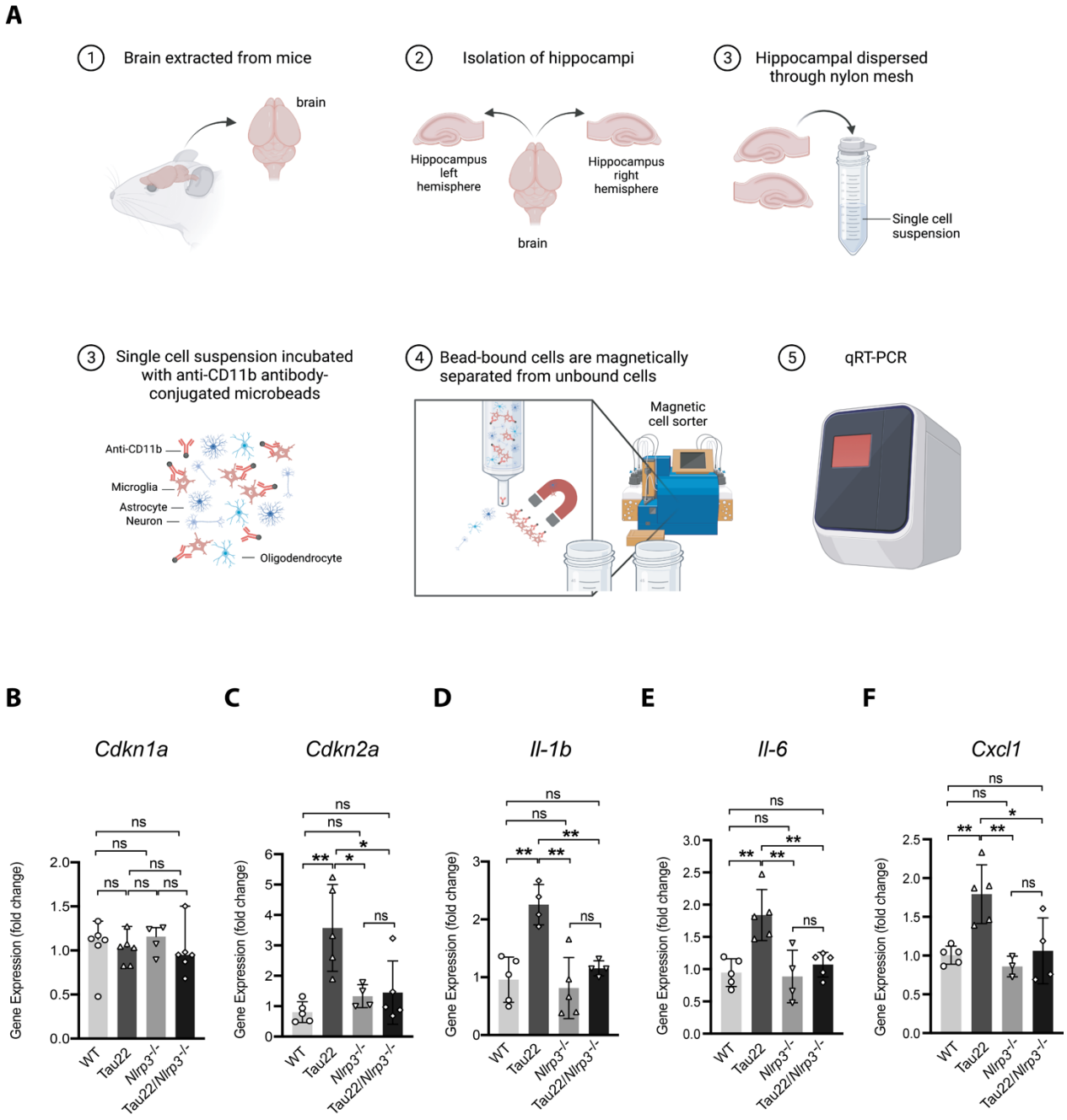

Fig. 7: Isolated adult hippocampal microglia from NLRP3 deficient Tau22 mice show a reduced expression of senescence-associated genes. **A.** Experimental setup of microglia isolation from the hippocampi of 11-month-old mice. **B-F.** Gene expression analysis of *Cdkn1a* **(B;** WT (n=6), Tau22 (n=6), *Nlrp3*$^{-/-}$ (n=4), Tau22/*Nlrp3*$^{-/-}$ (n=5)**)**, *Cdkn2a* **(C;** WT (n=5), Tau22 (n=5), *Nlrp3*$^{-/-}$ (n=4), Tau22/*Nlrp3*$^{-/-}$ (n=5)**)**, *IL-1b* (**D;** WT (n=5), Tau22 (n=4), *Nlrp3*$^{-/-}$ (n=5), Tau22/*Nlrp3*$^{-/-}$ (n=4)**)**, *Il-6* **(E;** WT (n=5), Tau22 (n=5), *Nlrp3*$^{-/-}$ (n=4), Tau22/*Nlrp3*$^{-/-}$ (n=5)**)** and *Cxcl1* (**F;** WT (n=5), Tau22 (n=5), *Nlrp3*$^{-/-}$ (n=3), Tau22/*Nlrp3*$^{-/-}$ (n=4)**)**. Data are represented as mean + SD and analyzed by one-way ANOVA with Tukey's test (**C:** F (3,15) = 8.309, *P* = 0.0017, **D**: F (3,14) = 11.89, *P*=0.0004), **E:** F (3,15) = 9.751, *P* = 0.0008 and **F:** F (3,13) = 8.485, *P* = 0.0022) or as median + 95% CI and analyzed by non-parametric Kruskal-Wallis test (**B:** *Cdkn1a*: Kruskal-wallis test = 2.466, *P*=0.4814). Statistical significance is presented as **P*<0.05 and ***P*<0.01. ns = non

significant. Exact *P* values are shown in *section 11, table 7 B-F* No exclusion criteria were pre-determined and no samples were excluded from the analysis

3.2 The effect of monomeric tau on the induction of microglial senescence: a cellular model

3.2.1 Microglia showed a senescent-like phenotype after tau exposure

Tau monomers transit into an oligomeric state before the formation of tau fibrils and eventually NFTs (Mamun et al., 2020). Strikingly, NFT-containing neurons are able to survive for decades (Morsch et al., 1999), suggesting that the pre-aggregated tau peptides are more toxic. Indeed, evidence points out that tau monomers and oligomers are associated with neuroinflammation (Gaikwad et al., 2021; Ising et al., 2019; Jin et al., 2021; Nilson et al., 2017). Although, it was demonstrated that microglia show features of senescence after phagocytosis of tau-aggregate bearing neurons (Brelstaff et al., 2021), the role of pre-aggregated tau peptides, such as monomers, on the induction of microglial senescence remain unclear. Since monomeric tau has been detected in the extracellular space (Yamada et al., 2011), the aim of the following experiments was to investigate the effect of monomeric tau on the induction of microglial senescence *in vitro*.

To begin with, we treated primary murine microglia for 18 hours with different concentrations of recombinant human tau monomers ranging from 0 (=control) over 5, 15 and 20 nM tau. After 18 hours, the medium was replaced with fresh medium and the cells incubated for another 48 hours. As microglia treated with 20 nM tau were found to detach from the cell culture plate during the incubation time, this concentration was excluded from the following analyses. We then investigated classical senescence markers at both mRNA and protein level in cells exposed to 5 and 15 nM of tau. We observed that exposure to 15 nM of tau increased the mRNA levels of *Cdkn2a* (Protein name: $p16^{INK4a}$) compared to control and 5 nM tau conditions (Fig. 8 A), but neither 5 nM nor 15 nM of tau altered the mRNA expression of *Cdkn1a* (Fig. 8 B) (Protein name: $p21^{WAF1}$) or *Lmnb1* (Protein name: lamin B1) (Fig. 8 C). In contrast, we found that microglia express increased protein levels of $p16^{INK4a}$ and $p21^{WAF1}$ independent of the tau concentration (Fig. 8 D-F). But interestingly, only exposure to 15 nM tau resulted in loss of lamin B1 at the protein level (Fig. 8 G).

To rule out that treatment with monomeric tau resulted in microglial cytotoxicity, we performed a cytotoxicity assay (LDH) on the conditioned medium after treatment (18 hours) and recovery (66 hours) (Fig. 8 H). Our results demonstrate that our selected treatment strategy did not result in microglial cytotoxicity (Fig. 8 H).

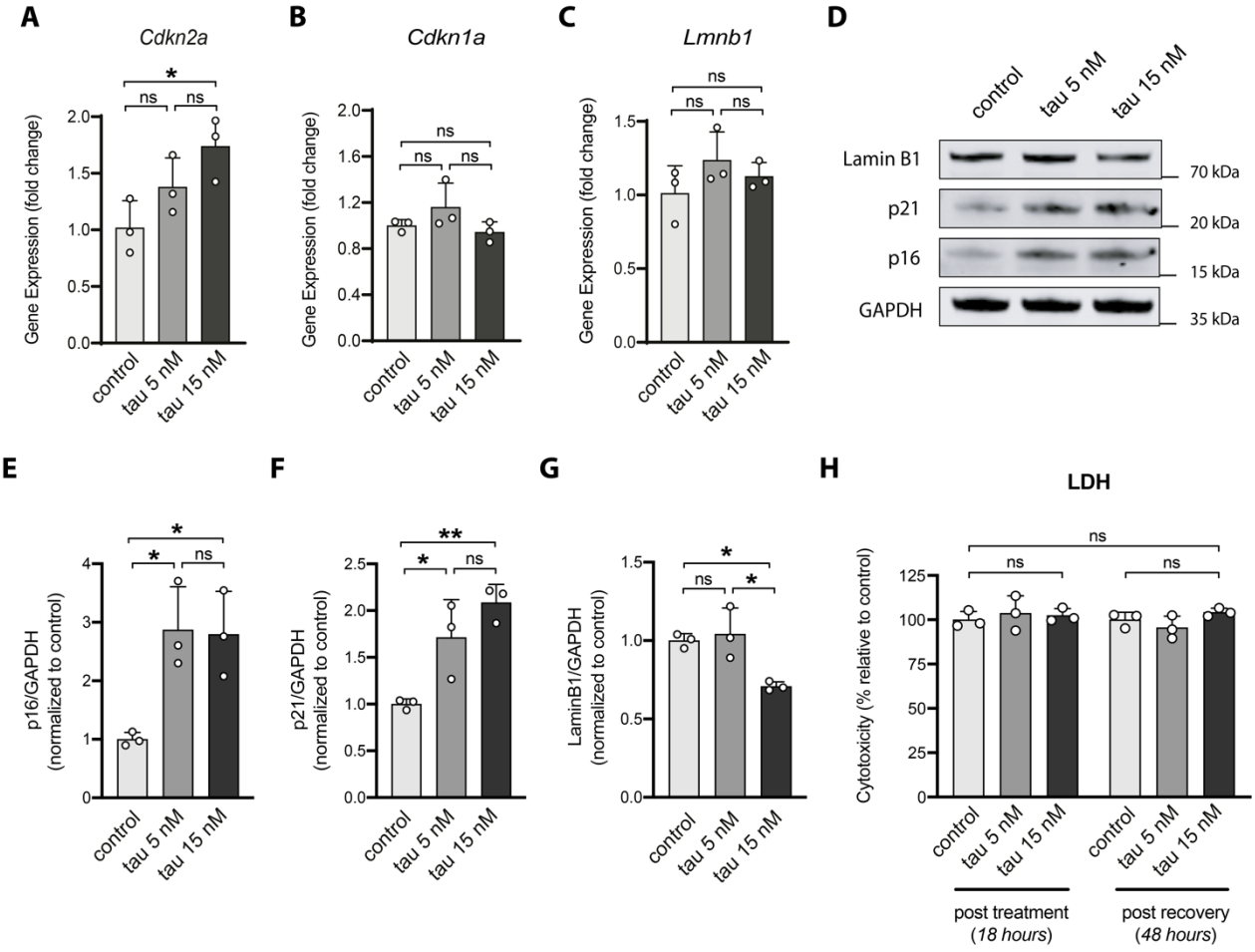

Fig. 8: Exposure to monomeric tau increased protein expression of $p16^{INK4a}$ and $p21^{WAF1}$ and induced loss of lamin B1 in murine primary microglia. **A.** *Cdkn2a* ($p16^{INK4a}$), **B.** *Cdkn1a* ($p21^{WAF1}$) and **C.** *Lmnb1* mRNA levels after exposure to monomeric tau. **D.** Immunoblot representing lamin B1, $p21^{WAF1}$, $p16^{INK4a}$ and GAPDH in murine primary microglia after exposure to tau monomers. **E-G.** Immunoblot quantification of $p16^{INK4a}$ (**E.)** $p21^{WAF1}$ (**F.**) and lamin B1 (**G.**) shown in D. **H.** Quantification of microglial cytotoxicity as a result of lactate dehydrogenase (LDH) release in the conditioned medium after exposure to monomeric tau at post treatment (18h) and post recovery (48h). Data are represented as mean + SD and analyzed by one-way ANOVA (**A:** F (2,6) = 5.791, *P*=0.0397; **B:** F (2,6) = 2.135, *P*=0.1994; **C:** F (2,6) = 1.422, *P*=0.3122; **E:** F (2,6) = 9.187, *P*=0.0149; **F:** F (2,6) = 13.49, *P*= 0.0060; **G:** F (2,6) = 9.879, *P*=0.0126) or as mean + SD and analyzed by two-way ANOVA (**H**: F (5,10) = 0.8804, *P*=0.5279 with multiple comparisons regardless of rows and columns) followed by Tukey's test. Significance is presented as **P*<0.05 and

**P<0.01. ns = not significant, n=3 independent cell culture preparations. Exact P values are shown in *section 11, table 8 A-C and 8 E-G.* No outliers were detected using ROUT test (Q = 1%). No exclusion criteria were pre-determined and no samples were excluded from the analysis. Adapted from (Karabag et al., 2023).

3.2.2 Characterization of a microglial SASP

Noteworthy, cell cycle arrest does not necessarily represent senescence since increased expression of $p16^{INK4a}$ and $p21^{WAF1}$ can also be observed during other states of cell cycle arrest, including quiescence (Terzi et al., 2016; Blagosklonny, 2011). However, one of the differences between senescent cells and quiescent cells is that senescent cells are additionally characterized by the secretion of a SASP, which might contribute to tissue damage and degeneration seen during aging and age-related diseases (Coppé et al., 2010; Cuollo et al., 2020). To investigate whether our model system is characterized by the presence of a SASP, we measured the release of several previously identified SASP molecules, namely IL-1β, IL-6, TNF-α, IL-15 and CXCL1 (Coppé et al., 2010; Schafer et al., 2020; Su et al., 2021), to the conditioned medium of murine primary microglia after exposure to monomeric tau. Our results showed that microglia exposed to 15 nM, but not 5 nM of monomeric tau secrete significantly higher levels of these SASP factors (Fig. 9 A-E) when compared to control treated microglia. Moreover, exposure to 15 nM tau enhanced the secretion of IL-27, a factor that to the extend of our knowledge is a potential newly identified SASP factor (Fig. 9 F). Notably, we observed a dose-dependent increase in the secretion of IL-33 and a dose-dependent decrease in the secretion of anti-inflammatory IL-10 from murine primary microglia after tau treatment (Fig. 9 G, H).

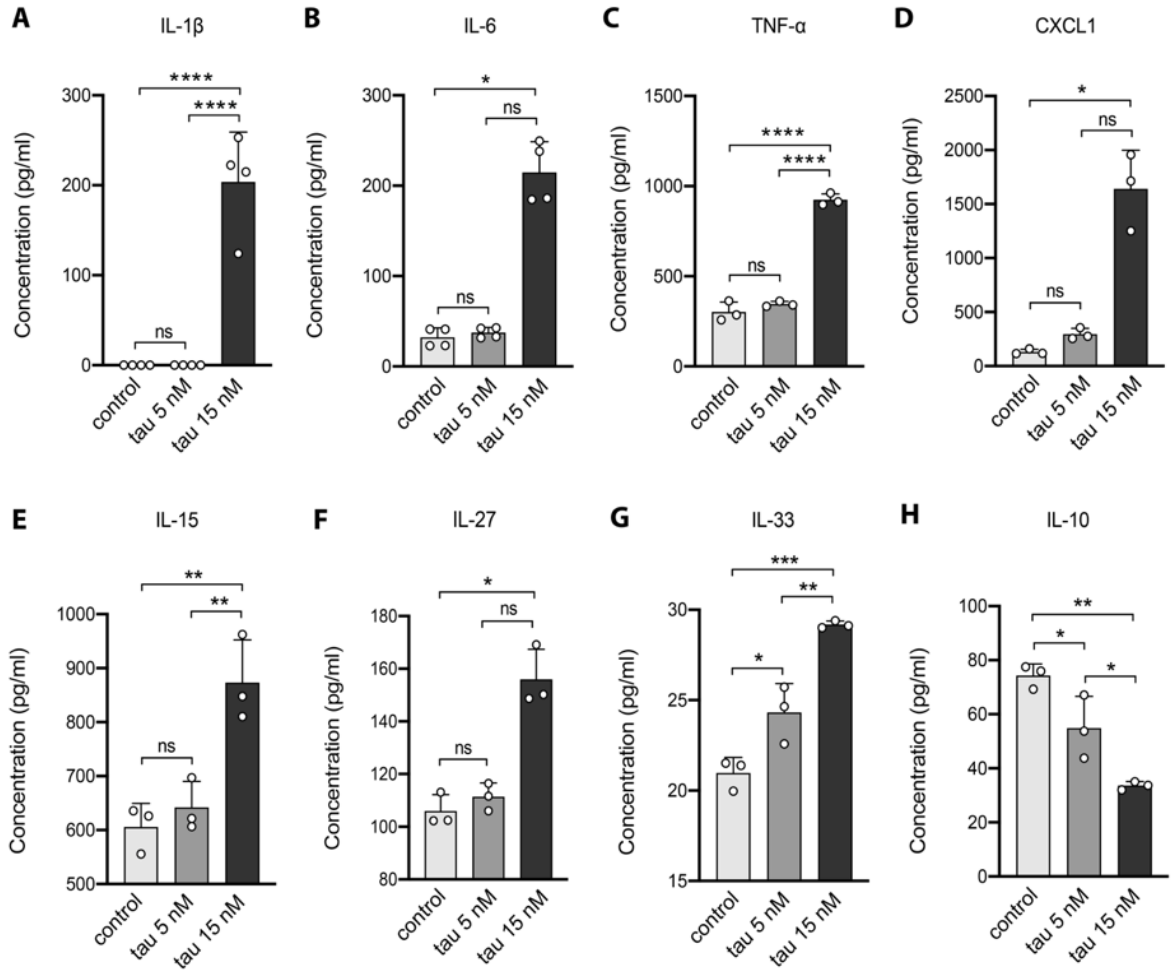

Fig. 9: Exposure to monomeric tau elicited the secretion of a senescence-associated secretory profile (SASP) from murine primary microglia. Secretion of **A.** Interleukin-1β (IL-1β), **B.** Interleukin-6 (IL-6;). **C.** Tumor necrosis factor alpha (TNF-α). **D.** Chemokine (C-X-C motif) ligand 1 (CXCL1). **E.** Interleukin-15 (IL-15). **F.** Interleukin-27 (IL-27), **G.** Interleukin-33 (IL-33) and **H.** Interleukin-10 (IL-10) from murine primary microglia after exposure to tau monomers. Data are represented as mean + SD **(A, C, E, G-H)** or median + 95% CI (**B, D and F)** and analyzed by one-way ANOVA followed by Tukey's test (**A:** F (2,9) = 53.74, *P*<0.0001; **C:** F (2,6) = 252.4, *P*<0.0001; **E:** F (2,6) = 18.03, *P*=0.0029; **G:** F (2,6) = 45.98, *P*=0.0002; **H:** F(2,6)=23.44, *P*=0.0015) and for non-parametric data, Kruskal-Wallis test with post hoc Dunn's test (**B:** Kruskal-wallis = 8.028, *P*=0.0040; **D:** Kruskal-wallis = 7.200, *P*=0.0036; **F**: Kruskal-wallis = 6.489, *P*=0.0107). n=3 independent cell culture experiments (**C-H**) or n=4 independent cell culture experiments (**A-B**). Significance is presented as **P*<0.05, ***P*<0.01 and ****P*<0.001. ns = not significant. Exact *P* values are shown in *section 11, table 9 A-H.* No outliers were identified using ROUT test (Q = 1%). No exclusion criteria were pre-determined and no samples were excluded from the analysis. Adapted from (Karabag et al., 2023)

3.2.3 Confirming the senescent phenotype using a positive control: treatment with phorbol 12-myristate 13-acetate (PMA) induced microglial senescence

The fact that primary cell cultures are limited in their proliferation capacity (Gillooly et al., 2012; Pan et al., 2009; Vay et al., 2018) raises questions whether the classical cell cycle arrest markers $p16^{INK4a}$ and $p21^{WAF1}$ are representative and suitable markers of senescence in our newly established cell culture model. Hence, we tried to confirm our findings based on a previous study showing that exposure to phorbol 12-myristate 13-acetate (PMA) for 72 h induced senescence in rat microglia *in vitro*, characterized by increased cell cycle arrest, release of a SASP and senescence-associated β-Gal positive cell stainings (Cao et al., 2020). In keeping with this, we show that exposure to PMA induces cell cycle arrest markers (Fig. 10 A-C) and formation of a SASP also in murine primary microglia (Fig. 10 D-F).

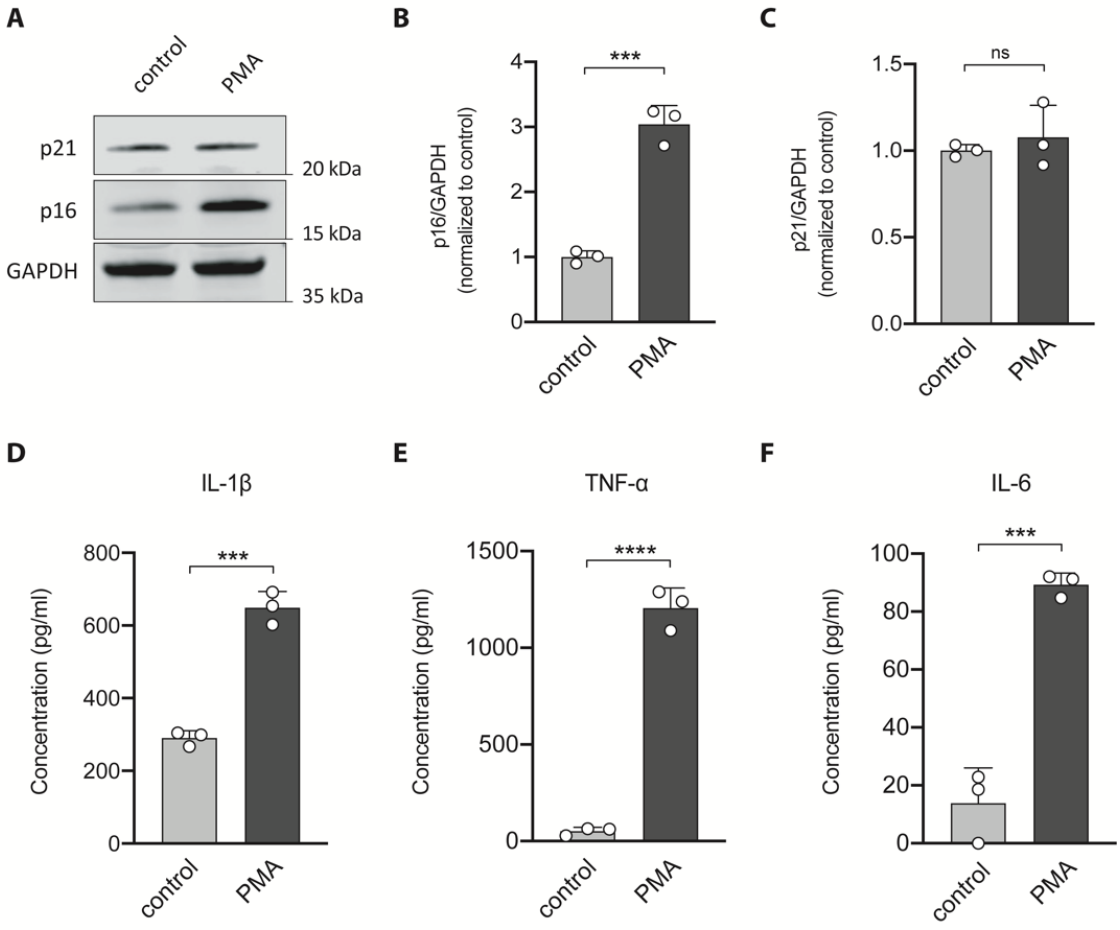

Fig. 10: Exposure to phorbol-12-myristat-13-acetat (PMA) induced senescence in murine primary microglia. **A.** Immunoblot representing $p16^{INK4a}$, $p21^{WAF1}$ and GAPDH after

exposure to 50 ng/ml phorbol-12-myristat-13-acetat (PMA) for 72 hours. **B-C**. Quantification of $p16^{INK4a}$ (**B**: ***P=0.0003) and $p21^{WAF1}$ (**C**: P=0.5262) shown in A. **D-F.** Exposure to PMA resulted in the secretion of IL-1β (**D**: ***P=0.0002), TNF-α (**E**: ****P<0.0001) and IL-6 (**F**: ***P=0.0005) from primary murine microglia. Data are represented as mean + SD and analyzed by two-tailed unpaired t-test. n=3 independent cell culture preparations. ROUT test (Q = 1%) showed no outliers. No exclusion criteria were pre-determined and no samples were excluded from the analysis. Adapted from (Karabag et al., 2023)

In addition to the use of PMA as a positive control showing that microglia can go into senescence in culture, we used multiple other markers to adequately assess the senescent phenotype of primary microglia after tau exposure in more detail. In the following section, we present evidence for nuclear changes in senescent microglia.

3.2.4 Microglia exhibited nuclear changes upon tau treatment

As a result of the loss of lamin B1 after tau exposure, we aimed to identify other nuclear changes associated with senescence in our model system (Camps et al., 2015; Lämmerhirt et al., 2022; Matias et al., 2022). One of the changes we wanted to verify involved the loss of lysine 9 trimethylation on histone H3 (H3K9me3) (Sidler et al., 2017; Tsurumi and Li, 2012; Zhang et al., 2021). As loss of H3K9me has been associated with astrocytes and neurons in tauopathies (Gil et al., 2021; Jury et al., 2020), it appeared plausible that exposure to tau might be accompanied by the loss of H3K9me3 in our model system. Indeed, murine primary microglia exposed to 15 nM, but not 5 nM of tau, showed a significant loss of H3K9me3 (Fig. 11 A, B). Another accepted marker associated with senescence (Mah et al., 2010), which is also present in tauopathies (Farmer et al., 2020; Musi et al., 2018), is phosphorylation of histone H2AX (yH2AX). Here, we report that exposure to 15 nM, but not 5 nM of tau significantly increased the levels of nuclear yH2AX in murine primary microglia (Fig. 11 C, D).

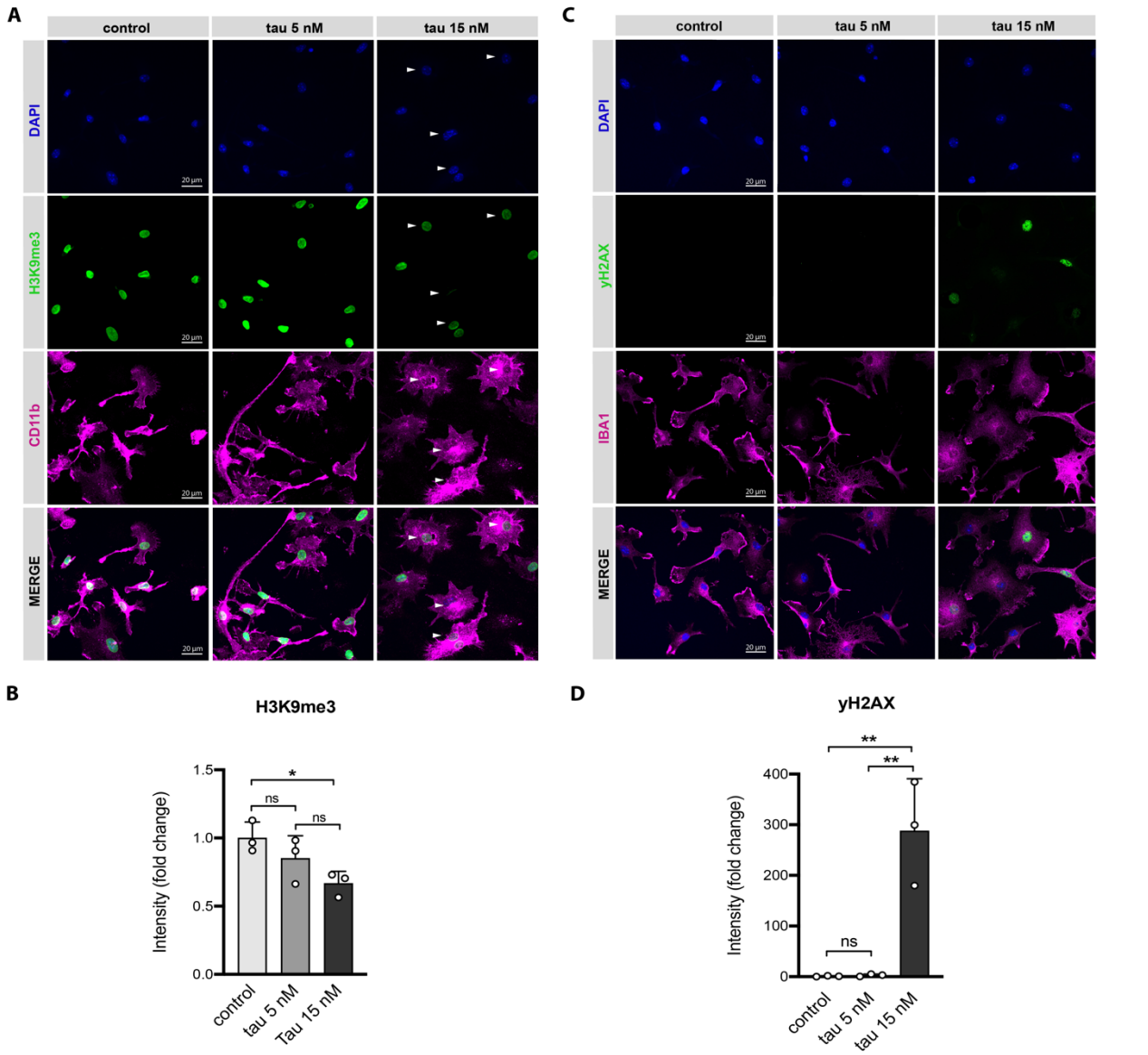

Fig. 11: Primary murine microglia demonstrated loss of H3K9me3 and increased formation of γH2AX foci after exposure to monomeric tau. **A.** Immunocytochemical staining representing trimethylation of lysine 9 on histone 3 (H3K9me3; green), cluster of differentiation molecule (CD11b; magenta) and 4′,6-diamidino-2-phenylindole (DAPI; blue) in murine primary microglia after exposure to monomeric tau. **B.** Quantification of H3K9me3. **C.** Representative immunocytochemical staining showing phosphorylation of H2AX (γH2AX; green), IBA1 (magenta) and DAPI (blue) in microglia after exposure to different concentrations of tau. **D.** Quantification of γH2AX. Data are represented as mean + SD and analyzed by one-way ANOVA with Tukey's test (**B**: F (2,6) = 5.142, *P*=0.0500; **D**: (F (2,6) = 23.24, *P*=0.0015)). Arrow heads indicate nuclei with H3K9me3 expression. Statistical significance is presented as **P*<0.05 and ***P*<0.01. ns = not significant, n=3 independent cell culture preparations. Exact *P* values are shown in *section 11, table 11 B, C.* ROUT test (Q = 1%) showed no outliers. No exclusion criteria were pre-determined and no samples were excluded from the analysis. Adapted from (Karabag et al., 2023).

3.2.5 Senescent microglia are impaired in their capability to clear tau

Microglia carry out important functions in the brain, including promotion of recovery after injury, modulation of neuronal synapses and maintenance of CNS homeostasis. In addition, other major functions of microglia include phagocytosis and clearance (Colonna and Butovsky, 2017; Galloway et al., 2019), which were shown to be impaired during senescence (Brelstaff et al., 2021). Therefore, we assessed whether our model system is characterized by an impaired ability to clear tau monomers. To test this, we first exposed murine primary microglia to 5 and 15 nM of monomeric tau as previously described, followed by adding 200 nM of fluorescently labeled tau monomers for 30 or 60 minutes. After the respective timepoints, we analyzed the ability of microglia to take up and clear tau monomers using flow cytometry (Fig. 12 A-F). In line with previous findings, we found that microglia pre-exposed to 15 nM, but not 5 nM of tau, presented with a decreased amount of tau in microglia as indicated by a reduction in fluorescence (Fig. 12E) and also a reduced percentage (%) of tau-positive microglia (Fig. 12F), overall showing a reduced capability of treated microglia to clear tau.

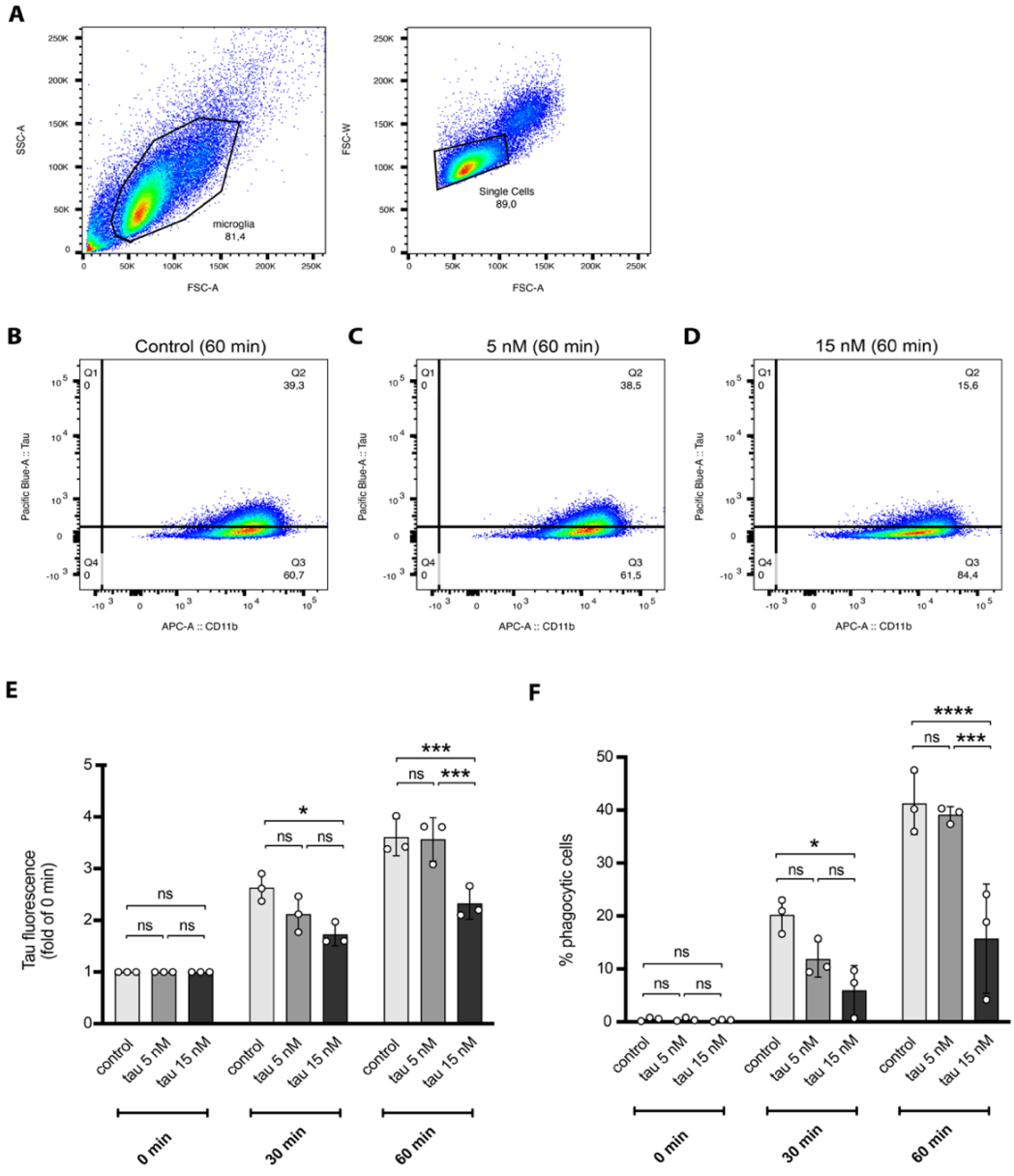

Fig. 12: Senescent murine primary microglia showed loss of tau clearance capabilities. **A.** FACS plot displaying the gating scheme for the assessment of tau clearance by murine primary microglia. **B-D.** Charts representing the engulfment of tau by control microglia **(B)** or microglia pre-exposed to tau monomers **(C-D)**. **E**. Quantified tau fluorescence in the microglia after exposure to 200 nM AlexaFluor-405-labeled monomeric tau for 0, 30 and 60 minutes. **F.** Quantification of the percentage (%) of tau-containing microglia after exposure to monomeric tau for 0, 30 and 60 minutes. Data are represented as mean + SD and analyzed by two-way ANOVA with multiple comparisons regardless of rows and columns (**E:** F (2,18) = 18.51, $P<0.0001$); **F:** F (2,18) = 20.60, $P<0.0001$). Statistical significance is presented as *$P<0.05$, ***$P<0.001$ and ****$P<0.0001$. ns = not significant, n=3 independent cell culture preparations. Exact *P* values are shown in *section 11, table 12 E-F.* ROUT test (Q = 1%) showed no outliers. No exclusion criteria were pre-determined and no samples were excluded from the analysis. Adapted from (Karabag et al., 2023).

3.2.6 Impaired migratory capacity in senescent microglia

Microglia rapidly change their ramified, highly motile branched shape to a reactive amoeboid shape during an insult to the CNS to support proper migration to the site of insult (Kettenmann et al., 2011; Scheiblich and Bicker, 2015; Zhang et al., 2016). Interestingly, the migration rate of various cell types, including microglia, was shown to be impaired during aging and senescence (Brelstaff et al., 2021; Caldeira et al., 2014, 2017; Damani et al., 2011). Given this, we examined the migration ability of murine primary microglia after senescence induction using an *in vitro* scratch wound assay (Fig. 13). We discovered that exposure to 15 nM, but not 5 nM of tau monomers, significantly impaired distance (Fig. 13 B) as well as speed (Fig. 13 C) traveled by microglia towards the wound.

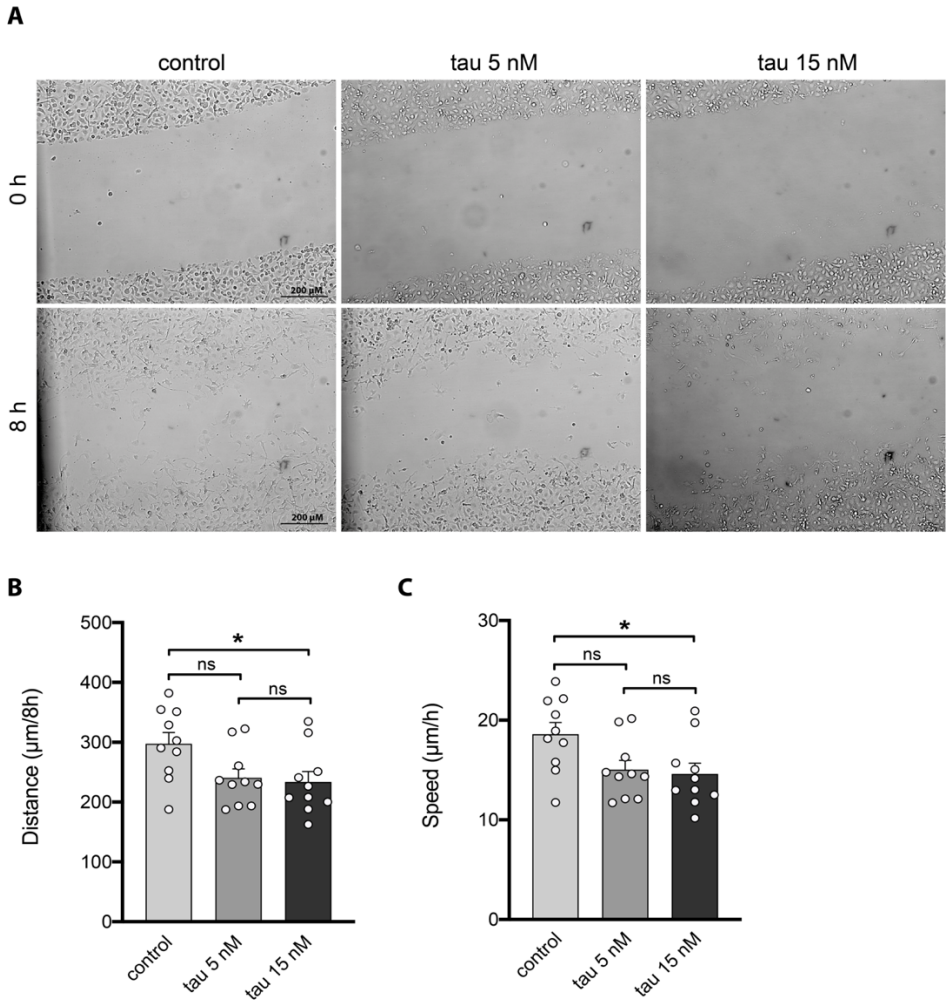

Fig. 13: Senescent murine primary microglia showed impaired migratory behavior. **A.** Images representing migratory behavior of primary microglia in a scratch assay at 0 and

8 hours (8h). **B.** Analysis of distance travelled in µm/8h. **C.** Quantification of the migration speed in µm/h. Data are shown as mean + SD and analyzed by one-way ANOVA with post hoc Tukey's test (**B-C**: F (2,27) = 4.174, *P*=0.0263). n=3 independent cell culture experiments with 3-4 technical replicates per experiment. Statistical significance is presented as **P*<0.05. ns = not significant. Exact *P* values are shown in *section 11, table 13 B-C.* ROUT test (Q = 1%) showed no outliers. No exclusion criteria were pre-determined and no samples were excluded from the analysis. Adapted from (Karabag et al., 2023).

3.2.7 Senescent microglia show changes in their cytoskeletal morphology

Impaired migratory behavior of senescent cells might be the consequence of re-organizations of the cytoskeleton (Wang, 1985; Nishio and Inoue, 2005; Moujaber et al., 2019; Reed et al., 2001). Changes in morphology, such as enlargements in cell size, are cardinal features of senescent cells (Greenberg et al., 1977; Wallis et al., 2022). Given this, we hypothesized that impaired migratory behavior during microglial senescence could be attributed to changes in morphology, which we measured by a Phalloidin staining. Interestingly, our results showed that exposure to 15 nM, but not 5 nM of tau, significantly increased the total skeletal length (µm) (Fig. 14 B), area (μm^2) (Fig. 14 C), perimeter (µm) (Fig. 14 D), number of trunks (No. of Trunks) (Fig. 14 E) and branches (No. of Branches) (Fig. 14 F) in murine primary microglia.

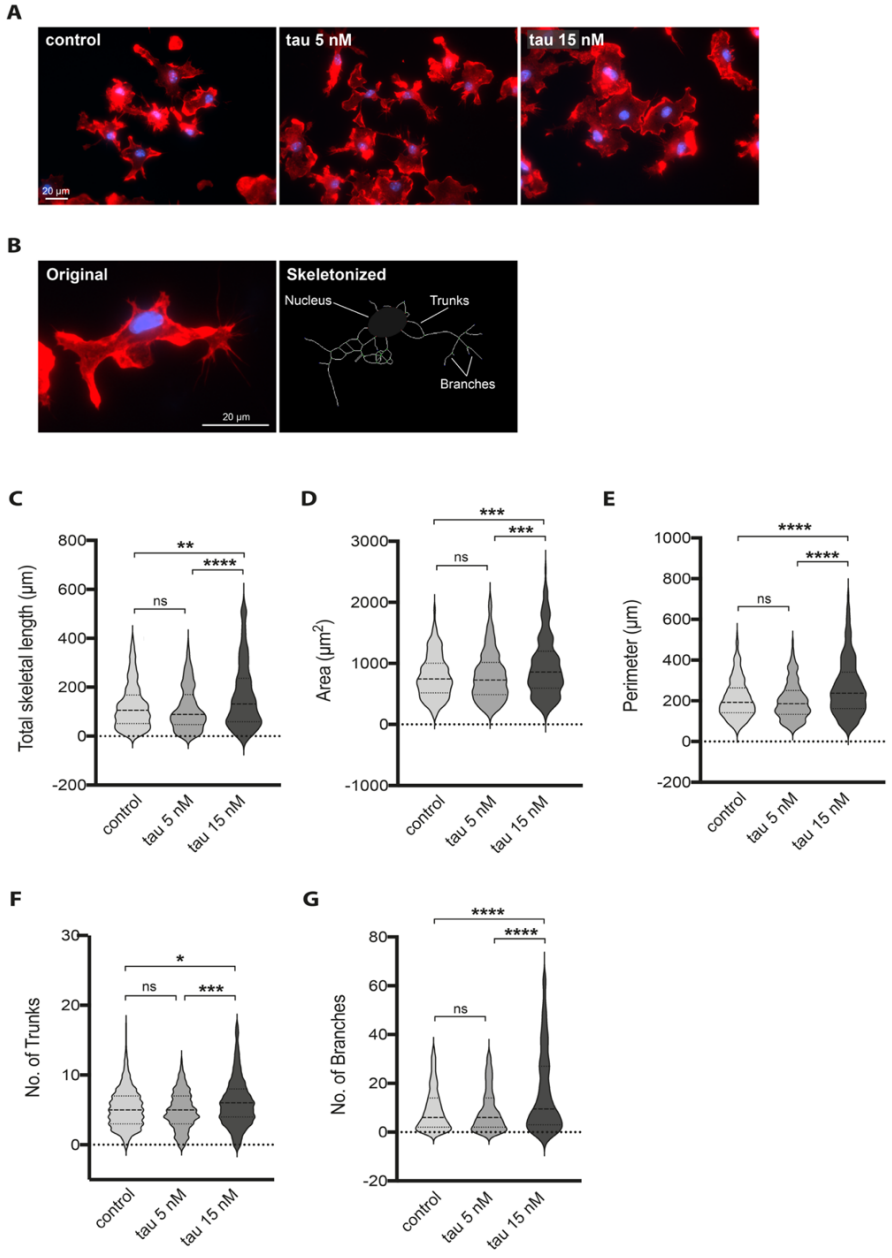

Fig. 14: Senescent murine primary microglia presented with changes in cytoskeletal morphology. **A.** Representative immunocytochemical staining showing Phalloidin (red) and DAPI (blue) in primary murine microglia after exposure to different concentrations of tau. **B.** "Original" is an example of a cell stained with phalloidin (to label the F-actin cytoskeleton) and DAPI as nuclear counterstain. "Skeletonized" is the cell after running the skeletonization tool for morphological analysis. Dark grey is the nucleus and white are the processes that can be devided into trunks (structurally attached to the nucleus) and branches (structurally attached to trunks). **C-G**. Quantification of microglial morphology, including total skeletal length **(C)**, cell area **(D)**, perimeter **(E)**, number of trunks **(F)** and number of branches **(G)**. Data are presented as violin plots and analyzed by non-parametric Kruskal-Wallis test with post hoc Dunn's test (**C:** Kruskal-wallis = 24.67, *P*<0.0001; **D:** Kruskal-wallis = 19.97, *P*<0.0001; **E:** Kruskal-wallis = 47.19, *P*<0.0001; **F:** Kruskal-wallis = 15.22, *P*=0.0005 and **G:** Kruskal-wallis = 31.61, *P*<0.0001). Outliers were

removed (ROUT test: Q = 1%) from all datasets. No exclusion criteria were pre-determined. Statistical significance is presented as *P<0.05, **P<0.01, ***P<0.001 and ****P<0.0001. ns = not significant, n=3 independent cell culture preparations with an estimate of 100 cells analyzed per preparation in each condition. Exact P values are shown in *section 11, table 14 C-G.* Adapted from (Karabag et al., 2023).

Taken together, our data indicated that exposure to 15 nM, but not 5 nM tau monomers results in the expression of markers that encompass most of the attributes associated with cellular senescence, including secretion of the SASP. Given this, we continued our experiments with 15 nM tau as the optimal concentration for inducing senescence in primary murine microglia.

3.3 The contribution of the NLRP3 inflammasome to tau-mediated microglial senescence *in vitro*

3.3.1 Activation of the NLRP3 inflammasome during microglial senescence

The fact that ablation of the NLRP3 inflammasome ameliorated microglial senescence *in vivo* (Fig. 6 and Fig. 7) prompted us to further investigate the role of the NLRP3 inflammasome in tau-mediated microglial senescence. To understand this, we first studied NLRP3 inflammasome activation in our established cell culture model. Interestingly, our results demonstrated that senescent microglia show increased release of cleaved caspase-1 (Fig. 15 B) and IL-1β (Fig. 15 C), both signs of NLRP3 inflammasome activation. These results are consistent with a previous study, showing activation of the NLRP3 inflammasome during senescence in another cell culture model (Tai et al., 2022; Wiggins and Clarke, 2019). To confirm that cleavage of caspase-1 as well as production of IL-1β are the result of NLRP3 inflammasome activation, we pre-treated the microglia with 1 µM of the selective NLRP3 inflammasome inhibitor CRID3 sodium salt (Tocris, Cat #5479). This concentration was based on previous experiments performed by colleagues in the laboratory (Scheiblich et al., 2021). In addition, a CRID3 treatment without exposure to tau (CRID3) (Fig. 15 A-D) was included. Our findings revealed that pre-treatment with CRID3 did significantly inhibit the release of cleaved caspase-1 (Fig. 15 B) as well as of IL-1β (Fig. 15 C).

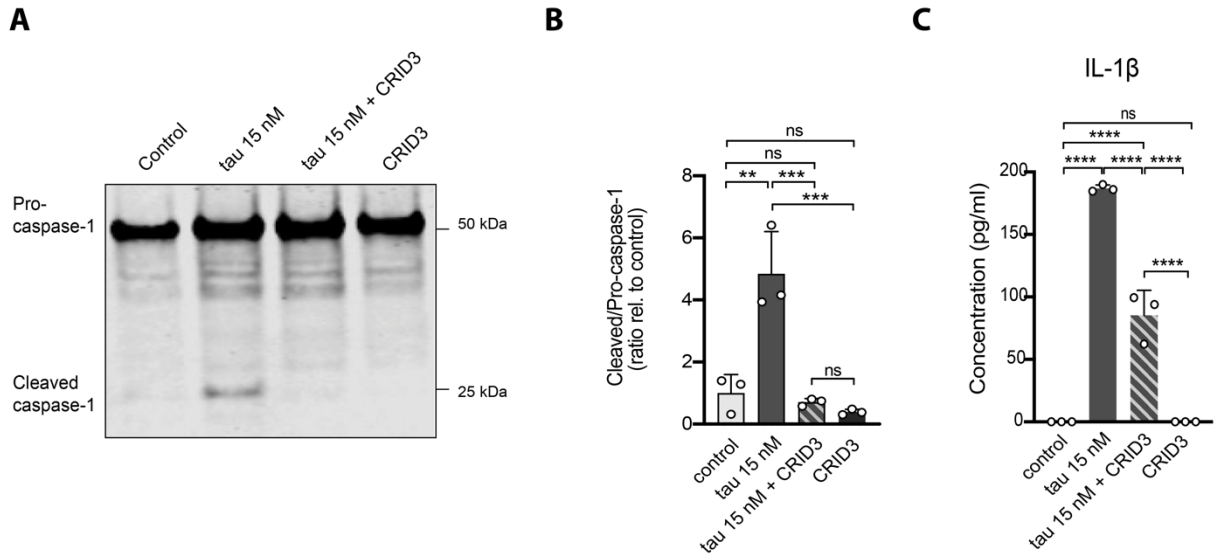

Fig. 15: Senescent murine primary microglia show activation of the NLRP3 inflammasome. **A.** Representative immunoblot of pro-caspase-1 and cleaved-caspase-1 in the conditioned medium after senescence induction. **B.** Quantification of the ratio cleaved/pro-caspase-1 and **C**. Release of IL-1β in the conditioned medium of senescent murine primary microglia. Data are represented as mean + SD and statistical significance for parametric data was analyzed by one-way ANOVA followed by Tukey's test (**B**: (3,8) = 23.13, P=0.0003 and **C**: F (3,8) = 229.5, P<0.0001). Statistical significance is presented as ***P*<0.01, ****P*<0.001 and *****P*<0.0001. ns = not significant, n=3 independent cell culture preparations. Exact *P* values are shown in *section 11, table 15 B-C*. ROUT test (Q = 1%) showed no outliers. Shapiro-Wilk test showed no violation of normality. No exclusion criteria were pre-determined and no samples were excluded from the analysis.

3.3.2 Inhibition of the NLRP3 inflammasome attenuates microglial senescence

As mentioned in section 1.3.3.1, inflammaging or immunosenescence is characterized by the release of pro-inflammatory molecules, in particular IL-1α, IL-1β, IL-6, IL8, interferon gamma (IFN-y) and tumor necrosis factor α (TNF-α). Interestingly, activation of the NLRP3 inflammasome was shown to control the SASP (Acosta et al., 2013) and pharmacological inhibition of the NLRP3 inflammasome was shown to be protective against cellular senescence (Romero et al., 2022; Shi et al., 2022). However, the contribution of the NLRP3 inflammasome to microglial senescence has not been investigated so far. Given this, we wanted to find out whether activation of the NLRP3 inflammasome mediates microglial senescence. To study this, murine primary microglia were pre-treated with 1 µM CRID3 for one hour prior to senescence indution. Here, we found that inhibition of the NLRP3 inflammasome prevented microglial senescence, as seen by normalization of

$p16^{INK4a}$ (Fig. 16 A, C) and $p21^{WAF1}$ protein levels (Fig. 16 A, B) and partial reduction of release of several components of the SASP, in particular IL-1β (Fig. 16 D), IL-6 (Fig. 16 E), TNF-α (Fig. 16 F) and CXCL1 (Fig. 16 G). In contrast, inhibition of the NLRP3 inflammasome did not affect the release of IL-15 (Fig. 16 H), IL-27 (Fig. 16 I), IL-33 (Fig. 16 J) and IL-10 (Fig. 16 K).

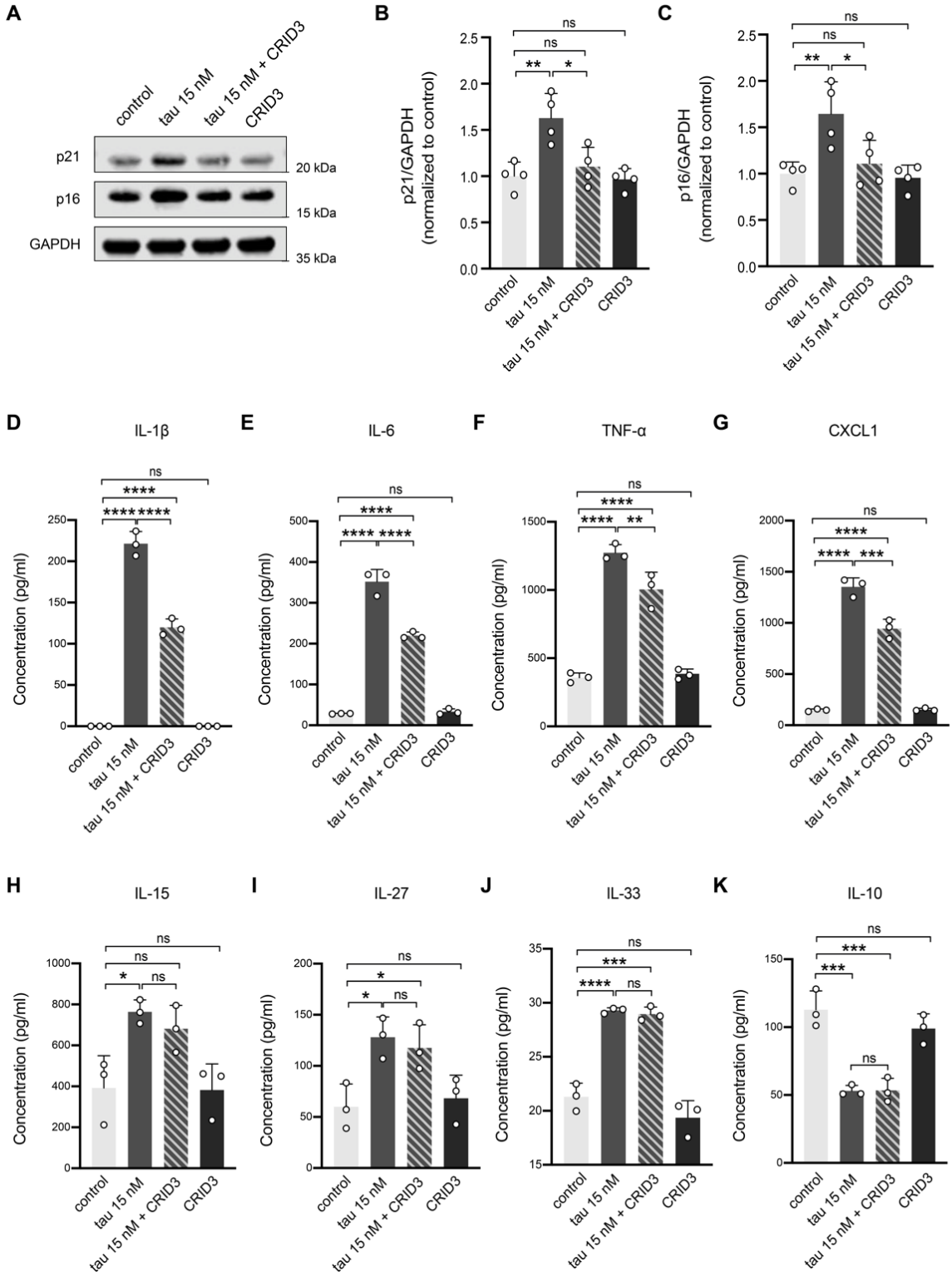

Fig. 16: Inhibition of the NLRP3 inflammasome using CRID3 prevented the senescent phenotype in murine primary microglia. **A**. Representative immunoblot for p16 and p21. **B-C**. Quantification of **B.** $p21^{WAF1}$ and **C.** $p16^{INK4a}$. Pre-treatment with CRID3 resulted in the suppression of **D**. IL-1β, **E**. IL-6, **F**. TNF-α, **G**: CXCL1, **H**. IL-15, **I**. IL-27, **J**: IL-33 and **K**. IL-10. Graphs are presented as mean + SD and analyzed by one-way ANOVA followed

by Tukey's test **B**: F (3,12) = 10.08, *P*=0.0013, **C**: F (3,12) = 7,412, *P*=0.0045, **D**: F (3,8) = 422.2, *P*<0.0001), **E:** F (3,8) = 286.1, *P*<0.0001**, F:** F (3,8) = 113.5, *P*<0.0001, **G:** F (3,8) = 262.1, *P*<0.0001**, H:** F (3,8) = 8.047, *P*=0.0084**, I:** F (3,8) =7.351, *P*=0.0110**, J:** F (3,8) = 68.93, *P*<0.0001 and **K:** F (3,8) = 29.29, *P*=0.0001), Statistical significance is presented as **P*<0.05, ***P*<0.01, ****P*<0.001 and *****P*<0.0001. ns = not significant, n=3 (**D-K**) or n=4 (**B-C**) n=3 independent cell culture preparations. Exact *P* values are shown in *section 11, table 16 B-K*. ROUT test (Q = 1%) showed no outliers. Shapiro-Wilk test showed no violation of normality. No exclusion criteria were pre-determined and no samples were excluded from the analysis.

To confirm these findings, we performed similar experiments using murine primary microglia from *Nlrp3*$^{-/-}$ mice (Fig. 17). Similar to the results obtained with CRID3 treatments, *Nlrp3*$^{-/-}$ microglia were protected against cell cycle arrest after tau exposure (Fig. 17 A-C), indicated by normalization of p21^{WAF1} (Fig. 17 B) and p16^{INK4a} protein levels (Fig. 17 C). In addition, the release of major components of the SASP, including IL-1β (Fig. 17 D), IL-6 (Fig. 17 E) and TNF-α (Fig. 17 F) were significantly reduced. These findings are in concordance with the results of previous studies showing a protective effect of NLRP3 inhibition on cellular senescence (Marín-Aguilar et al., 2020; Tai et al., 2022; Youm et al., 2012).

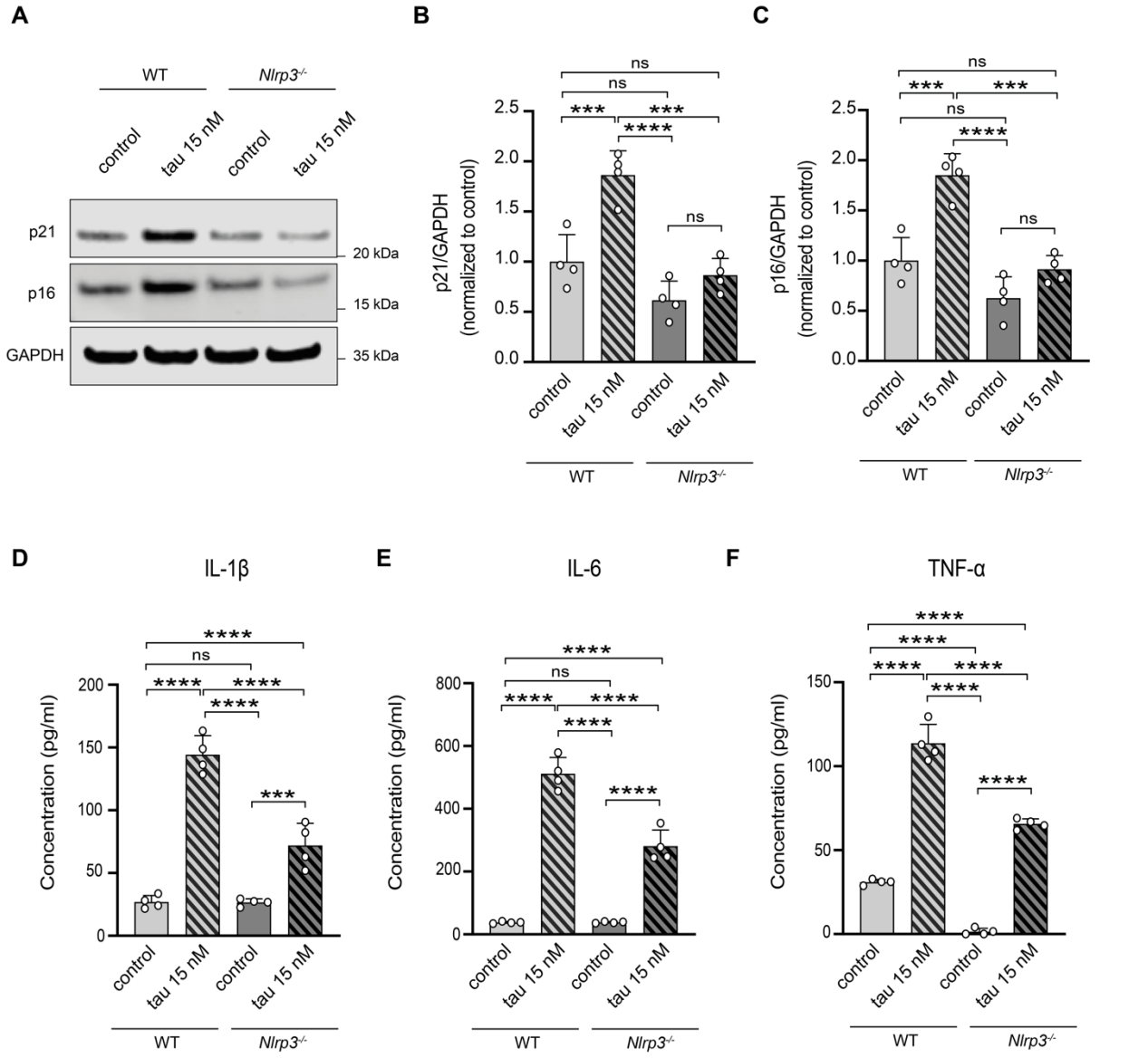

Fig. 17: Nlrp3 deficiency (*Nlrp3*$^{-/-}$) ameliorated the senescent phenotype in murine primary microglia. **A.** Representative immunoblot for p16^{INK4a} and p21^{WAF1} after tau treatment of *Nlrp3*$^{-/-}$ murine primary microglia. **B-C**. Quantification of **B.** p21^{WAF1} and **C.** p16^{INK4a}. *Nlrp3*$^{-/-}$ inhibited the release of **D.** IL-1β, **E.** IL-6 and **F.** TNF-α in tau-induced senescent microglia. ROUT test (Q= 1%) showed no outliers. Shapiro-Wilk test showed no violation of normality. Graphs are presented as mean + SD and statistical significance was analyzed by one-way ANOVA followed by Tukey's test (**B:** F (3,12) = 24.00, *P*<0.0001; **C:** F (3,12) = 27.13, *P*<0.0001; **D:** F (3,12) = 85.72, *P*<0.0001, **E:** F (3,12) = 154.0, *P*<0.0001 and **F:** F (3,12) = 262.3, *P*<0.0001). Statistical significance is presented as ***P<0.001 and ****P<0.0001. ns = not significant, n=4 independent cell culture preparations. Exact *P* values are shown in *section 11, table 17 B-F.* No exclusion criteria were pre-determined and no samples were excluded from the analysis.

3.4 NLRP3 and mitophagy during microglial senescence

3.4.1 Activation of NLRP3 impairs mitophagy during microglial senescence

Intriguingly, activation of the NLRP3 inflammasome has been shown to block mitophagy and mediate mitochondrial dysfunction (Yu et al., 2014). Proteins involved in the regulation of mitophagy include Parkin and PINK1 (Ham et al., 2020; Ye et al., 2015). Interestingly, previous findings have demonstrated the importance of mitophagy in cellular senescence. For instance, normalization of Parkin in RhoA-depleted cardiomyocytes rescued mitophagy and ameliorated mitochondrial damage and cardiomyocyte senescence in mice (Soh et al., 2023). In addition, overexpression of Parkin attenuated airway endothelial cell (AEC) senescence in a mouse model of chronic obstructive pulmonary disease (COPD). In line with this, our data indicated that the expression of Parkin is significantly reduced in tau-induced senescent microglia and that inhibition of the NLRP3 inflammasome rescues the expression of Parkin (Fig. 18). This rescue effect might be an explanation to why NLRP3 deficiency attenuated cellular senescence in microglia.

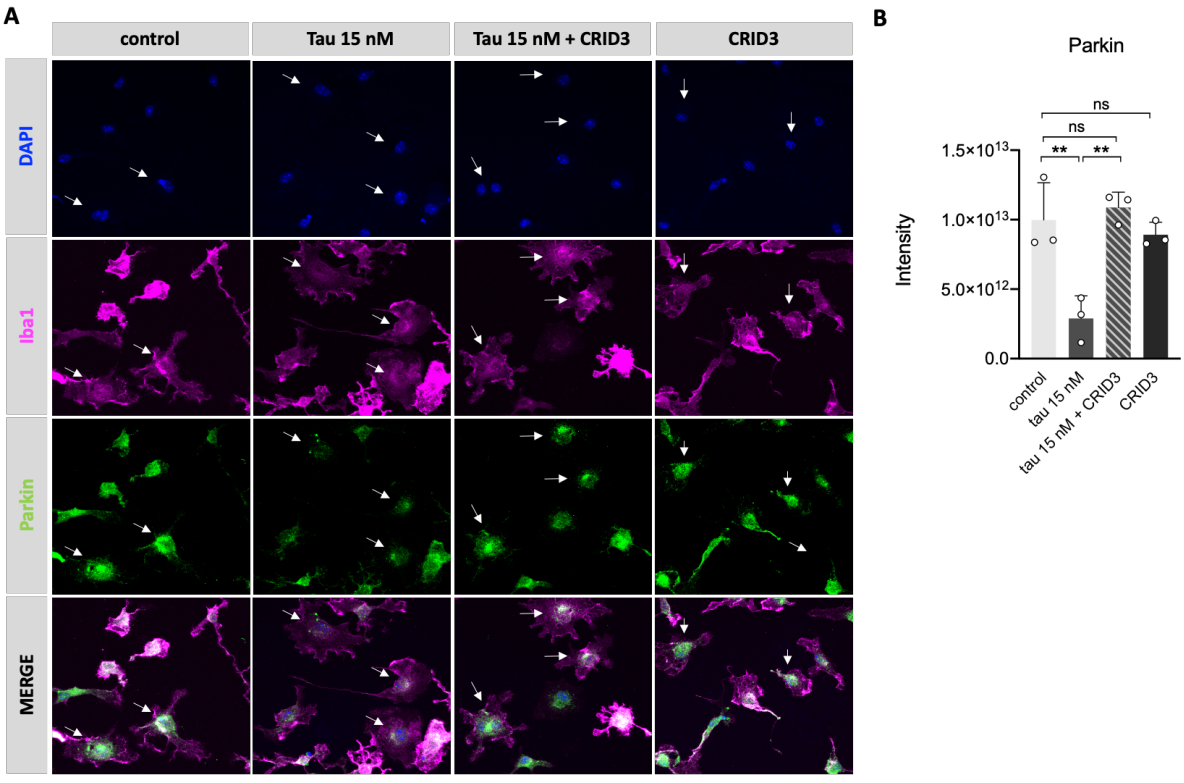

Fig. 18: Senescent microglia showed loss of Parkin which is rescued upon NLRP3 inhibition. **A.** Staining for Iba1 (magenta), Parkin (green) and DAPI (blue) after senescence induction in the presence or absence of CRID3. **B.** Quantification of Parkin in microglia (control vs tau 15 nM: **P=0.0043, control vs. tau 15 nM + CRID3: P=0.9165, control vs. CRID3: P=0.8694 and tau 15 nM vs. tau 15 nM + CRID3: **P=0.0020). Graph is presented as mean ± SD and analyzed using one-way ANOVA with Tukey's test ($F(3,8) = 13.27$, P=0.0018). Exact *P* values are shown in *section 11, table 18 B.* Arrows indicate the expression of Parkin in microglia.

3.5 NLRP3 independent pathways involved in formation of the SASP

3.5.1 Activation of signal transducer and activator of transcription (STAT3)

Although ablation of the NLRP3 inflammasome rescued cell cycle arrest *in vitro*, it did not prevent release of the SASP. These findings imply that NLRP3 independent mechanisms are involved in formation of the SASP during tau-induced microglial senescence. One of these mechanisms might be mediated via signal transducer and activator of transcription (STAT3), a transcription factor that has been shown to play a key role in proliferation, migration and cell fate (Bromberg and Darnell, 2000; Kojima et al., 2013). Interestingly, STAT3 signaling serves an important role during the development of cellular senescence (Kojima et al., 2012; Kuilman et al., 2008) and the production of pro-inflammatory cytokines related to the SASP (Birch and Gil, 2020; Chen et al., 2021; Wu et al., 2020). To explore a potential NLRP3 independent effect of STAT3 during microglial senescence, we investigated the expression of total and Tyr705-phosphorylated, active STAT3 in our culture model (Fig. 19). Interestingly, our data showed that senescent murine primary microglia do not show differences in total levels of STAT3 (Fig. 19 A, B), but express significantly more phosphorylated STAT3 (Fig. 19 A, C) in comparison to control microglia. Strikingly, suppression of the NLRP3 inflammasome using CRID3 did not affect the levels of phosphorylated STAT3 in senescent microglia (Fig. 19 A, C), indicating that STAT3 activation is NLRP3 independent. To be able to further test a role of STAT3 for induction of the SASP, we also probed for the effect of stattic, a selective STAT3 phosphorylation inhibitor (Schust et al., 2006), on the levels of total and phosphorylated STAT3 after senescence induction. Therefore, we pre-treated murine primary microglia with 2.5 µM of the selective STAT3 phosphorylation inhibitor stattic. The concentration used in this study

is within the range of the established doses used in previous studies (Li et al., 2020; Liu et al., 2013; Lu et al., 2014; Tong et al., 2017). Akin to previous findings, our results indicated that pre-treatment with stattic prevented phosphorylation of STAT3 (Fig. 19 C).

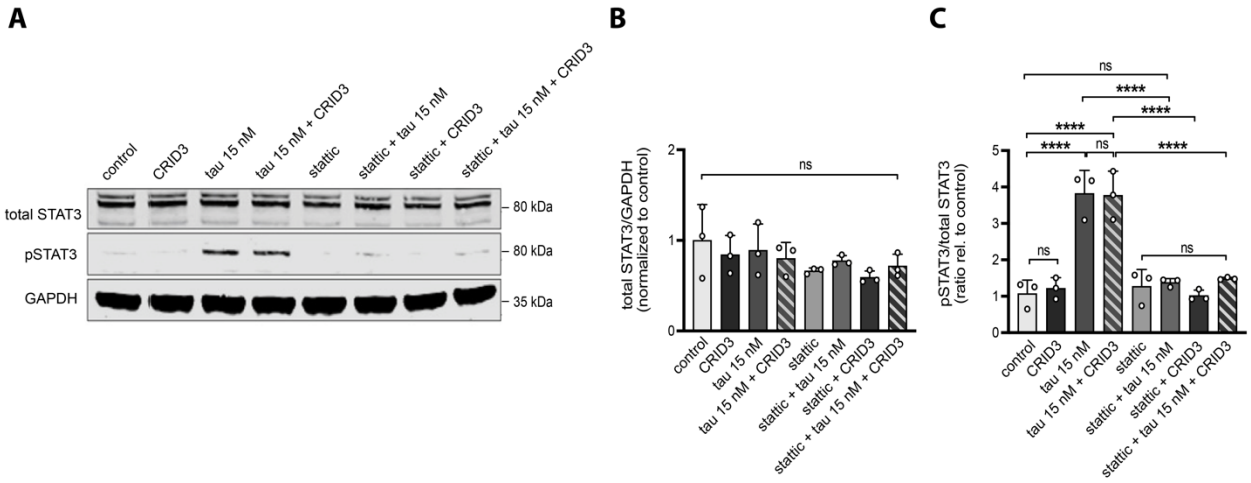

Fig. 19: Tau-treated murine primary microglia exhibited NLRP3 independent phosphorylation of STAT3. **A**. Representative immunoblot for total STAT3 (totalSTAT3) and Tyr705-phosphorylated STAT3 (pSTAT3) after senescence induction in murine primary microglia. **B.** Quantification of total STAT3. **C.** Quantification of phosphorylated STAT3. Data are represented as mean + SD and statistical significance was analyzed by one-way ANOVA followed by Tukey's test (**B**: $F(7,16)=1.166$, $P=0.3740$, **C**: $F(7,16) = 26.04$, $P<0.0001$). Statistical significance is presented as ****$P<0.0001$. ns = not significant, n=3 independent cell culture preparations. Exact *P* values are shown in *section 11, table 19 B-C.* ROUT test (Q= 1%) showed no outliers. Shapiro-Wilk test showed no violation of normality. No exclusion criteria were pre-determined and no samples were excluded from the analysis.

3.5.2 STAT3 activation is a key driver of the SASP

In the previous section, we have demonstrated that activation of STAT3 coincided with microglial senescence in a NLRP3 independent manner. Additionally, we showed that pre-treatment with stattic prevented activation of STAT3. Given these findings, we then analyzed whether activation of STAT3 contributes to formation of the SASP. To study this, we examined the effect of stattic on the release of our previously identified SASP factors in our model system (Fig. 20). Remarkably, we found that pre-treatment with stattic prevented the release of IL-1β (Fig. 20 A), IL-6 (Fig. 20 B), TNF-α (Fig. 20 C), CXCL1 (Fig. 20 D), IL-15 (Fig. 20 E), IL-27 (Fig. 20 F) and IL-33 (Fig. 20 G). In contrast, pre-treatment with stattic significantly enhanced the release of IL-10 (Fig. 20 H).

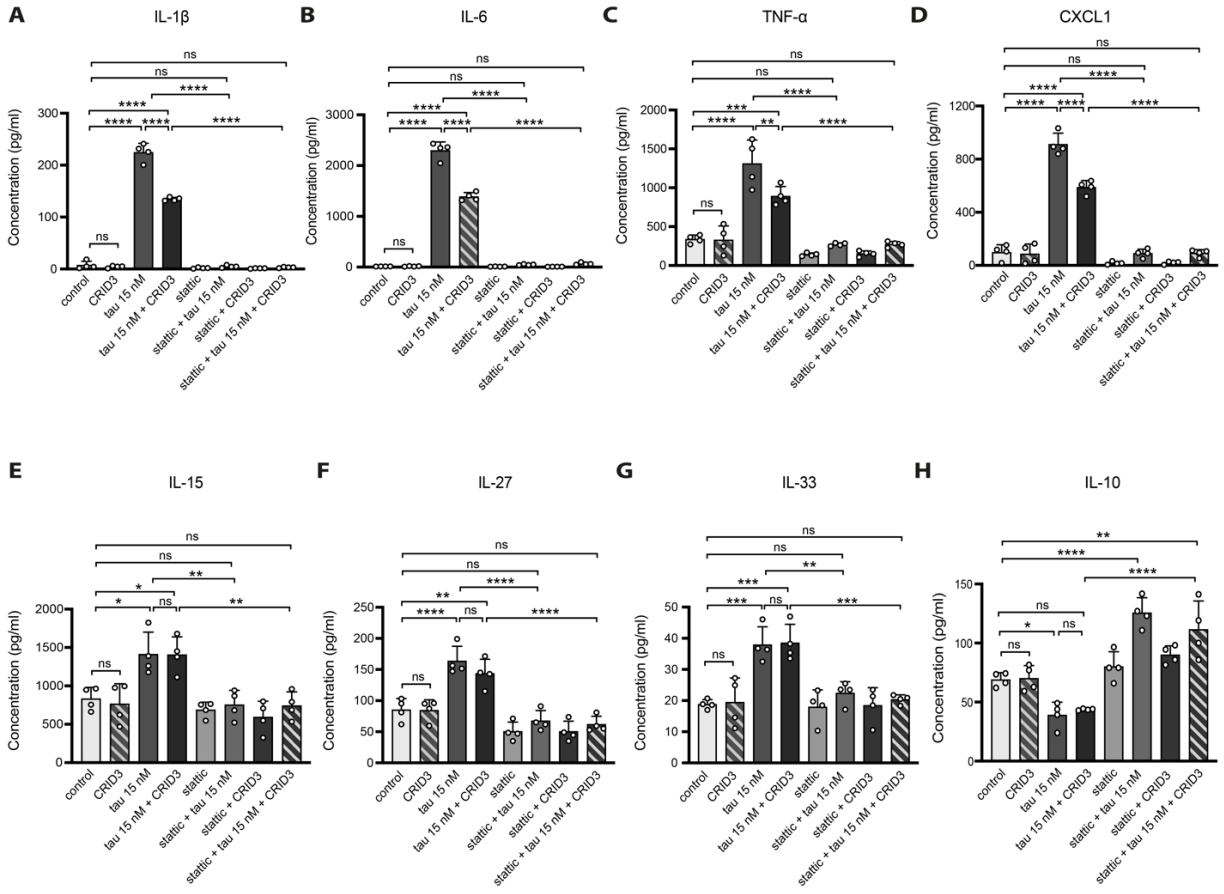

Fig. 20: Activation of STAT3 drives the SASP in senescent murine primary microglia. Blocking STAT3 phosphorylation using stattic prevented the formation of **A.** IL-1β, **B.** IL-6, **C.** TNF-α, **D.** CXCL1, **E.** IL-15, **F.** IL-27 and **G.** IL-33 and increased the release of **H.** IL-10. Data are represented as mean + SD and statistical significance was analyzed by one-way ANOVA followed by Tukey's test (**A**: F (7,24) = 600.7, *P*<0.0001; **B**: F(7,24) = 671.6, *P*<0.0001; **C**: F(7,24) = 37.80, *P*<0.0001; **D:** F (7,24) = 172.4, *P*<0.0001; **E:** F (7,24) = 9.513, *P*<0.0001; **F:** F (7,24) = 21.94, *P*<0.0001; **G:** F (7,24) = 11.68, *P*<0.0001 and **H:** F (7,24) = 23.80, *P*<0.0001. Statistical significance is presented as **P*<0.05, ***P*<0.01, ****P*<0.001 and *****P*<0.0001. ns = not significant, n=4 independent cell culture preparations. Exact *P* values are shown in *section 11, table 20 A-H.* ROUT test (Q= 1%) showed no outliers. Shapiro-Wilk test showed no violation of normality. No exclusion criteria were pre-determined and no samples were excluded from the analysis.

3.5.3 STAT3 controls NLRP3 inflammasome activation

Activation of STAT3 has been implicated with inflammation in numerous diseases, including inflammatory bowel disease (IBD) (Sugimoto, 2008), Multiple Sclerosis (MS) (Alhazzani et al., 2021), Alzheimer's Disease (AD) (Millot et al., 2020; Reichenbach et al., 2019) and Amyotrophic Lateral Sclerosis (ALS) (Shibata et al., 2010). Interestingly,

inhibition of STAT3 was shown to prevent NLRP3 inflammasome activation in acute lung injury (Liu et al., 2023), osteolysis (Zhu et al., 2023) and LPS-induced sepsis (Kang et al., 2023). Given that STAT3 was shown to regulate the NLRP3 inflammasome (Cao et al., 2020; Zhu et al., 2023), we hypothesized that also activation of the NLRP3 inflammasome during microglial senescence is regulated by STAT3. Since our previous results indicated that pre-treatment with stattic blocks the release of IL-1β (Fig. 20 A) from murine primary microglia, we investigated whether release of cleaved caspase-1 is prevented as well (Fig. 21). Our data showed that stattic significantly reduced the levels of pro-caspase-1 (Fig. 21 B) and cleavage of caspase-1 in the conditioned medium (Fig. 21 C), supporting our hypothesis of a contribution of STAT3 signaling to NLRP3 inflammasome activation in senescence.

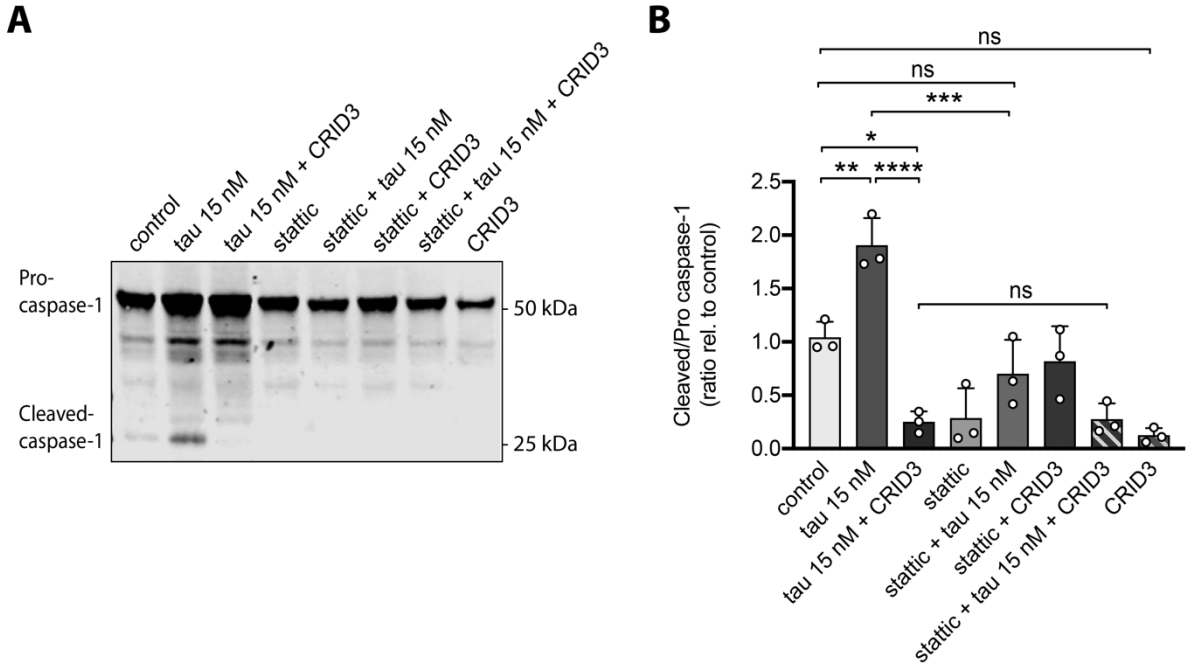

Fig. 21: Stattic prevented NLRP3 inflammasome activation in senescent murine primary microglia. **A.** Representative immunoblot analysis of pro-caspase-1 and cleaved-caspase-1. **B.** Quantification of the ratio cleaved/pro-caspase-1. Data are represented as mean ± SD and statistical significance was analyzed by one-way ANOVA followed by Tukey's test (**B**: (7,16) = 20.35, *P*<0.0001. Statistical significance is presented as **P*<0.05, ***P*<0.01, ****P*<0.001 and *****P*<0.0001. ns = not significant, n=3 independent cell culture preparations. Exact *P* values are shown in *section 11, table 21 B.* ROUT test (Q = 1%) showed no outliers. Shapiro-Wilk test showed no violation of normality. No exclusion criteria were pre-determined and no samples were excluded from the analysis.

4 Discussion

4.1 Microglial senescence in the hippocampus of aged Tau22 mice

Our findings demonstrated that lamin B1 is significantly reduced in microglia in the stratum radiatum close to the CA1 cell body region of Tau22 mice in comparison to microglia in the same anatomical region of WT mice. Interestingly, loss of lamin B1 was also detected in microglia of rats bearing an amyotrophic lateral sclerosis (ALS) linked SOD1-mutation and was associated with senescence (Trias et al., 2019), suggesting that microglial senescence might be a common characteristic of several neurodegenerative diseases.

Lamin B1 plays a key role in maintaining the structural and functional integrity of the nucleus (Garvalov et al., 2019; Vergnes et al., 2004). Moreover, loss of lamin B1 has been associated with the DNA damage response (Gonzalo, 2014). For example, silencing of lamin B1 in human osteosarcoma U-2-OS and colorectal carcinoma HCT116 cell lines increased the formation of double-strand breaks, indicated by phosphorylation of histone H2AX (yH2AX) and disturbed DNA damage repair mechanisms (Butin-Israeli et al., 2015). In this thesis work we demonstrated that microglia close to the CA1 cell body region of aged Tau22 mice showed increased formation of yH2AX foci and loss of lamin B1 in comparison to microglia close to the CA1 cell body region of WT mice. Our findings contribute to previous findings showing an association between the loss of lamin B1 and phosphorylation of H2Av, a chimera of H2AZ and H2AX, in the brains of tau transgenic Drosophila. Additionally, the study demonstrated that neurons in *post-mortem* brains of AD patients show a significant decline in lamin B1 (Frost et al., 2016).

Under physiological conditions, microglia contribute to the development of a neurogenic niche through their fundamental role on neuronal proliferation, differentiation and survival of newborn neurons into the existing, developing thereby contributing to the formation of a functional neuronal network (Gemma and Bachstetter, 2013; Pérez-Rodríguez et al., 2021). Nevertheless, microglia activation and subsequent cerebral inflammation can be deleterious for adult hippocampal neurogenesis (Ekdahl et al., 2003; Monje et al., 2003). For example, intracortical infusions of lipopolysaccharide (LPS) in adult rats resulted in microglial activation and correlated with impaired neurogenesis. Suppression of microglial

activation using minocycline reduced inflammation and restored hippocampal neurogenesis (Ekdahl et al., 2003). Interestingly, increased DNA damage has been associated with the proinflammatory profile expressed by senescent cells. For example, primary irradiated (IR) WI-38 human embryonic fibroblasts exhibited DNA damage, which was accompanied by release of the SASP, in particular IL-6 and IL-8 upon entering an IR-induced senescent state (Isermann, 2020). In line with this, another study demonstrated that persistent DNA damage signaling in IR HCA2 human foreskin fibroblasts correlated with the release of IL-6 from these cells (Rodier, 2009). Lastly, the persistent DNA damage response in OIS primary human fetal lung fibroblasts was typified by the secretion of IL-6, IL-8 and CXCL1 (Chen et al., 2015). Here, we demonstrated that isolated adult hippocampal microglia from Tau22 – which are at least partially characterized by an increase in the DNA damage marker yH2AX - expressed a proinflammatory gene expression profile that is likely part of the SASP. Our findings are in line with previously reported findings on increased *Il-6* and *Il-1b* gene expression levels, which were part of the SASP in neurons containing NFTs (Musi et al., 2018) and microglia isolated from cortices of PS19 mice (Bussian et al., 2018).

Taken together, this thesis work confirmed the presence of senescent microglia in a mouse model of tauopathy (Tau22 mice). Although no behavioral experiments were performed in this study, the Tau22 is a valuable model that recapitulates most of the aspects of the neuropathological spectrum of primary tauopathies and also aspects of secondary, AD-like tau pathology. Future experiments could test whether senolytics protect from tau pathology-associated cognitive dysfunction.

A potential limitation of the present study is that we cannot conclude that microglial senescence *in vivo* is driven by the accumulation of pathogenic tau, due to its crossectional nature. Future directions should investigate the correlation between the accumulation of pathological tau over time and assessing the occurrence of senescent microglia over time.

4.2 The effect of monomeric tau on the induction of microglial senescence: nuclear changes and formation of a SASP

Despite the presence of senescent microglia in the brains of AD patients as well as mouse models of tauopathy, it remains unknown what drives microglia into a senescent state. Hence, this thesis work aimed to study whether tau is able to induce senescence in microglia.

When treating primary microglia with two different concentrations of tau, we detected an increased $p16^{INK4a}$ and $p21^{WAF}$ protein expression independent of the concentration used. In contrast, neither tau concentration increased the gene expression levels of *Cdkn1a (*$p21^{WAF1}$). Interestingly, however, exposure to 15 nM but not 5 nM of tau increased the gene expression levels of *Cdkn2a (*$p16^{INK4A}$). A potential explanation for the inconsistency in these results might be that $p21^{WAF1}$ is more important for initiating senescence, whereas $p16^{INK4a}$ was shown to be more involved in its maintenance (Stein et al., 1999). Therefore, it could be possible that microglia exposed to 15 nM of tau show increased *Cdkn1a* ($p21^{WAF1}$) gene expression at an earlier timepoint. Another potential explanation for the lack of *Cdkn1a* ($p21^{WAF1}$) expression in our model is that senescent cells are highly variable in their expression of senescence-associated mRNA levels, resulting in a heterogenous population of cells (Cohn et al., 2022; Wiley et al., 2017). Hence, it remains possible that the fraction of microglia expressing *Cdkn1a* is too small to show changes on the population level.

Increased expression of the classical cell cycle markers $p16^{INK4a}$ and $p21^{WAF1}$ are widely used to study cellular senescence (González-Gualda et al., 2021; Sikora et al., 2013). However, expression of these markers was also found to be upregulated in quiescent cells, terminal differentiated cells, including fibroblasts and actived macrophages (Blagosklonny, 2011; Ogrodnik, 2021). In line with this, ectopical expression of $p16^{INK4a}$ resulted in cell cycle arrest, but did not elicit release of the SASP (Coppé et al., 2011). These findings confirm that the use of classical cell cycle arrest markers alone are not sufficient to identify or characterize senescence and raises doubts about the sole use of these markers in earlier studies on senescence in the context of tauopathies (Musi et al.,

2018; Bussian et al., 2018). To overcome this issue, the work present here pointed out that further biomarkers are essential to adequately characterize senescence in microglia.

For instance, despite increased expression of $p16^{INK4a}$ and $p21^{WAF1}$ irrespective of the tau concentration, only treatment with 15 nM of tau resulted in loss of lamin B1. Interestingly, loss of lamin B1 was also present in microglia close to the stratum radiatum close to the CA1 cell body region of Tau22 mice (Fig. 4). Furthermore, a decline in lamin B1 levels was also observed in neurons of tau transgenic Drosophila (Frost et al., 2016) and senescent astrocytes of Parkinson's Disease (PD) patients (Chinta et al., 2018), suggesting that loss of lamin B1 is a common characteristic shared by senescent cells during neurodegenerative conditions. Next, we found that primary murine microglia exposed to tau 15 nM, but not 5 nM showed increased levels of yH2AX. This finding is supported by our *in vivo* data showing that microglia in the stratum radiatum close to the CA1 cell body region of Tau22 mice showed increased levels of yH2AX.

Nuclear lamins as well as double-stranded breaks are associated with nuclear changes, such as heterochromatin remodeling (Butin-Israeli et al., 2015; Camps et al., 2015). Heterochromatin remodeling is not only part of chronological aging, but also premature aging (Lee et al., 2020) and neurodegeneration (Gil et al., 2021; Jury et al., 2020). More specifically, loss of heterochromatin mark H3K9me3 has been associated with genomic instability during cellular senescence (Sidler et al., 2017; Tsurumi and Li, 2012; Zhang et al., 2021). Interestingly, neurons and astrocytes in the spinal cord and motor cortex of C9ALS/FTD BAC mice, a model harboring mutations present in ALS and FTD patients, are characterized by the loss H3K9me3 (Jury et al., 2020). Furthermore, pyramidal neurons in the CA1 region of AD patients show a progressive decline in H3K9me3 over the course of disease (Gil et al., 2021). Here, we showed that microglia treated with the highest concentration of tau presented with loss of H3K9me3, supporting the idea that heterochromatin loss in tauopathies could be a sign of cellular senescence.

Neuroinflammation has been considered a key feature in the brain during aging, tauopathies and other forms of dementia (Bauer et al., 1991; Kiecolt-Glaser et al., 2003; Lasry & Ben-Neriah, 2015; Rea et al., 2018). Heightened microglial activation preceding

the formation of NFTs is one of the earliest events observed in a mouse model of tauopathy (Yoshiyama et al., 2007). More recently, studies have shown that early microglia activation in the context of tauopathies is driven by soluble forms of tau, rather than fibrils (Ising et al., 2019; Perea et al., 2018). Here, we report that primary murine microglia exposed to the highest concentration of tau responded with the release of (pro)inflammatory factors, which are not the result of cellular cytotoxicity but are likely part of the SASP. Noteworthy, the final composition of the SASP in senescent cells can vary depending on the inducer as well as cell type investigated (Basisty et al., 2020; Coppé et al., 2008). Interestingly, the release of various SASP factors presented in this study, such as IL-1β and IL-6 have been negatively associated with hippocampal neurogenesis. For example, cultured neural progenitor cells (NPC) of adult rats showed an impaired neurogenesis after exposure to IL-1β (Ryan et al., 2013). In addition, IL-6 mediated inflammation inhibited neurogenesis after cranial irradiation (Monje et al., 2003). On the other hand, release of IL-10, which is decreased in senescent microglia, was found to regulate adult hippocampal neurogenesis by promoting cell cycle exit (Pereira et al., 2015). These findings might suggest that cellular senescence, and the SASP in particular, contribute to impairments in AHN and that preventing release of the SASP might be a potential treatment strategy to restore AHN. However, whether microglial senescence contributes to impairments in AHN as observed in tauopathies (Komuro et al., 2015; Moreno-Jiménez et al., 2019; Zheng et al., 2020) requires further investigations.

Despite incomplete understanding on mechanisms involved in SASP formation, research has demonstrated that the transcriptional factor nuclear factor κB (NF-κB) was the highest associated regulator of the SASP gene pathway (Musi et al., 2018). Activation of NF-κB is required for the expression of various SASP factors, including IL-1β, IL-6, TNF-α and CXCL1 (Rodier and Campisi, 2011), all factors that have been shown in this study to be released by senescent microglia. Although these finding demonstrate that targeting NF-κB signaling might be a therapeutic approach during cellular senescence, it should be considered that targeting this pathway will affect many more processes, including mitochondrial dynamics, respiratory control, cellular development and survival (Albensi, 2019; Shishodia & Aggarwal, 2002) potentially causing side effects. Another interesting pathway that might be involved in driving the SASP is the cGAS-STING pathway (Glück

et al., 2017). During senescence, degradation of laminB1 is followed by the formation of abnormal cytoplasmic DNA fragments, called cytosolic chromatin fragments (CCFs), which act as a ligand for the cGAS-STING pathway (Glück et al., 2017). This triggers the production of various inflammatory cytokines, chemokines and interferons (IFNs) (Chen et al., 2018; Loo et al., 2020). In this study, we did not observe any CCF formation after treatment with tau. However, it could be that tau itself acts as a ligand for cGAS-STING signaling as previously demonstrated (Jin et al., 2021) and that CCF formation is sufficient, but not necessary for the activation of the cGAS-STING pathway. Another possibility might be that the microglia in our study are in an intermediate, rather than deep senescent state in which lamin B1 levels are still stable enough to prevent the formation of CCFs.

Together, our data show that monomeric tau is a driver of microglial senescence. Despite the fact that exposure to 5 nM tau increased the expression of cell cycle markers, it did not result in loss of either lamin B1 or H3K9me3 and did not induce release of a SASP. This raises questions about the cellular state of these cells. Although we cannot rule out that longer 5 nM tau-treated microglia would finally enter a full senescent state, our results still emphasize the importance of using multiple biomarkers to adequately assess the senescent state of cells at a given time point. Further studies are warranted to investigate the exact mechanism(s) by which monomeric tau induces senescence in microglia and how this affects bystander cells. In addition, future directions should extent on investigating pathways that are involved in formation of the SASP during microglial senescence.

4.3 The outcome of tau-induced microglial senescence: functional and morphological changes

Senescent cells also present with functional disabilities, such as impairments in migration and phagocytosis. Microglia are the main phagocytic cells in the CNS that serve to maintain homeostasis under physiological conditions and to respond to injury or infection (Colonna & Butovsky, 2017; Galloway et al., 2019). In order for microglia to efficiently phagocytose, they need to be able to properly migrate towards the site of insult (Kettenmann et al., 2011; Scheiblich & Bicker, 2015). Interestingly, young adult 5xFAD transgenic mice, an AD mouse model, presented with hypophagocytic microglia that were

impaired in their capability to clear β-amyloid plaques (Hellwig et al., 2015). Moreover, microglia that phagocytose tau-aggregate containing neurons present with a senescent-like phenotype afterwards, characterized by the loss of phagocytic capabilities (Brelstaff et al., 2021). Not only did our results show that pre-treatment with the highest concentration of tau resulted in microglia with reduced tau clearance capabilities but also impaired in migratory capacity. In addition to functional disabilities, senescent cells present with morphological alterations, including enlargements in cell size. Morphological alterations might result in the loss of proper migration in reponse to a threat. Strikingly, loss of migratory capability was related to morphological changes as a result of cellular senescence (Moujaber et al., 2019; Nishio & Inoue, 2005; Reed et al., 2001; Wang, 1985). To support these findings, the findings presented in this study showed that exposure to the highest concentration of tau significantly decreased the migration distance and speed in primary murine microglia. Interestingly, however, a non-significant trend towards reduction in migration distance and speed was also observed after exposure to the lower tau concentration. Together with the increased expression in $p16^{INK4a}$ and $p21^{WAF1}$, it might be hypothesized that microglia treated with the lower tau concentration have entered an inactive, quiescent phase, which impairs their migratory capability in the short term. Given this, an examination of the migration time and speed over a longer time period might be valuable to study whether the migratory capacity can be restored despite the tau treatment.

Interestingly, monomeric tau was found to be released in the brain interstitial fluid (ISF), the fluid surrounding the parenchymal cells of the brain and spinal cord (Shetty & Zanirati, 2020). Strikingly, endogenous tau can be detected in the ISF of WT mice in a concentration significantly higher than in CSF and in P301S human tau transgenic mice, murine as well as human tau were detectable in the ISF before the onset of neurodegeneration (Yamada et al., 2011), suggesting that microglia are constantly exposed to monomeric tau. Since we demonstrate that monomeric tau can induce microglial senescence, it might be speculated that senescence-mediated inflammation, subsequently reduced tau clearance represents a key driver of tau seeding, aggregation and spreading (Ising et al., 2019; Langworth-Green et al., 2023; Stancu et al., 2019).

Ultimately, senescent microglia may be part of a a vicious cycle that further drives neuronal pathology and death.

4.4 The contribution of the NLRP3 inflammasome to microglial senescence *in vitro* and *in vivo*

Suppression of NLRP3-mediated inflammation was shown to be protective against various age-related diseases. For example, NLRP3 deficiency extended the lifespan and protected against cardiac aging in C57/BL6/J mice (Marín-Aguilar et al., 2020), protected against the aging phenotype and inflammation in Hutchinson-Gilford Progeria Syndrome (HGPS) patient-derived skin fibroblasts (González-Dominguez et al., 2021) and significantly reduced microglia-mediated tau pathology and cognitive deficits in Tau22 mice (Ising et al., 2019). Although these findings highlight the contribution of the NLRP3 inflammasome to inflammation-driven disease pathology, the mechanism(s) underlying NLRP3-driven inflammation are poorly studied. Since activation of the NLRP3 inflammasome has been associated with inflammaging (Sebastian-Valverde and Pasinetti, 2020), it could be speculated that activation of NLRP3 is associated with cellular senescence. Therefore, the present study aimed to better understand the contribution of the NLRP3 inflammasome to microglial senescence in the context of tauopathies.

The data presented in this study demonstrated that the NLRP3 inflammasome is activated in an *in vitro* model of microglial senescence induced by tau. Interestingly, inhibition and deletion of the NLRP3 inflammasome was protective against senescence-associated cell cycle arrest in murine primary microglia after exposure to monomeric tau. These results were supported by our *in vivo* findings, showing that microglia from *Nlrp3*$^{-/-}$ mice are protected against loss of lamin B1, cell cycle arrest and increased expression of the SASP.

Ablation of the NLRP3 inflammasome *in vitro* significantly reduced, but did not completely prevent the release of IL-1β, IL-6, TNF-α and CXCL1. However, the release of other SASP factors, including IL-10, IL-15, IL-27 and IL-33 remained unaffected, indicating that these factors are NLRP3 independent. In contrast, gene expression levels of IL-1β, IL-6, TNF-α were completely abolished in microglia isolated from Tau22/*Nlrp3*$^{-/-}$ mice *in vivo.* Nevertheless, one has to bear in mind that the gene expression levels of the SASP

presented *in vivo* might not represent the expression at the protein level. The isolation of adult hippocampal microglia only gives a limited number of cells to work with, which makes it difficult to perform an extensive analysis of the SASP at the protein level. Furthermore, analysis of SASP factors in the brain tissue is hindered by the fact that those factors are expressed only at an overall low concentration undetectable by commercial ELISA kits. To overcome this issue, an immunohistochemical approach could be used to detect the presence of selected SASP factors at the protein level in the future. In addition, more sensitive assays to detect SASP factors in the brain tissue should be employed to confirm their presence *in vivo*.

Overall, this study showed that activation of the NLRP3 inflammasome mediated microglial senescence *in vivo* as well as *in vitro*. A possible explanation for the mechanism by which NLRP3 inhibition ameliorated inflammation-mediated neurodegeneration in tau pathology in Tau22 mice (Ising et al., 2019) might be the fact that inhibition of the NLRP3 inflammasome reduces senescence-mediated inflammation and subsequently promotes AHN. However, the role of AHN in Tau22 mice as well as the contribution of the NLRP3 inflammasome to AHN should be further explored in the future. In addition, it might be possible that release of the SASP acts on tau kinases and phosphatases that can modulate tau pathology. For instance, hippocampal neurons exposed to different concentrations of IL-6 show activation of cyclin-dependent kinase 5 (CDK5) (Quintanilla et al., 2004), a key kinase involved in pathogenic tau phosphorylation (Hashiguchi et al., 2002; Liu et al., 2002; Lund et al., 2001), aggregation and tangle formation (Noble et al., 2003). In addition, rat pheochromocytoma PC12 cells treated with TNF-α showed a dose-dependent increase in CDK5 activation (Utreras et al., 2009). Lastly, macrophage-induced release of IL-1β resulted in increased phosphorylation of GSK3β, another kinase involved in tauopathies (Dolan and Johnson, 2010), in colorectal carcinoma cell lines (Kaler et al., 2009).

4.5 The role of STAT3 signaling during microglial senescence *in vitro*

The fact that inhibition of the NLRP3 inflammasome did not completely rescue release of the SASP encouraged us to find other potential pathways involved in senescence-mediated inflammation. Interestingly, activation of the NLRP3 inflammasome was shown

to be dependent on STAT3 activation. As an illustration, activation of STAT3 in macrophages in a mouse model of infection-induced apical periodontitis was strongly associated with the production of IL-1β. Remarkably, pharmacological inhibition of STAT3 significantly reduced the production of IL-1β and cleavage of caspase-1 (Zhu et al., 2023). Additionally, evidence showed that inhibition of STAT3 ameliorated LPS-induced acute lung injury in mice via suppression of the NLRP3 inflammasome (Cao et al., 2020).

Furthermore, STAT3 signalling has been shown to play a key role in the regulation of cytokines related to the SASP. For instance, premature senescent human TIG3 fibroblasts show activation of STAT3 and subsequent increased gene expression of *Il-1b* and *Il-6* (Kojima et al., 2012). In addition, oxidant-induced senescent primary human lung fibroblasts showed activation of STAT3 and release of IL-6 (Waters et al., 2019).

The findings presented in this study demonstrate that STAT3 signaling plays a key role in formation of the SASP during microglial senescence. Our analyses revealed that senescent microglia show a significant increase in phosphorylated (e.g., activated) STAT3, even after ablation of the NLRP3 inflammasome. Our findings are in line with previous results showing that activation of STAT3 is associated with cellular senescence. For instance, activation of STAT3 has been shown to drive premature senescence in human fibroblasts (Kojima et al., 2013), estrogen-depleted bone marrow mesenchymal stem cell senescence (Wu et al., 2020) and oxidative stress-induced senescence in human lung fibroblasts (Waters et al., 2019).

Furthermore, we explored whether NLRP3 independent activation of STAT3 accounts for the release of the SASP from senescent murine primary microglia. Our analyses revealed that inhibition of STAT3 completely prevented the release of all analyzed SASP factors, including IL-1β, IL-6, TNF-α, CXCL1, IL-15, IL-27 and IL-33. Additionally, inhibition of STAT3 drastically increased the release of anti-inflammatory IL-10. As previously discussed (section 3.2), the release of proinflammatory factors such as IL-1β and IL-6 were shown to negatively impact AHN. On the contrary, release of anti-inflammatory IL-10 was shown to positively correlate with AHN. It is intriguing to note that the release of IL-10 dramatically increased after pre-treatment with stattic, indicating that inhibition of

STAT3 significantly promotes an anti-inflammatory response by microglia. This finding is in line with a recent observation showing that deletion of STAT3 in microglia resulted in improved neurological function and inhibited early neuronal loss after subarachnoid haemorrhage (SAH) induction in mice. Strikingly, this was the result of STAT3-mediated inhibition of SAH-induced inflammation and promotion of anti-inflammatory signaling (Zheng et al., 2022). In addition, another study reported that microglial STAT3 activation contributed to IL-6 mediated death in hippocampal neurons in a mouse model of streptozotocin-induced type 1 Diabetes Mellitus (DM) (Yun et al., 2021). These findings strongly imply that microglial STAT3 activation contributes to inflammation-mediated neuronal death and subsequent cognitive impairment.

Interestingly, increased expression of phosphorylated STAT3 was also observed in microglia in aged PS19 mice (Litvinchuk et al., 2018). Moreover, inhibition of STAT3 using Stattic attenuated astrocyte activation and impairments in learning and memory in 5XFAD mice (Choi et al., 2020). Given the role of STAT3 in senescence and tau-mediated neurodegeneration, it is plausible to speculate that microglia in the stratum radiatum close to the CA1 cell body region of Tau22 mice express increased levels of phosphorylated STAT3, which could exacerbates cognitive dysfunction via tau pathology. Future work should further assess this and elucidate the contribution of microglial STAT3 signaling to AHN, neuronal apoptosis and cognitive decline in Tau22 mice.

4.6 Other mechanisms underlying tau-induced microglial senescence

Phosphorylated STAT3 has been shown to regulate mitochondrial dynamics (Rincon and Pereira, 2018) by interacting with the mitochondria-associated endoplasmic reticulum membranes (MAMs) (Su et al., 2020). The MAMs are a physical structure that connects the endoplasmic reticulum (ER) and mitochondria and plays a fundamental role in calcium (Ca^{2+}) homeostasis, autophagy, lipid metabolism, apoptosis, and tumor growth (Giorgi et al., 2015; Missiroli et al., 2018). More specifically, Ca^{2+} homeostasis between the ER and mitochondria is regulated by the inositol 1,4,5-trisphosphate receptor (IP3R) located on the ER membrane and by the voltage-dependent anion channel 1 (VDAC1) located on the outer membrane of mitochondria (OMM). The IP3Rs and VDAC1s are physically connected through the glucose-regulated protein 75 (GRP75), which creates the IP_3Rs-

GRP75-VDAC1 complex that is essential in ER-mitochondria Ca^{2+} trafficking (Giorgi et al., 2015; Liu & Yang, 2022; Missiroli et al., 2018). These findings illustrate the importance of STAT3-signaling in the regulation of mitochondrial dynamics.

Previously, VDAC1 was found to interact with Aβ and phosphorylated tau in postmortem brains of AD patients as well as AD mouse models (e.g., APP, APP/PS1 and 3XTg.AD mice) (Manczak and Reddy, 2012). More recently, recombinant human tau was shown to bind to the SAH hydrolase–like protein 1/inositol 1,4,5-trisphosphate receptor (IP3R)–binding protein released by IP_3 (AHCYL1/IRBIT), which is a modulator of IP_3R (Wischhof et al., 2022). IP_3R-mediated Ca^{2+} release has been associated with oxidative-stress induced senescence (Vijayan et al., 2022; Wischhof et al., 2022) and oncogene induced senescence (Wiel et al., 2014). However, the role of tau on the function of IP_3R in the context of microglial senescence remains unknown. Moreover, the role of tau on the function of GRP75 and VDAC1 is poorly understood and remains to be investigated.

Although mitochondria have the ability to buffer Ca^{2+} coming from the ER, excessive mitochondrial Ca^{2+} uptake leads to mitochondrial disruption, which contributes to leakage of Ca^{2+} in the cytoplasm (Lemasters et al., 2009; Rizzuto et al., 2012). Previous findings pointed out that senescent microglia have an increased mitochondrial mass (Lee et al., 2002; Martini and Passos, 2023), which might be indicative of mitochondrial swellings as a result of intracellular Ca^{2+} accumulation (Kobayashi et al., 2003; Li et al., 2018). In turn, this might cause mitochondrial membrane disruption and the release of cytosolic Ca^{2+} (Strubbe-Rivera et al., 2021).

Interestingly, the NLRP3 inflammasome is known to be activated by cytosolic Ca^{2+} (Elliott and Sutterwala, 2015; Murakami et al., 2012) and inhibition of IP_3R was shown to attenuate Ca^{2+}-mediated NLRP3 activation (Murakami et al., 2012). It remains unknown, however, whether Ca^{2+}-mediated NLRP3 inflammasome activation during microglial senescence is the result of alteration in IP_3R, GRP75 or VDAC1.

Together, these findings from the literature imply that STAT3 signaling is one likely potential cellular mechanism that drives senescence in microglia in tauopathies by binding

to components of the MAM, thereby altering ER-mitochondria Ca^{2+} trafficking, inducing mitochondrial damage and production of ROS and subsequently induce a DDR that triggers senescence and inflammation (Fig. 22).

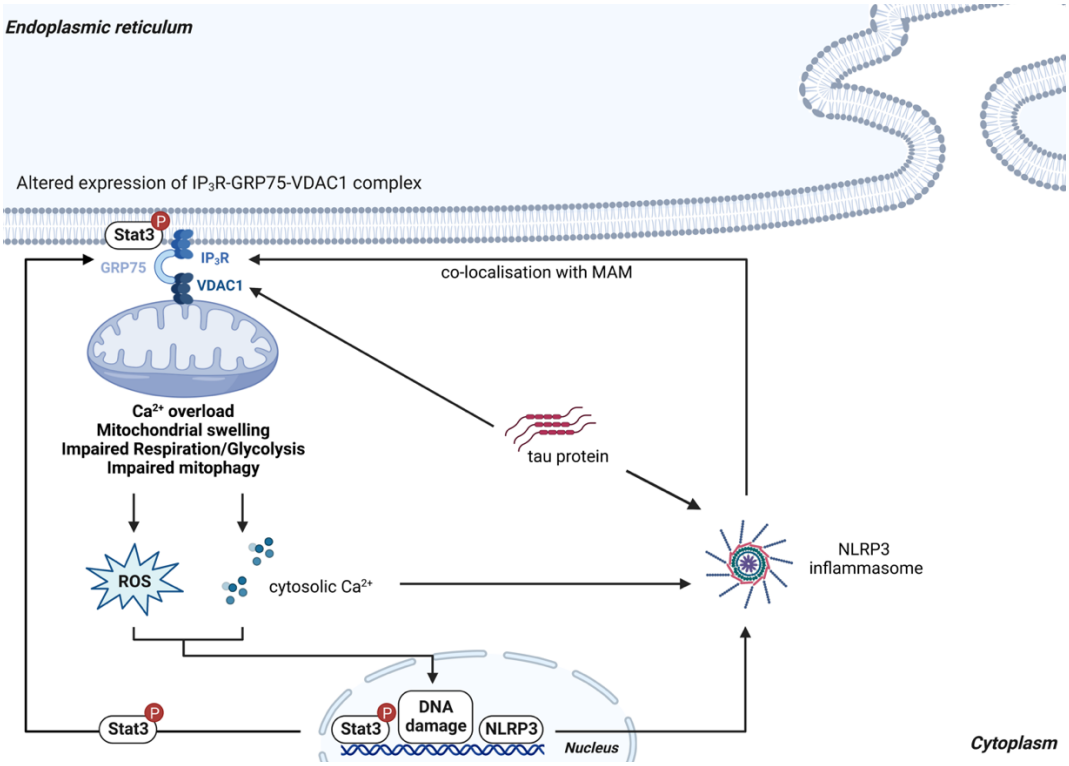

Fig. 22: Graphical representation of potential mechanism underlying tau-induced microglial senescence. Tau-induced microglia senescence is accompanied by changes in mitochondrial dynamics. Does tau modulate the activity of the IP3R-GRP75-VDAC1 complex, thereby impairing ER-mitochondrial Ca^{2+} trafficking and subsequently inducing mitochondrial dysfunction? Does phosphorylation of STAT3 modulate the activity of the IP3R-GRP75-VDAC1 complex in senescent microglia, consequently contributing to impaired mitochondrial dynamics? Is activation of the NLRP3 inflammasome triggered by the release of cytosolic Ca^{2+} from impaired mitochondria?

To end, it is plausible that mitochondrial dysfunction precedes microglial senescence and that this is driven by phosphorylation of STAT3. Future research will be needed to investigate if senescent microglia present with mitochondrial changes. In addition, future work should elucidate the role of STAT3 on mitochondrial dynamics and its potential contribution to microglial senescence.

5 Abstract

Tauopathies are a group of heterogenous neurodegenerative diseases in which patients clinically present with symptoms ranging from cognitive and behavioral deficits to movement disabilities. Pathologically, tauopathies are defined by the abnormal accumulation and deposition of the tau protein in the brain. Aging is regarded as the main risk factor for the development of dementia, in particular Alzheimer's disease (AD), which is the most prevalent form of tauopathies. Many physiological decrements underlying aging are linked to cellular senescence. Senescent cells are characterized by an irreversible growth arrest and formation of a potentially disease-modifying senescence-associated secretory profile (SASP) which has been recently shown to contribute to disease progression.

Microglia, the immune cells of our brain, are susceptible to entering a senescent state during age-related conditions. In addition, senescent microglia have been identified in the brains of tau transgenic mice and patients suffering from tauopathies even before the development of disease pathology. Interestingly, activation of the NLRP3 inflammasome has been associated with cellular senescence and was shown to drive tau accumulation and accelerate tau-mediated neurodegeneration in a mouse model of tauopathy. However, the role of the NLRP3 inflammasome for microglial senescence in the context of tauopathies remains unknown. Moreover, it is not clear whether tau can act as a driver of senescence in microglia and how the NLRP3 inflammasome might contribute to this.

The aim of the present study was to investigate the presence of senescent microglia in a mouse model of tauopathy and the impact of the NLRP3 inflammasome on the development of microglial senescence in this context. In addition, we aimed to investigate the effect of monomeric tau on the induction of microglial senescence and the contribution of the NLRP3 inflammasome to tau-induced microglial senescence *in vitro*.

We demonstrated that microglia of Tau22 mice showed elevated gene expression levels of *Cdkn2a*, *Il-1b, Tnfa, Cxcl1* as well as increasd yH2AX foci and loss of lamin B1 in comparison to WT microglia. Deficiency in NLRP3 normalized the levels of *Cdkn2a, Il-1b, Tnfa, Cxcl1* and lamin B1. In vitro, we showed that exposure to tau increased levels of cell cycle arrest and DNA damage markers, induced loss of the nuclear envelope protein lamin

B1 and the histone marker H3K9me3, impaired phagocytosis and migration, altered the cell morphology and resulted in formation of a SASP, collectively suggesting the cells to be in a senescent state. Ablation of NLRP3 *in vitro* rescued cell cycle arrest and ameliorated release of the SASP.

Lastly, we identified a NLRP3-independent contributer to the SASP, namely activation of STAT3. Here, we showed that activation of STAT3 is a key driver of the SASP and that it controls activation of the NLRP3 inflammasome.

In conclusion, we demonstrated that senescent microglia emerge in a tauopathy mouse model and that NLRP3-deficiency mitigated microglial senescence *in vivo*. Furthermore, we developed a model to study microglial senescence in culture and found that the NLRP3 inflammasome is a mediator in tau-induced microglial senescence. Lastly, we found a NLRP3 independent signaling pathway, namely STAT3, to be a key driver of the SASP. Employing this model in the future will be instrumental to investigate the mechanism underlying STAT3 induced microglial senescence, focusing on mitochondria dysfunction and the interaction between STAT3 and NLRP3.

6 List of Figures

12	Senescent murine primary microglia showed loss of tau clearance capabilities	63
13	Senescent murine primary microglia showed impaired migratory behavior	64
14	Senescent murine primary microglia presented with changes in cytoskeletal morphology	66
15	Senescent murine primary microglia show activation of the NLRP3 inflammasome	68
16	Inhibition of the NLRP3 inflammasome using CRID3 prevented the senescent phenotype in murine primary microglia	70
17	Nlrp3 deficiency *(Nlrp3$^{-/-}$)* ameliorated the senescent phenotype in murine primary microglia	72
18	Senescent microglia showed loss of Parkin which is rescued upon NLRP3 inhibition	74
19	Tau-treated murine primary microglia exhibited NLRP3 independent phosphorylation of STAT3	75
20	Activation of STAT3 drives the SASP in senescent murine primary microglia	76
21	Stattic prevented NLRP3 inflammasome activation in senescent murine primary microglia	77
22	Graphical representation of potential mechanism underlying tau-induced microglial senescence	89

7 List of tables

8 References

Acosta, JC., Banito, A., Wuestefeld, T., Georgilis, A., Janich, P., Morton, JP., Athineos, D., Kang, TW., Lasitschka, F., Andrulis, M. A complex secretory program orchestrated by the inflammasome controls paracrine senescence. Nature Cell Biology 2013; 15(8): 978–990

Agarwal, P., DeInnocentes, P., Bird, RC. Evaluation of 14-3-3 sigma as a potential partner of p16 in quiescence and differentiation. In Vitro Cellular & Developmental Biology 2018; 54(9): 658–665

Agarwal, P., Sandey, M., DeInnocentes, P., Bird, RC. Tumor suppressor gene p16/INK4A/CDKN2A-dependent regulation into and out of the cell cycle in a spontaneous canine model of breast cancer. Journal of Cellular Biochemistry 2013; 114(6), 1355–1363

Aiello, A., Farzaneh, F., Candore, G., Caruso, C., Davinelli, S., Gambino, CM., Ligotti, M. E., Zareian, N., Accardi, G. Immunosenescence and Its Hallmarks: How to Oppose Aging Strategically? A Review of Potential Options for Therapeutic Intervention. Frontiers in Immunology 2019; 10: 2247

Albensi, BC. What Is Nuclear Factor Kappa B (NF-κB) Doing in and to the Mitochondrion? Frontiers in Cell and Developmental Biology 2019; 7: 154

Alessio, N., Aprile, D., Cappabianca, S., Peluso, G., Di Bernardo, G., Galderisi, U. Different Stages of Quiescence, Senescence, and Cell Stress Identified by Molecular Algorithm Based on the Expression of Ki67, RPS6, and Beta-Galactosidase Activity. International Journal of Molecular Sciences 2021; 22(6): 3102

Alhazzani, K., Ahmad, SF., Al-Harbi, NO., Attia, SM., Bakheet, SA., Sarawi, W., Alqarni, SA., Algahtani, M., Nadeem, A. Pharmacological Inhibition of STAT3 by Stattic Ameliorates Clinical Symptoms and Reduces Autoinflammation in Myeloid, Lymphoid, and Neuronal Tissue Compartments in Relapsing–Remitting Model of Experimental Autoimmune Encephalomyelitis in SJL/J Mice. Pharmaceutics 2021; 13(7): 925

Ampie, L., McGavern, DB. Immunological defense of CNS barriers against infections. Immunity 2022; 55(5): 781–799

Asai, H., Ikezu, S., Tsunoda, S., Medalla, M., Luebke, J., Haydar, T., Wolozin, B., Butovsky, O., Kügler, S., Ikezu, T. Depletion of microglia and inhibition of exosome synthesis halt tau propagation. Nature Neuroscience 2015; 18(11): 1584–1593

Augusto-Oliveira, M., Arrifano, GP., Lopes-Araújo, A., Santos-Sacramento, L., Takeda, P. Y., Anthony, DC., Malva, JO., Crespo-Lopez, ME. What Do Microglia Really Do in Healthy Adult Brain? Cells 2019; 8(10): 1293

Avila, J., Lucas, JJ., Perez, M., Hernandez, F. Role of tau protein in both physiological and pathological conditions. Physiological Reviews 2014; 84(2): 361–384

Avila, J., Santa-María, I., Pérez, M., Hernández, F., Moreno, F. Tau phosphorylation, aggregation, and cell toxicity. Journal of Biomedicine & Biotechnology 2006; 3: 74539

Aw, D., Silva, AB., Palmer, DB. Immunosenescence: Emerging challenges for an ageing population. Immunology 2007; 120(4): 435–446

Bachmann, S., Bell, M., Klimek, J., Zempel, H. Differential Effects of the Six Human TAU Isoforms: Somatic Retention of 2N-TAU and Increased Microtubule Number Induced by 4R-TAU. Frontiers in Neuroscience 2021; 15: 643115

Bai, J., Wang, Y., Wang, J., Zhai, J., He, F., & Zhu, G. (2020). Irradiation-induced senescence of bone marrow mesenchymal stem cells aggravates osteogenic differentiation dysfunction via paracrine signaling. American Journal of Physiology. Cell Physiology 2020; 318(5): 1005–1017

Baker, D. J., & Petersen, R. C. Cellular senescence in brain aging and neurodegenerative diseases: Evidence and perspectives. The Journal of Clinical Investigation 2018; 128(4): 1208–1216

Baker, D. J., Wijshake, T., Tchkonia, T., LeBrasseur, N. K., Childs, B. G., van de Sluis, B., Kirkland, J. L., & van Deursen, J. M. Clearance of p16Ink4a-positive senescent cells delays ageing-associated disorders. Nature 2011; 479(7372): 232–236

Barbier, P., Zejneli, O., Martinho, M., Lasorsa, A., Belle, V., Smet-Nocca, C., Tsvetkov, P. O., Devred, F., & Landrieu, I. Role of Tau as a Microtubule-Associated Protein: Structural and Functional Aspects. Frontiers in Aging Neuroscience 2019; 11: 204

Basisty, N., Kale, A., Jeon, O. H., Kuehnemann, C., Payne, T., Rao, C., Holtz, A., Shah, S., Sharma, V., Ferrucci, L., Campisi, J., & Schilling, B. A proteomic atlas of

senescence-associated secretomes for aging biomarker development. PLOS Biology 2020; 18(1), e3000599

Bauer, J., Strauss, S., Schreiter-Gasser, U., Ganter, U., Schlegel, P., Witt, I., Yolk, B., & Berger, M. Interleukin-6 and alpha-2-macroglobulin indicate an acute-phase state in Alzheimer's disease cortices. FEBS Letters 1991; 285(1): 111–114

Ben-Porath, I., & Weinberg, R. A. The signals and pathways activating cellular senescence. The International Journal of Biochemistry & Cell Biology 2005; 37(5): 961–976

Beyne-Rauzy, O., Recher, C., Dastugue, N., Demur, C., Pottier, G., Laurent, G., Sabatier, L., & Mansat-De Mas, V. Tumor necrosis factor alpha induces senescence and chromosomal instability in human leukemic cells. Oncogene 2004; 23(45), Article 45

Bhat, R., Crowe, EP., Bitto, A., Moh, M., Katsetos, CD., Garcia, FU., Johnson, FB., Trojanowski, JQ., Sell, C., Torres, C. Astrocyte senescence as a component of Alzheimer's disease. PloS One 2012; 7(9): e45069

Birch, J., Gil, J. Senescence and the SASP: Many therapeutic avenues. Genes & Development 2020; 34(23–24): 1565–1576

Blagosklonny, MV. Cell cycle arrest is not senescence. Aging 2011; 3(2): 94–101

Bolós, M., Llorens-Martín, M., Jurado-Arjona, J., Hernández, F., Rábano, A., Avila, J. Direct Evidence of Internalization of Tau by Microglia In Vitro and In Vivo. Journal of Alzheimer's Disease 2016; 50(1): 77–87

Borodkina, AV., Shatrova, AN., Deryabin, PI., Griukova, AA., Abushik, PA., Antonov, S. M., Nikolsky, NN., Burova, EB. Calcium alterations signal either to senescence or to autophagy induction in stem cells upon oxidative stress. Aging (Albany NY) 2016; 8(12): 3400–3416

Brelstaff, JH., Mason, M., Katsinelos, T., McEwan, WA., Ghetti, B., Tolkovsky, AM., Spillantini, MG. Microglia become hypofunctional and release metalloproteases and tau seeds when phagocytosing live neurons with P301S tau aggregates. Science Advances 2021; 7(43): eabg4980

Bromberg, J., Darnell, JE. The role of STATs in transcriptional control and their impact on cellular function. Oncogene 2000; 19(21): 2468–2473

Bussian, TJ., Aziz, A., Meyer, CF., Swenson, BL., van Deursen, JM., Baker, DJ. Clearance of senescent glial cells prevents tau-dependent pathology and cognitive decline. Nature 2018; 562(7728): 578–582

Butin-Israeli, V., Adam, SA., Jain, N., Otte, GL., Neems, D., Wiesmüller, L., Berger, SL., Goldman, RD. Role of lamin b1 in chromatin instability. Molecular and Cellular Biology 2015; 35(5): 884–898

Caldeira, C., Cunha, C., Vaz, AR., Falcão, AS., Barateiro, A., Seixas, E., Fernandes, A., Brites, D. Key Aging-Associated Alterations in Primary Microglia Response to Beta-Amyloid Stimulation. Frontiers in Aging Neuroscience 2017; 9: 277

Caldeira, C., Oliveira, AF., Cunha, C., Vaz, AR., Falcão, AS., Fernandes, A., Brites, D. Microglia change from a reactive to an age-like phenotype with the time in culture. Frontiers in Cellular Neuroscience 2014; 8: 152

Campisi, J., Di Fagagna, FD. Cellular senescence: When bad things happen to good cells. Nature Reviews Molecular Cell Biology 2007; 8(9): 729–740

Camps, J., Erdos, MR., Ried, T. The role of lamin B1 for the maintenance of nuclear structure and function. Nucleus 2015; 6(1): 8–14

Cao, D., Li, XH., Luo, XG., Yu, HM., Wan, LS., Wei, L., Ren, Y. Phorbol myristate acetate induces cellular senescence in rat microglia in vitro. International Journal of Molecular Medicine 2020; 46(1): 415–426

Cao, F., Tian, X., Li, Z., Lv, Y., Han, J., Zhuang, R., Cheng, B., Gong, Y., Ying, B., Jin, S., Gao, Y. Suppression of NLRP3 Inflammasome by Erythropoietin via the EPOR/JAK2/STAT3 Pathway Contributes to Attenuation of Acute Lung Injury in Mice. Frontiers in Pharmacology 2020; 11: 306

Chapman, J., Fielder, E., Passos, JF. Mitochondrial dysfunction and cell senescence: Deciphering a complex relationship. FEBS Letters 2019; 593(13): 1566–1579

Chen, H., Ruiz, PD., McKimpson, WM., Novikov, L., Kitsis, RN., Gamble, MJ. MacroH2A1 and ATM play opposing roles in paracrine senescence and the senescence-associated secretory phenotype. Molecular Cell 2015; 59(5): 719–731

Chen, K., Liu, J., Cao, X. CGAS-STING pathway in senescence-related inflammation. National Science Review 2018; 5(3): 308–310

Chen, M., Xiao, L., Dai, G., Lu, P., Zhang, Y., Li, Y., Ni, M., Rui, Y. Inhibition of JAK-STAT Signaling Pathway Alleviates Age-Related Phenotypes in Tendon Stem/Progenitor Cells. Frontiers in Cell and Developmental Biology 2021; 9: 650250

Chen, Q., Fischer, A., Reagan, JD., Yan, LJ., Ames, BN. Oxidative DNA damage and senescence of human diploid fibroblast cells. Proceedings of the National Academy of Sciences 1995; 92(10): 4337–4341

Chien, Y., Scuoppo, C., Wang, X., Fang, X., Balgley, B., Bolden, JE., Premsrirut, P., Luo, W., Chicas, A., Lee, CS., Kogan, SC., Lowe, SW. Control of the senescence-associated secretory phenotype by NF-κB promotes senescence and enhances chemosensitivity. Genes & Development 2011; 25(20): 2125–2136

Childs, BG., Durik, M., Baker, DJ., Van Deursen, JM. Cellular senescence in aging and age-related disease: From mechanisms to therapy. Nature Medicine 2015; 21(12): 1424–1435

Chinta, SJ., Woods, G., Demaria, M., Rane, A., Zou, Y., McQuade, A., Rajagopalan, S., Limbad, C., Madden, DT., Campisi, J., Andersen, JK. Cellular Senescence Is Induced by the Environmental Neurotoxin Paraquat and Contributes to Neuropathology Linked to Parkinson's Disease. Cell Reports 2018; 22(4): 930–940

Chinta, SJ., Woods, G., Rane, A., Demaria, M., Campisi, J., Andersen, JK. Cellular senescence and the aging brain. Experimental Gerontology 2015; 68: 3–7

Choi, M., Kim, H., Yang, EJ., Kim, HS. Inhibition of STAT3 phosphorylation attenuates impairments in learning and memory in 5XFAD mice, an animal model of Alzheimer's disease. Journal of Pharmacological Sciences 2020; 143(4): 290–299

Chu, CT., Ji, J., Dagda, RK., Jiang, JF., Tyurina, YY., Kapralov, AA., Tyurin, VA., Yanamala, N., Shrivastava, IH., Mohammadyani, D., Wang, KZQ., Zhu, J., Klein-Seetharaman, J., Balasubramanian, K., Amoscato, AA., Borisenko, G., Huang, Z., Gusdon, AM., Cheikhi, A., Cheikhi, A., Steer, EK., Wang, R., Baty, C., Watkins, S., Bahar, I., Bayir, H., Kagan, VE. Cardiolipin externalization to the outer mitochondrial membrane acts as an elimination signal for mitophagy in neuronal cells. Nature Cell Biology 2013; 15(10): 1197–1205

Codolo, G., Plotegher, N., Pozzobon, T., Brucale, M., Tessari, I., Bubacco, L., de Bernard, M. Triggering of inflammasome by aggregated α-synuclein, an inflammatory response in synucleinopathies. PloS One 2013; 8(1): e55375

Cohn, RL., Gasek, NS., Kuchel, GA., Xu, M. The heterogeneity of cellular senescence: Insights at the single-cell level. Trends in Cell Biology 2022; 33(1): 9-17

Colonna, M. TREMs in the immune system and beyond. Nature Reviews. Immunology 2003; 3(6): 445–453

Colonna, M., Butovsky, O. Microglia Function in the Central Nervous System During Health and Neurodegeneration. Annual Review of Immunology 2017; 35: 441–468

Congdon, EE., Kim, S., Bonchak, J., Songrug, T., Matzavinos, A., Kuret, J. Nucleation-dependent tau filament formation: The importance of dimerization and an estimation of elementary rate constants. The Journal of Biological Chemistry 2008; 283(20): 13806–13816

Coppé, JP., Desprez, PY., Krtolica, A., Campisi, J. The senescence-associated secretory phenotype: The dark side of tumor suppression. Annual Review of Pathology: Mechanisms of Disease 2010; 5: 99–118

Coppé, JP., Patil, CK., Rodier, F., Sun, Y., Muñoz, DP., Goldstein, J., Nelson, PS., Desprez, PY., Campisi, J. Senescence-Associated Secretory Phenotypes Reveal Cell-Nonautonomous Functions of Oncogenic RAS and the p53 Tumor Suppressor. PLOS Biology 2008; 6(12): e301

Coppé, JP., Rodier, F., Patil, CK., Freund, A., Desprez, PY., Campisi, J. Tumor suppressor and aging biomarker p16(INK4a) induces cellular senescence without the associated inflammatory secretory phenotype. The Journal of Biological Chemistry 2011; 286(42): 36396–36403

Corder, EH., Saunders, AM., Strittmatter, WJ., Schmechel, DE., Gaskell, PC., Small, G. W., Roses, AD., Haines, JL., Pericak-Vance, MA. Gene dose of apolipoprotein E type 4 allele and the risk of Alzheimer's disease in late onset families. Science 1993; 261(5123): 921–923

Correia-Melo, C., Marques, FD., Anderson, R., Hewitt, G., Hewitt, R., Cole, J., Carroll, B. M., Miwa, S., Birch, J., Merz, A. Mitochondria are required for pro-ageing features of the senescent phenotype. The EMBO Journal 2016; 35(7): 724–742

Cras, P., Kawai, M., Siedlak, S., Perry, G. Microglia are associated with the extracellular neurofibrillary tangles of Alzheimer disease. Brain Research 1991; 558(2): 312–314

Csak, T., Ganz, M., Pespisa, J., Kodys, K., Dolganiuc, A., & Szabo, G. Fatty acid and endotoxin activate inflammasomes in mouse hepatocytes that release danger signals to stimulate immune cells. Hepatology 2011; 54(1): 133–144

Cuollo, L., Antonangeli, F., Santoni, A., Soriani, A. The Senescence-Associated Secretory Phenotype (SASP) in the Challenging Future of Cancer Therapy and Age-Related Diseases. Biology 2020; 9(12): 485

Damani, MR., Zhao, L., Fontainhas, AM., Amaral, J., Fariss, RN., Wong, WT. Age-related Alterations in the Dynamic Behavior of Microglia. Aging Cell 2011; 10(2): 263–276

de Zoete, MR., Palm, NW., Zhu, S., Flavell, RA. Inflammasomes. Cold Spring Harbor Perspectives in Biology 2014; 6(12): a016287

Dela Cruz, CS., Kang, MJ. Mitochondrial Dysfunction and Damage Associated Molecular Patterns (DAMPs) in Chronic Inflammatory Diseases. Mitochondrion 2018; 41: 37–44

DeVos, SL., Corjuc, BT., Oakley, DH., Nobuhara, CK., Bannon, RN., Chase, A., Commins, C., Gonzalez, JA., Dooley, PM., Frosch, MP., Hyman, BT. Synaptic Tau Seeding Precedes Tau Pathology in Human Alzheimer's Disease Brain. Frontiers in Neuroscience 2018; 12: 267

Di Micco, R., Krizhanovsky, V., Baker, D., di Fagagna, F. Cellular senescence in ageing: From mechanisms to therapeutic opportunities. Nature Reviews Molecular Cell Biology 2021; 22(2): 75–95

Didonna, A. Tau at the interface between neurodegeneration and neuroinflammation. Genes and Immunity 2020; 21(5): 288–300

Dodig, S., Čepelak, I., Pavić, I. Hallmarks of senescence and aging. Biochemia Medica 2019; 29(3): 483–497

Dolan, PJ., Johnson, GV. The role of tau kinases in Alzheimer's disease. Current Opinion in Drug Discovery & Development 2010; 13(5): 595–603

Duez, H., Pourcet, B. Nuclear Receptors in the Control of the NLRP3 Inflammasome Pathway. Frontiers in Endocrinology (Lausanne) 2021; 12: 630536

Ekdahl, CT., Claasen, JH., Bonde, S., Kokaia, Z., Lindvall, O. Inflammation is detrimental for neurogenesis in adult brain. Proceedings of the National Academy of Sciences of the United States of America 2013; 100(23): 13632–13637

Elhage, R., Jawien, J., Rudling, M., Ljunggren, HG., Takeda, K., Akira, S., Bayard, F., Hansson, GK. Reduced atherosclerosis in interleukin-18 deficient apolipoprotein E-knockout mice. Cardiovascular Research 2003; 59(1): 234–240

Elliott, EI., Sutterwala, FS. Initiation and perpetuation of NLRP3 inflammasome activation and assembly. Immunological Reviews 2015; 265(1): 35–52

Erlich, Z., Shlomovitz, I., Edry-Botzer, L., Cohen, H., Frank, D., Wang, H., Lew, AM., Lawlor, KE., Zhan, Y., Vince, JE., Gerlic, M. Macrophages, rather than DCs, are responsible for inflammasome activity in the GM-CSF BMDC model. Nature Immunology 2019; 20(4): 397–406

Eysert, F., Kinoshita, PF., Mary, A., Vaillant-Beuchot, L., Checler, F., Chami, M. Molecular Dysfunctions of Mitochondria-Associated Membranes (MAMs) in Alzheimer's Disease. International Journal of Molecular Sciences 2020; 21(24): 9521

Farmer, KM., Ghag, G., Puangmalai, N., Montalbano, M., Bhatt, N., Kayed, R. P53 aggregation, interactions with tau, and impaired DNA damage response in Alzheimer's disease. Acta Neuropathologica Communications 2020; 8(1): 132

Forrester, JV., McMenamin, PG., Dando, SJ. CNS infection and immune privilege. Nature Reviews Neuroscience 2018; 19(11): 655–671

Freund, A., Laberge, RM., Demaria, M., Campisi, J. Lamin B1 loss is a senescence-associated biomarker. Molecular Biology of the Cell 2012; 23(11): 2066–2075

Friedhoff, P., von Bergen, M., Mandelkow, EM., Davies, P., Mandelkow, EA nucleated assembly mechanism of Alzheimer paired helical filaments. Proceedings of the National Academy of Sciences of the United States of America 1998; 95(26): 15712–15717

Frost, B., Bardai, FH., Feany, MB. Lamin Dysfunction Mediates Neurodegeneration in Tauopathies. Current Biology 2016; 26(1): 129–136

Frost, B., Hemberg, M., Lewis, J., Feany, MB. Tau promotes neurodegeneration through global chromatin relaxation. Nature Neuroscience 2014; 17(3): 357–366

Frost, JL., Schafer, DP. Microglia: Architects of the Developing Nervous System. Trends in Cell Biology 2016; 26(8): 587–597

Gaikwad, S., Puangmalai, N., Bittar, A., Montalbano, M., Garcia, S., McAllen, S., Bhatt, N., Sonawane, M., Sengupta, U., Kayed, R. Tau oligomer induced HMGB1 release

contributes to cellular senescence and neuropathology linked to Alzheimer's disease and frontotemporal dementia. Cell Reports 2021; 36(3): 109419

Galloway, DA., Phillips, AEM., Owen, DRJ., Moore, CS. Phagocytosis in the Brain: Homeostasis and Disease. Frontiers in Immunology 2019; 10: 790

Gao, YL., Wang, N., Sun, FR., Cao, XP., Zhang, W., Yu, JT. Tau in neurodegenerative disease. Annals of Translational Medicine 2018; 6(10): 175

Garvalov, BK., Muhammad, S., Dobreva, G. Lamin B1 in cancer and aging. Aging 2019; 11(18): 7336–7338

Garwood, CJ., Simpson, JE., Al Mashhadi, S., Axe, C., Wilson, S., Heath, PR., Shaw, P. J., Matthews, FE., Brayne, C., Ince, PG., Wharton, SB. DNA damage response and senescence in endothelial cells of human cerebral cortex and relation to Alzheimer's neuropathology progression: A population-based study in the Medical Research Council Cognitive Function and Ageing Study (MRC-CFAS) cohort. Neuropathology and Applied Neurobiology 2014; 40(7): 802–814

Gemma, C., Bachstetter, AD. The role of microglia in adult hippocampal neurogenesis. Frontiers in Cellular Neuroscience 2013; 7: 229

Gil, L., Niño, S. A., Guerrero, C., Jiménez-Capdeville, ME. Phospho-Tau and Chromatin Landscapes in Early and Late Alzheimer's Disease. International Journal of Molecular Sciences 2021; 22(19): 10283

Gillooly, JF., Hayward, A., Hou, C., Burleigh, JG. Explaining differences in the lifespan and replicative capacity of cells: A general model and comparative analysis of vertebrates. Proceedings. Biological Sciences 2012; 279(1744): 3976–3980

Ginhoux, F., Prinz, M. Origin of Microglia: Current Concepts and Past Controversies. Cold Spring Harbor Perspectives in Biology 2015, 7(8): a020537

Giorgi, C., Missiroli, S., Patergnani, S., Duszynski, J., Wieckowski, MR., Pinton, P. Mitochondria-Associated Membranes: Composition, Molecular Mechanisms, and Physiopathological Implications. Antioxidants & Redox Signaling 2015; 22(12): 995–1019

Giunta, B., Fernandez, F., Nikolic, WV., Obregon, D., Rrapo, E., Town, T., Tan, J. Inflammaging as a prodrome to Alzheimer's disease. Journal of Neuroinflammation 2008; 5(1): 51

Glück, S., Guey, B., Gulen, MF., Wolter, K., Kang, TW., Schmacke, NA., Bridgeman, A., Rehwinkel, J., Zender, L., Ablasser, A. Innate immune sensing of cytosolic chromatin fragments through cGAS promotes senescence. Nature Cell Biology 2017; 19(9): 1061–1070

Goedert, M. Tau protein and neurodegeneration. Seminars in Cell & Developmental Biology 2004; 15(1): 45–49

Goedert, M., Spillantini, MG., Jakes, R., Rutherford, D., Crowther, RA. Multiple isoforms of human microtubule-associated protein tau: Sequences and localization in neurofibrillary tangles of Alzheimer's disease. Neuron 1889; 3(4): 519–526

Gong, CX., Iqbal, K. Hyperphosphorylation of microtubule-associated protein tau: A promising therapeutic target for Alzheimer disease. Current Medicinal Chemistry 2008; 15(23): 2321–2328

Gong, T., Liu, L., Jiang, W., Zhou, R. DAMP-sensing receptors in sterile inflammation and inflammatory diseases. Nature Reviews. Immunology 2020; 20(2): 95–112

González-Dominguez, A., Montañez, R., Castejón-Vega, B., Nuñez-Vasco, J., Lendines-Cordero, D., Wang, C., Mbalaviele, G., Navarro-Pando, JM., Alcocer-Gómez, E., Cordero, MD. Inhibition of the NLRP3 inflammasome improves lifespan in animal murine model of Hutchinson-Gilford Progeria. EMBO Molecular Medicine 2021; 13(10): e14012

González-Gualda, E., Baker, AG., Fruk, L., Muñoz-Espín, DA guide to assessing cellular senescence in vitro and in vivo. The FEBS Journal 2021; 288(1): 56–80

Gonzalo, S. DNA Damage and Lamins. Advances in Experimental Medicine and Biology 2014; 773: 377–399

Gosselin, D., Rivest, S. Getting Too Old Too Quickly for Their Job: Senescent Glial Cells Promote Neurodegeneration. Neuron 2018; 100(4): 777–779

Greenberg, SB., Grove, GL., Cristofalo, VJ. Cell size in aging monolayer cultures. In Vitro 1977; 13(5): 297–300

Greenwood, EK., Brown, DR. Senescent Microglia: The Key to the Ageing Brain? International Journal of Molecular Sciences 2021; 22(9): 4402

Griciuc, A., Serrano-Pozo, A., Parrado, AR., Lesinski, AN., Asselin, CN., Mullin, K., Hooli, B., Choi, SH., Hyman, BT., Tanzi, RE. Alzheimer's disease risk gene CD33 inhibits microglial uptake of amyloid beta. Neuron 2013; 78(4): 631–643

Griffin, WS. T., Liu, L., Li, Y., Mrak, RE., Barger, SW. Interleukin-1 mediates Alzheimer and Lewy body pathologies. Journal of Neuroinflammation 2006; 3: 5

Guo, T., Noble, W., Hanger, DP. Roles of tau protein in health and disease. Acta Neuropathologica 2017; 133(5): 665–704

Halle, A., Hornung, V., Petzold, GC., Stewart, CR., Monks, BG., Reinheckel, T., Fitzgerald, K. A., Latz, E., Moore, KJ., Golenbock, DT. The NALP3 inflammasome is involved in the innate immune response to amyloid-beta. Nature Immunology 2008; 9(8): 857–865

Ham, SJ., Lee, D., Yoo, H., Jun, K., Shin, H., Chung, J. Decision between mitophagy and apoptosis by Parkin via VDAC1 ubiquitination. Proceedings of the National Academy of Sciences of the United States of America 2020; 117(8): 4281–4291

Han, L., Zhang, Y., Zhang, M., Guo, L., Wang, J., Zeng, F., Xu, D., Yin, Z., Xu, Y., Wang, D., Zhou, H. Interleukin-1β-Induced Senescence Promotes Osteoblastic Transition of Vascular Smooth Muscle Cells. Kidney & Blood Pressure Research 2020; 45(2): 314–330

Hashiguchi, M., Saito, T., Hisanaga, S., Hashiguchi, T. Truncation of CDK5 activator p35 induces intensive phosphorylation of Ser202/Thr205 of human tau. The Journal of Biological Chemistry 2002; 277(46): 44525–44530

Hayflick, L., Moorhead, PS. The serial cultivation of human diploid cell strains. Experimental Cell Research 1961; 25(3): 585–621

He, S., Sharpless, NE. Senescence in Health and Disease. Cell 2017; 169(6): 1000–1011

Hellwig, S., Masuch, A., Nestel, S., Katzmarski, N., Meyer-Luehmann, M., Biber, K. Forebrain microglia from wild-type but not adult 5xFAD mice prevent amyloid-β plaque formation in organotypic hippocampal slice cultures. Scientific Reports 2015; 5: 14624

Heneka MT, Carson MJ, El Khoury J, Landreth GE, Brosseron F, Feinstein DL, Jacobs AH, Wyss-Coray T, Vitorica J, Ransohoff RM, Herrup K, Frautschy SA, Finsen B, Brown GC, Verkhratsky A, Yamanaka K, Koistinaho J, Latz E, Halle A, Petzold GC, Town T, Morgan D, Shinohara ML, Perry VH, Holmes C, Bazan NG, Brooks DJ, Hunot S, Joseph B, Deigendesch N, Garaschuk O, Boddeke E, Dinarello CA, Breitner JC, Cole GM, Golenbock DT, Kummer MP. Neuroinflammation in Alzheimer's disease. The Lancet. Neurology 2015; 14(4): 388–405

Heneka, MT., Kummer, MP., Latz, E. Innate immune activation in neurodegenerative disease. Nature Reviews. Immunology 2014; 14(7): 463–477

Heneka, MT., Kummer, MP., Stutz, A., Delekate, A., Schwartz, S., Vieira-Saecker, A., Griep, A., Axt, D., Remus, A., Tzeng, TC., Gelpi, E., Halle, A., Korte, M., Latz, E., Golenbock, D. T. NLRP3 is activated in Alzheimer's disease and contributes to pathology in APP/PS1 mice. Nature 2013; 493(7434): 674–678

Hernandez-Segura, A., Nehme, J., Demaria, M. Hallmarks of cellular senescence. Trends in Cell Biology 2018; 28(6): 436–453

Herranz, N., Gil, J. Mechanisms and functions of cellular senescence. The Journal of Clinical Investigation 2018; 128(4): 1238–1246

Höglinger, GU., Respondek, G., Kovacs, GG. New classification of tauopathies. Revue Neurologique 2019; 174(9): 664–668

Hollingworth, P., Harold, D., Sims, R., Gerrish, A., Lambert, JC., Carrasquillo, MM., Abraham, R., Hamshere, ML., Pahwa, JS., Moskvina, V., Dowzell, K., Jones, N., Stretton, A., Thomas, C., Richards, A., Ivanov, D., Widdowson, C., Chapman, J., Lovestone, S., … Williams, J. Common variants at ABCA7, MS4A6A/MS4A4E, EPHA1, CD33 and CD2AP are associated with Alzheimer's disease. Nature Genetics 2011; 43(5): 429–435

Hopp, SC., Lin, Y., Oakley, D., Roe, AD., DeVos, SL., Hanlon, D., Hyman, BT. The role of microglia in processing and spreading of bioactive tau seeds in Alzheimer's disease. Journal of Neuroinflammation 2018; 15(1): 269

Hu, Y., Fryatt, GL., Ghorbani, M., Obst, J., Menassa, DA., Martin-Estebane, M., Muntslag, TAO., Olmos-Alonso, A., Guerrero-Carrasco, M., Thomas, D., Cragg, MS., Gomez-Nicola, D. Replicative senescence dictates the emergence of disease-associated microglia and contributes to Aβ pathology. Cell Reports 2021; 35(10): 109228

Huang, Z., Lan, J., Gao, X. Feprazone Mitigates IL-1β-Induced Cellular Senescence in Chondrocytes. ACS Omega 2021; 6(14): 9442–9448

Ising, C., Venegas, C., Zhang, S., Scheiblich, H., Schmidt, SV., Vieira-Saecker, A., Schwartz, S., Albasset, S., McManus, RM., Tejera, D., Griep, A., Santarelli, F., Brosseron, F., Opitz, S., Stunden, J., Merten, M., Kayed, R., Golenbock, DT., Blum, D., Latz, E., Buée, L., Heneka, MT. NLRP3 inflammasome activation drives tau pathology. Nature 2019; 575(7784): 669–673

Janeway, CA. The immune system evolved to discriminate infectious nonself from noninfectious self. Immunology Today 1992; 13(1): 11–16

Jessen, NA., Munk, AS. F., Lundgaard, I., Nedergaard, M. The Glymphatic System – A Beginner's Guide. Neurochemical Research 2015; 40(12): 2583–2599

Jiang, D., Chen, S., Sun, R., Zhang, X., Wang, D. The NLRP3 inflammasome: Role in metabolic disorders and regulation by metabolic pathways. Cancer Letters 2018; 419: 8–19

Jiang, T., Yu, JT., Hu, N., Tan, MS., Zhu, XC., Tan, L. CD33 in Alzheimer's disease. Molecular Neurobiology 2014; 49(1): 529–535

Jin, M., Shiwaku, H., Tanaka, H., Obita, T., Ohuchi, S., Yoshioka, Y., Jin, X., Kondo, K., Fujita, K., Homma, H., Nakajima, K., Mizuguchi, M., & Okazawa, H. Tau activates microglia via the PQBP1-cGAS-STING pathway to promote brain inflammation. Nature Communications 2021; 12(1): 6565

Jung, ES., Suh, K., Han, J., Kim, H., Kang, HS., Choi, WS., Mook-Jung, I. Amyloid-β activates NLRP3 inflammasomes by affecting microglial immunometabolism through the Syk-AMPK pathway. Aging Cell 2022; 21(5): e13623

Jury, N., Abarzua, S., Diaz, I., Guerra, MV., Ampuero, E., Cubillos, P., Martinez, P., Herrera-Soto, A., Arredondo, C., Rojas, F., Manterola, M., Rojas, A., Montecino, M., Varela-Nallar, L., van Zundert, B. Widespread loss of the silencing epigenetic mark H3K9me3 in astrocytes and neurons along with hippocampal-dependent cognitive impairment in C9orf72 BAC transgenic mice. Clinical Epigenetics 2020; 12(1): 32

Kaler, P., Augenlicht, L., Klampfer, L. Macrophage-derived IL-1beta stimulates Wnt signaling and growth of colon cancer cells: A crosstalk interrupted by vitamin D3. Oncogene 2009; 28(44): 3892–3902

Kamentsky, L., Jones, TR., Fraser, A., Bray, MA., Logan, DJ., Madden, KL., Ljosa, V., Rueden, C., Eliceiri, KW., Carpenter, AE. Improved structure, function and compatibility for CellProfiler: Modular high-throughput image analysis software. Bioinformatics 2011; 27(8): 1179–1180

Kang, JH., Lee, SB., Seok, J., Kim, DH., Ma, G., Park, J., Jeong, AJ., Ye, SK., Kang, TB. Novel Activity of ODZ10117, a STAT3 Inhibitor, for Regulation of NLRP3

Inflammasome Activation. International Journal of Molecular Sciences 2023; 24(7): 6079

Kanneganti, TD., Ozören, N., Body-Malapel, M., Amer, A., Park, JH., Franchi, L., Whitfield, J., Barchet, W., Colonna, M., Vandenabeele, P., Bertin, J., Coyle, A., Grant, EP., Akira, S., Núñez, G. Bacterial RNA and small antiviral compounds activate caspase-1 through cryopyrin/Nalp3. Nature 2006; 440(7081): 233–236

Karabag, D., Scheiblich, H., Griep, A., Santarelli, F., Schwartz, S., Heneka, MT., Ising, C. Characterizing microglial senescence: Tau as a key player. Journal of Neurochemistry 2023; 166(3): 517–533. DOI: 10.1111/jnc.15866

Kelley, N., Jeltema, D., Duan, Y., He, Y. The NLRP3 Inflammasome: An Overview of Mechanisms of Activation and Regulation. International Journal of Molecular Sciences 2019; 20(13): 3328

Kettenmann, H., Hanisch, UK., Noda, M., Verkhratsky, A. Physiology of microglia. Physiological Reviews 2011; 91(2): 461–553

Kiecolt-Glaser, JK., Preacher, KJ., MacCallum, RC., Atkinson, C., Malarkey, WB., Glaser, R. Chronic stress and age-related increases in the proinflammatory cytokine IL-6. Proceedings of the National Academy of Sciences 2003; 100(15): 9090–9095

Kigerl, KA., de Rivero Vaccari, JP., Dietrich, WD., Popovich, PG., Keane, RW. Pattern recognition receptors and central nervous system repair. Experimental Neurology 2014; 258: 5–16

Kobayashi, T., Kuroda, S., Tada, M., Houkin, K., Iwasaki, Y., Abe, H. Calcium-induced mitochondrial swelling and cytochrome c release in the brain: Its biochemical characteristics and implication in ischemic neuronal injury. Brain Research 2003; 960(1–2): 62–70

Kojima, H., Inoue, T., Kunimoto, H., Nakajima, K. IL-6-STAT3 signaling and premature senescence. JAKSTAT 2013; 2(4): e25763

Kojima, H., Kunimoto, H., Inoue, T., Nakajima, K. The STAT3-IGFBP5 axis is critical for IL-6/gp130-induced premature senescence in human fibroblasts. Cell Cycle 2012; 11(4): 730–739

Komuro, Y., Xu, G., Bhaskar, K., Lamb, BT. Human tau expression reduces adult neurogenesis in a mouse model of tauopathy. Neurobiology of Aging 2015; 36(6): 2034–2042

Kosik, KS., Orecchio, LD., Bakalis, S., Neve, RL. Developmentally regulated expression of specific tau sequences. Neuron 1989; 2(4): 1389–1397

Kovacs, GG. Tauopathies. Handbook of Clinical Neurology 2017; 145: 355–368

Krasemann, S., Madore, C., Cialic, R., Baufeld, C., Calcagno, N., El Fatimy, R., Beckers, L., O'Loughlin, E., Xu, Y., Fanek, Z., Greco, D. J., Smith, S. T., Tweet, G., Humulock, Z., Zrzavy, T., Conde-Sanroman, P., Gacias, M., Weng, Z., Chen, H., Tjon, E., Mazaheri, F., Hartmann, K., Madi, A., Ulrich, JD., Glatzel, M., Worthmann, A., Heeren, J., Budnik, B., Lemere, C., Ikezu, T., Heppner, FL., Litvak, V., Holtzman, DM., Lassmann, H., Weiner, HL., Ochando, J., Haass, C., Butovsky, O. The TREM2-APOE Pathway Drives the Transcriptional Phenotype of Dysfunctional Microglia in Neurodegenerative Diseases. Immunity 2017; 47(3): 566-581

Kritsilis, M., V Rizou, S., Koutsoudaki, PN., Evangelou, K., Gorgoulis, VG., Papadopoulos, D. Ageing, cellular senescence and neurodegenerative disease. International Journal of Molecular Sciences 2018; 19(10): 2937

Krizhanovsky, V., Yon, M., Dickins, RA., Hearn, S., Simon, J., Miething, C., Yee, H., Zender, L., Lowe, SW. Senescence of activated stellate cells limits liver fibrosis. Cell 2018; 134(4): 657–667

Kuilman, T., Michaloglou, C., Mooi, WJ., Peeper, DS. (2010). The essence of senescence. Genes Dev 2010; 24(22): 2463–2479

Kuilman, T., Michaloglou, C., Vredeveld, LCW., Douma, S., van Doorn, R., Desmet, CJ., Aarden, LA., Mooi, WJ., Peeper, DS. Oncogene-induced senescence relayed by an interleukin-dependent inflammatory network. Cel 2008; 133(6): 1019–1031

Kumari, R., Jat, P. Mechanisms of Cellular Senescence: Cell Cycle Arrest and Senescence Associated Secretory Phenotype. Frontiers in Cell and Developmental Biology 2021; 9: 645593

Kyjacova, L., Saup, R., Rönsch, K., Wallbaum, S., Dukowic-Schulze, S., Foss, A., Scherer, SD., Rothley, M., Neeb, A., Grau, N., Thiele, W., Thaler, S., Cremers, N., Sticht, C., Gretz, N., Garvalov, BK., Utikal, J., Sleeman, JP. IER2-induced senescence drives melanoma invasion through osteopontin. Oncogene 2021; 40(47): 6494–6512

Lai, KSP., Liu, CS., Rau, A., Lanctôt, KL., Köhler, CA., Pakosh, M., Carvalho, AF., Herrmann, N. Peripheral inflammatory markers in Alzheimer's disease: A

systematic review and meta-analysis of 175 studies. Journal of Neurology, Neurosurgery & Psychiatry 2017; 88(10): 876–882

Lämmerhirt, L., Kappelmann-Fenzl, M., Fischer, S., Pommer, M., Zimmermann, T., Kluge, V., Matthies, A., Kuphal, S., Bosserhoff, AK. Knockdown of Lamin B1 and the Corresponding Lamin B Receptor Leads to Changes in Heterochromatin State and Senescence Induction in Malignant Melanoma. Cells 2022; 11(14): 2154

Langworth-Green, C., Patel, S., Jaunmuktane, Z., Jabbari, E., Morris, H., Thom, M., Lees, A., Hardy, J., Zandi, M., Duff, K. Chronic effects of inflammation on tauopathies. The Lancet. Neurology 2023; 22(5): 430–442

Lasry, A., Ben-Neriah, Y. Senescence-associated inflammatory responses: Aging and cancer perspectives. Trends in Immunology 2015; 36(4): 217–228

Lasser, M., Tiber, J., Lowery, LA. The Role of the Microtubule Cytoskeleton in Neurodevelopmental Disorders. Frontiers in Cellular Neuroscience 2018; 12: 165

Lathuiliere, A., Hyman, BT. Quantitative Methods for the Detection of Tau Seeding Activity in Human Biofluids. Frontiers in Neuroscience 2021; 15: 654176

Lee, HC., Yin, PH., Chi, CW., Wei, YH. Increase in mitochondrial mass in human fibroblasts under oxidative stress and during replicative cell senescence. Journal of Biomedical Science 2002; 9(6 Pt 1): 517–526

Lee, JH., Kim, EW., Croteau, DL., Bohr, VA. Heterochromatin: An epigenetic point of view in aging. Experimental & Molecular Medicine 2020; 52(9): 1466–1474

Lee, VMY., Goedert, M., Trojanowski, JQ. Neurodegenerative Tauopathies. Annual Review Neuroscience 2001; 24: 1121–1159

Lemasters, JJ., Theruvath, TP., Zhong, Z., Nieminen, AL. Mitochondrial calcium and the permeability transition in cell death. Biochimica Et Biophysica Acta 2009; 1787(11): 1395–1401

Leyns, CEG., Ulrich, JD., Finn, MB., Stewart, FR., Koscal, LJ., Remolina Serrano, J., Robinson, GO., Anderson, E., Colonna, M., Holtzman, DM. TREM2 deficiency attenuates neuroinflammation and protects against neurodegeneration in a mouse model of tauopathy. Proceedings of the National Academy of Sciences of the United States of America 2017; 114(43): 11524–11529

Li, C., Fan, C., Zhao, J., Di, M., Sui, C., Han, L., Hu, L. Panaxatriol Saponins Promote M2 Polarization of BV2 Cells to Reduce Inflammation and Apoptosis after

Glucose/Oxygen Deprivation by Activating STAT3. Inflammation 2020; 43(6): 2109–2118

Li, D., Wu, M. Pattern recognition receptors in health and diseases. Signal Transduction and Targeted Therapy 2021; 4(6), 291

Li, Q., Barres, BA. Microglia and macrophages in brain homeostasis and disease. Nature Reviews Immunology 2018; 18(4), 225–242

Li, W., Zhang, C., Sun, X. Mitochondrial Ca2+ Retention Capacity Assay and Ca2+-triggered Mitochondrial Swelling Assay. Journal of Visualized Experiments 2018; 135: 56236

Liang, CC., Park, AY., Guan, JL. In vitro scratch assay: A convenient and inexpensive method for analysis of cell migration in vitro. Nature Protocols 2007; 2(2): 329–333

Linnartz, B., Neumann, H. Microglial activatory (immunoreceptor tyrosine-based activation motif)- and inhibitory (immunoreceptor tyrosine-based inhibition motif)-signaling receptors for recognition of the neuronal glycocalyx. Glia 2013; 61(1): 37–46

Litvinchuk, A., Wan, YW., Swartzlander, DB., Chen, F., Cole, A., Propson, NE., Wang, Q., Zhang, B., Liu, Z., Zheng, H. Complement C3aR inactivation attenuates tau pathology and reverses an immune network deregulated in tauopathy models and Alzheimer's disease. Neuron 2018; 100(6): 1337-1353

Liu, F., Iqbal, K., Grundke-Iqbal, I., Gong, CX. Involvement of aberrant glycosylation in phosphorylation of tau by cdk5 and GSK-3beta. FEBS Letters 2002; 530(1–3): 209–214

Liu, J., Yang, J.. Mitochondria-associated membranes: A hub for neurodegenerative diseases. Biomedicine & Pharmacotherapy 2022; 149: 112890

Liu, X., Ding, J., Meng, L. Oncogene-induced senescence: A double edged sword in cancer. Acta Pharmacologica Sinica 2018; 39(10): 1553–1558

Liu, X., Tian, Y., Lu, N., Gin, T., Cheng, CHK., Chan, MTV. Stat3 Inhibition Attenuates Mechanical Allodynia through Transcriptional Regulation of Chemokine Expression in Spinal Astrocytes. PLoS ONE 2013; 8(10): e75804

Liu, X., Zhang, Z., Ruan, J., Pan, Y., Magupalli, VG., Wu, H., Lieberman, J. Inflammasome-activated gasdermin D causes pyroptosis by forming membrane pores. Nature 2016; 535(7610): 153–158

Liu, Y., Yang, H., Zhu, F., Ouyang, Y., Pan, P. Inhibition of STAT3 phosphorylation by colchicine regulates NLRP3 activation to alleviate sepsis-induced acute lung injury. Inflammopharmacology 2023; 31(4): 2007–2021

Loo, TM., Miyata, K., Tanaka, Y., Takahashi, A. Cellular senescence and senescence-associated secretory phenotype via the cGAS-STING signaling pathway in cancer. Cancer Science 2020; 111(2): 304–311

Lopes-Paciencia, S., Saint-Germain, E., Rowell, MC., Ruiz, AF., Kalegari, P., Ferbeyre, G. The senescence-associated secretory phenotype and its regulation. Cytokine 2019; 117: 15–22

Lu, Y., He, M., Zhang, Y., Xu, S., Zhang, L., He, Y., Chen, C., Liu, C., Pi, H., Yu, Z., Zhou, Z. Differential pro-inflammatory responses of astrocytes and microglia involve STAT3 activation in response to 1800 MHz radiofrequency fields. PloS One 2014; 9(9): e108318

Lund, ET., McKenna, R., Evans, DB., Sharma, SK., Mathews, WR. Characterization of the in vitro phosphorylation of human tau by tau protein kinase II (cdk5/p20) using mass spectrometry. Journal of Neurochemistry 2001; 76(4): 1221–1232

Maciel-Barón, LA., Morales-Rosales, SL., Aquino-Cruz, AA., Triana-Martínez, F., Galván-Arzate, S., Luna-López, A., González-Puertos, VY., López-Díazguerrero, NE., Torres, C., Königsberg, M. Senescence associated secretory phenotype profile from primary lung mice fibroblasts depends on the senescence induction stimuli. Age 2016; 38(1): 26

Maeda, S., Sahara, N., Saito, Y., Murayama, S., Ikai, A., Takashima, A. Increased levels of granular tau oligomers: An early sign of brain aging and Alzheimer's disease. Neuroscience Research 2006; 54(3): 197–201

Mah, LJ., El-Osta, A., Karagiannis, TC. gammaH2AX as a molecular marker of aging and disease. Epigenetics 2010; 5(2): 129–136

Mamun, AA., Uddin, MS., Mathew, B., Ashraf, GM. Toxic tau: Structural origins of tau aggregation in Alzheimer's disease. Neural Regeneration Research 2020; 15(8): 1417–1420

Manczak, M., Reddy, PH. Abnormal interaction of VDAC1 with amyloid beta and phosphorylated tau causes mitochondrial dysfunction in Alzheimer's disease. Human Molecular Genetics 2012; 21(23): 5131–5146

Mangan, MSJ., Olhava, EJ., Roush, WR., Seidel, HM., Glick, GD., Latz, E. Targeting the NLRP3 inflammasome in inflammatory diseases. Nature Reviews. Drug Discovery 2018; 17(8): 588–606

Maphis, N., Xu, G., Kokiko-Cochran, ON., Jiang, S., Cardona, A., Ransohoff, RM., Lamb, BT., Bhaskar, K. Reactive microglia drive tau pathology and contribute to the spreading of pathological tau in the brain. Brain 2015; 138(6): 1738–1755

Mapunda, JA., Tibar, H., Regragui, W., Engelhardt, B. How Does the Immune System Enter the Brain? Frontiers in Immunology 2022; 13: 805657

Marín-Aguilar, F., Lechuga-Vieco, AV., Alcocer-Gómez, E., Castejón-Vega, B., Lucas, J., Garrido, C., Peralta-Garcia, A., Pérez-Pulido, AJ., Varela-López, A., Quiles, JL., Ryffel, B., Flores, I., Bullón, P., Ruiz-Cabello, J., Cordero, MD. NLRP3 inflammasome suppression improves longevity and prevents cardiac aging in male mice. Aging Cell 2020; 19(1): e13050

Marshall, JS., Warrington, R., Watson, W., Kim, HL. An introduction to immunology and immunopathology. Allergy, Asthma & Clinical Immunology 2018; 14(2): 49

Martínez-Cué, C., Rueda, N. Cellular Senescence in Neurodegenerative Diseases. Frontiers in Cellular Neuroscience 2020; 14: 16

Martini, H., Passos, J. F. Cellular senescence: All roads lead to mitochondria. The FEBS Journal 2023; 290(5): 1186–1202

Martinon, F., Burns, K., Tschopp, J. The Inflammasome: A Molecular Platform Triggering Activation of Inflammatory Caspases and Processing of proIL-β. Molecular Cell 2002; 10(2): 417–426

Matias, I., Diniz, LP., Damico, IV., Araujo, APB., Neves, L., Vargas, G., Leite, REP., Suemoto, CK., Nitrini, R., Jacob-Filho, W., Grinberg, LT., Hol, EM., Middeldorp, J., Gomes, FCA. Loss of lamin-B1 and defective nuclear morphology are hallmarks of astrocyte senescence in vitro and in the aging human hippocampus. Aging Cell 2022; 21(1): e13521

McHugh, D., Gil, J. Senescence and aging: Causes, consequences, and therapeutic avenues. The Journal of Cell Biology 2018; 217(1): 65–77

McKee, CM., Coll, RC. NLRP3 inflammasome priming: A riddle wrapped in a mystery inside an enigma. Journal of Leukocyte Biology 2020; 108(3): 937–952

McQuade, A., Blurton-Jones, M. Microglia in Alzheimer's Disease: Exploring How Genetics and Phenotype Influence Risk. Journal of Molecular Biology 2019; 431(9): 1805–1817

McShea, A., Harris, PL., Webster, KR., Wahl, AF., Smith, MA. Abnormal expression of the cell cycle regulators P16 and CDK4 in Alzheimer's disease. The American Journal of Pathology 1997; 150(6): 1933–1939

Mendelsohn, AR., Larrick, J. Cellular senescence as the key intermediate in tau-mediated neurodegeneration. Rejuvenation Research 2018; 21(6): 572–579

Millot, P., San, C., Bennana, E., Porte, B., Vignal, N., Hugon, J., Paquet, C., Hosten, B., Mouton-Liger, F. STAT3 inhibition protects against neuroinflammation and BACE1 upregulation induced by systemic inflammation. Immunology Letters 2020; 228: 129–134

Mirbaha, H., Chen, D., Morazova, OA., Ruff, KM., Sharma, AM., Liu, X., Goodarzi, M., Pappu, RV., Colby, DW., Mirzaei, H., Joachimiak, LA., Diamond, MI. Inert and seed-competent tau monomers suggest structural origins of aggregation. ELife 2018; 7: e36584

Missiroli, S., Patergnani, S., Caroccia, N., Pedriali, G., Perrone, M., Previati, M., Wieckowski, MR., Giorgi, C. Mitochondria-associated membranes (MAMs) and inflammation. Cell Death & Disease 2018; 9(3): 329

Miwa, S., Kashyap, S., Chini, E., Zglinicki, T. Mitochondrial dysfunction in cell senescence and aging. The Journal of Clinical Investigation 2022; 132(13): e158447

Mongi-Bragato, B., Grondona, E., Sosa, LD. V., Zlocowski, N., Venier, AC., Torres, AI., Latini, A., Leal, RB., Gutiérrez, S., De Paul, AL. Pivotal role of NF-κB in cellular senescence of experimental pituitary tumours. The Journal of Endocrinology 2020; 245(2): 179–191

Monje, ML., Toda, H., Palmer, TD. Inflammatory blockade restores adult hippocampal neurogenesis. Science 2003; 302(5651): 1760–1765

Moreno-Jiménez, EP., Flor-García, M., Terreros-Roncal, J., Rábano, A., Cafini, F., Pallas-Bazarra, N., Ávila, J., Llorens-Martín, M. Adult hippocampal neurogenesis is abundant in neurologically healthy subjects and drops sharply in patients with Alzheimer's disease. Nature Medicine 2019; 25(4): 554–560

Morsch, R., Simon, W., Coleman, PD. Neurons May Live for Decades with Neurofibrillary Tangles. Journal of Neuropathology & Experimental Neurology 1999; 58(2): 188–197

Moujaber, O., Fishbein, F., Omran, N., Liang, Y., Colmegna, I., Presley, JF., Stochaj, U. Cellular senescence is associated with reorganization of the microtubule cytoskeleton. Cellular and Molecular Life Sciences 2019; 76(6): 1169–1183

Muñoz-Espín, D., Serrano, M. Cellular senescence: From physiology to pathology. Nature Reviews Molecular Cell Biology 2014; 15(7): 482–496

Murakami, T., Ockinger, J., Yu, J., Byles, V., McColl, A., Hofer, AM., Horng, T. Critical role for calcium mobilization in activation of the NLRP3 inflammasome. Proceedings of the National Academy of Sciences 2012; 109(28): 11282–11287

Musi, N., Valentine, JM., Sickora, KR., Baeuerle, E., Thompson, CS., Shen, Q., Orr, M. E. Tau protein aggregation is associated with cellular senescence in the brain. Aging Cell 2018; 17(6): e12840

Nadalutti, CA., Stefanick, DF., Zhao, ML., Horton, JK., Prasad, R., Brooks, AM., Griffith, JD., Wilson, SH. Mitochondrial dysfunction and DNA damage accompany enhanced levels of formaldehyde in cultured primary human fibroblasts. Scientific Reports 2020; 10(1): 5575

Nakahira, K., Hisata, S., Choi, AMK. The Roles of Mitochondrial Damage-Associated Molecular Patterns in Diseases. Antioxidants & Redox Signaling 2015; 23(17): 1329–1350

Nilson, AN., English, KC., Gerson, JE., Barton Whittle, T., Nicolas Crain, C., Xue, J., Sengupta, U., Castillo-Carranza, DL., Zhang, W., Gupta, P., Kayed, R. Tau Oligomers Associate with Inflammation in the Brain and Retina of Tauopathy Mice and in Neurodegenerative Diseases. Journal of Alzheimer's Disease 2017; 55(3): 1083–1099

Nishio, K., Inoue, A. Senescence-associated alterations of cytoskeleton: Extraordinary production of vimentin that anchors cytoplasmic p53 in senescent human fibroblasts. Histochemistry and Cell Biology 2005; 123(3): 263–273

Noble, W., Olm, V., Takata, K., Casey, E., Mary, O., Meyerson, J., Gaynor, K., LaFrancois, J., Wang, L., Kondo, T., Davies, P., Burns, M., Veeranna, null, Nixon, R., Dickson,

D., Matsuoka, Y., Ahlijanian, M., Lau, LF., Duff, K. Cdk5 is a key factor in tau aggregation and tangle formation in vivo. Neuron 2003; 38(4): 555–565

Norden, DM., Godbout, JP. Review: Microglia of the aged brain: primed to be activated and resistant to regulation. Neuropathology and Applied Neurobiology 2013; 39(1): 19–34

Norris, GT., Kipnis, J. Immune cells and CNS physiology: Microglia and beyond. Journal of Experimental Medicine 2018; 216(1): 60–70

Ogrodnik, M. Cellular aging beyond cellular senescence: Markers of senescence prior to cell cycle arrest in vitro and in vivo. Aging Cell 2021; 20(4): e13338

Olfati, N., Shoeibi, A., Litvan, I. Clinical Spectrum of Tauopathies. Frontiers in Neurology 2022; 13: 944806

Overton, KW., Spencer, SL., Noderer, WL., Meyer, T., Wang, CL. Basal p21 controls population heterogeneity in cycling and quiescent cell cycle states. Proceedings of the National Academy of Sciences 2014; 111(41): E4386–E4393

Paluvai, H., Di Giorgio, E., Brancolini, C. The Histone Code of Senescence. Cells 2020; 9(2): 466

Pan, C., Kumar, C., Bohl, S., Klingmueller, U., Mann, M. Comparative Proteomic Phenotyping of Cell Lines and Primary Cells to Assess Preservation of Cell Type-specific Functions. Molecular & Cellular Proteomics 2009; 8(3): 443–450

Paonessa, F., Evans, LD., Solanki, R., Larrieu, D., Wray, S., Hardy, J., Jackson, SP., Livesey, FJ. Microtubules Deform the Nuclear Membrane and Disrupt Nucleocytoplasmic Transport in Tau-Mediated Frontotemporal Dementia. Cell Reports 2019; 26(3): 582-593

Perea, JR., Ávila, J., Bolós, M. Dephosphorylated rather than hyperphosphorylated Tau triggers a pro-inflammatory profile in microglia through the p38 MAPK pathway. Experimental Neurology 2018; 310: 14–21

Pereira, CA., Carlos, D., Ferreira, NS., Silva, JF., Zanotto, CZ., Zamboni, DS., Garcia, V. D., Ventura, DF., Silva, JS., Tostes, RC. Mitochondrial DNA Promotes NLRP3 Inflammasome Activation and Contributes to Endothelial Dysfunction and Inflammation in Type 1 Diabetes. Frontiers in Physiology 2019; 10: 1557

Pereira, L., Font-Nieves, M., Van den Haute, C., Baekelandt, V., Planas, AM., Pozas, E. IL-10 regulates adult neurogenesis by modulating ERK and STAT3 activity. Frontiers in Cellular Neuroscience 2015; 9: 57

Pérez-Rodríguez, DR., Blanco-Luquin, I., Mendioroz, M. The Participation of Microglia in Neurogenesis: A Review. Brain Sciences 2021; 11(5): 658

Perucca, P., Cazzalini, O., Madine, M., Savio, M., Laskey, RA., Vannini, V., Prosperi, E., & Stivala, LA. Loss of p21 CDKN1A impairs entry to quiescence and activates a DNA damage response in normal fibroblasts induced to quiescence. Cell Cycle 2009; 8(1): 105–114

Pike, AF., Varanita, T., Herrebout, MAC., Plug, BC., Kole, J., Musters, RJP., Teunissen, CE., Hoozemans, JJM., Bubacco, L., Veerhuis, R. α-Synuclein evokes NLRP3 inflammasome-mediated IL-1β secretion from primary human microglia. Glia 2021; 69(6): 1413–1428

Pretre, V., Papadopoulos, D., Regard, J., Pelletier, M., Woo, J. Interleukin-1 (IL-1) and the inflammasome in cancer. Cytokine 2022; 153: 155850

Qiang, L., Sun, X., Austin, TO., Muralidharan, H., Jean, DC., Liu, M., Yu, W., Baas, PW. Tau Does Not Stabilize Axonal Microtubules but Rather Enables Them to Have Long Labile Domains. Current Biology 2018; 28(13): 2181-2189

Quintanilla, RA., Orellana, DI., González-Billault, C., Maccioni, RB. Interleukin-6 induces Alzheimer-type phosphorylation of tau protein by deregulating the cdk5/p35 pathway. Experimental Cell Research 2004; 295(1): 245–257

Ransohoff, RM., Brown, MA. Innate immunity in the central nervous system. The Journal of Clinical Investigation 2012; 122(4): 1164–1171

Rea, I. M., Gibson, DS., McGilligan, V., McNerlan, SE., Alexander, HD., Ross, OA. Age and age-related diseases: Role of inflammation triggers and cytokines. Frontiers in Immunology 2018; 9: 586

Reed, MJ., Ferara, NS., Vernon, RB. Impaired migration, integrin function, and actin cytoskeletal organization in dermal fibroblasts from a subset of aged human donors. Mechanisms of Ageing and Development 2001; 122(11): 1203–1220

Reichenbach, N., Delekate, A., Plescher, M., Schmitt, F., Krauss, S., Blank, N., Halle, A., Petzold, GC. Inhibition of Stat3-mediated astrogliosis ameliorates pathology in an Alzheimer's disease model. EMBO Molecular Medicine 2019; 11(2): e9665

Rimessi, A., Bezzerri, V., Patergnani, S., Marchi, S., Cabrini, G., Pinton, P. Mitochondrial Ca2+-dependent NLRP3 activation exacerbates the Pseudomonas aeruginosa-driven inflammatory response in cystic fibrosis. Nature Communications 2015; 6: 6201

Rincon, M., Pereira, FV. A New Perspective: Mitochondrial Stat3 as a Regulator for Lymphocyte Function. International Journal of Molecular Sciences 2018; 19(6): 1656

Río-Hortega, P. The microglia. The Lancet 1939; 233(6036): 1023–1026

Rizzuto, R., De Stefani, D., Raffaello, A., Mammucari, C. Mitochondria as sensors and regulators of calcium signalling. Nature Reviews. Molecular Cell Biology 2012; 13(9): 566–578

Rodier, F., Campisi, J. Four faces of cellular senescence. Journal of Cell Biology 2011; 192(4): 547–556

Rodier, F., Coppé, JP., Patil, CK., Hoeijmakers, WAM., Muñoz, DP., Raza, SR., Freund, A., Campeau, E., Davalos, AR., Campisi, J. Persistent DNA damage signalling triggers senescence-associated inflammatory cytokine secretion. Nature Cell Biology 2009; 11(8): 973–979

Romero, A., Dongil, P., Valencia, I., Vallejo, S., Hipólito-Luengo, ÁS., Díaz-Araya, G., Bartha, JL., González-Arlanzón, MM., Rivilla, F., Cuesta, F., Sánchez-Ferrer, CF., Peiró, C. Pharmacological Blockade of NLRP3 Inflammasome/IL-1β-Positive Loop Mitigates Endothelial Cell Senescence and Dysfunction. Aging and Disease 2022; 13(1): 284–297

Ryan, SM., O'Keeffe, GW., O'Connor, C., Keeshan, K., Nolan, YM. Negative regulation of TLX by IL-1β correlates with an inhibition of adult hippocampal neural precursor cell proliferation. Brain, Behavior, and Immunity 2013; 33: 7–13

Saha, P., Sen, N. Tauopathy: A common mechanism for neurodegeneration and brain aging. Mechanisms of Ageing and Development 2019; 178: 72–79

Saito, N., Araya, J., Ito, S., Tsubouchi, K., Minagawa, S., Hara, H., Ito, A., Nakano, T., Hosaka, Y., Ichikawa, A., Kadota, T., Yoshida, M., Fujita, Y., Utsumi, H., Kurita, Y., Kobayashi, K., Hashimoto, M., Wakui, H., Numata, T., Kaneko, Y., Asano, H., Odaka, M., Ohtsuka, T., Morikawa, T., Nakayama, K., Kuwano, K. Involvement of Lamin B1 Reduction in Accelerated Cellular Senescence during Chronic

Obstructive Pulmonary Disease Pathogenesis. The Journal of Immunology 2019; 202(5): 1428–1440

Saker, M., Lipskaia, L., Marcos, E., Abid, S., Parpaleix, A., Houssaini, A., Validire, P., Girard, P., Noureddine, H., Boyer, L., Vienney, N., Amsellem, V., Marguerit, L., Maitre, B., Derumeaux, G., Dubois-Rande, JL., Jourdan-Lesaux, C., Delcroix, M., Quarck, R., Adnot, S. Osteopontin, a Key Mediator Expressed by Senescent Pulmonary Vascular Cells in Pulmonary Hypertension. Arteriosclerosis, Thrombosis, and Vascular Biology 2016; 36(9): 1879–1890

Salminen, A., Kauppinen, A., Kaarniranta, K. Emerging role of NF-κB signaling in the induction of senescence-associated secretory phenotype (SASP). Cellular Signalling 2012; 24(4): 835–845

Salotti, J., Johnson, PF. Regulation of senescence and the SASP by the transcription factor C/EBPβ. Experimental Gerontology 2019; 128: 110752

Sandanger, Ø., Ranheim, T., Vinge, LE., Bliksøen, M., Alfsnes, K., Finsen, AV., Dahl, CP., Askevold, ET., Florholmen, G., Christensen, G., Fitzgerald, KA., Lien, E., Valen, G., Espevik, T., Aukrust, P., Yndestad, A. The NLRP3 inflammasome is up-regulated in cardiac fibroblasts and mediates myocardial ischaemia-reperfusion injury. Cardiovascular Research 2013; 99(1): 164–174

Schafer, MJ., Zhang, X., Kumar, A., Atkinson, EJ., Zhu, Y., Jachim, S., Mazula, DL., Brown, AK., Berning, M., Aversa, Z., Kotajarvi, B., Bruce, CJ., Greason, KL., Suri, RM., Tracy, RP., Cummings, SR., White, TA., LeBrasseur, NK. The senescence-associated secretome as an indicator of age and medical risk. JCI Insight 2020; 5(12): 133668

Scheiblich, H., Bicker, G. Regulation of microglial migration, phagocytosis, and neurite outgrowth by HO-1/CO signaling. Developmental Neurobiology 2015; 75(8): 854–876

Scheiblich, H., Bousset, L., Schwartz, S., Griep, A., Latz, E., Melki, R., Heneka, MT. Microglial NLRP3 Inflammasome Activation upon TLR2 and TLR5 Ligation by Distinct α-Synuclein Assemblies. Journal of Immunology 2021; 207(8): 2143–2154

Schindowski, K., Bretteville, A., Leroy, K., Bégard, S., Brion, JP., Hamdane, M., Buée, L. Alzheimer's disease-like tau neuropathology leads to memory deficits and loss of

functional synapses in a novel mutated tau transgenic mouse without any motor deficits. The American Journal of Pathology 2006; 169(2): 599–616

Schroder, K., Tschopp, J. The inflammasomes. Cell 2010; 140(6): 821–832

Schust, J., Sperl, B., Hollis, A., Mayer, TU., Berg, T. Stattic: A small-molecule inhibitor of STAT3 activation and dimerization. Chemistry & Biology 2006; 13(11): 1235–1242

Sebastian-Valverde, M., Pasinetti, GM. The NLRP3 Inflammasome as a Critical Actor in the Inflammaging Process. Cells 2020; 9(6): 1552

Shang, D., Hong, Y., Xie, W., Tu, Z., Xu, J. Interleukin-1β Drives Cellular Senescence of Rat Astrocytes Induced by Oligomerized Amyloid β Peptide and Oxidative Stress. Frontiers in Neurology 2020; 11: 929

Shetty, AK., Zanirati, G. The Interstitial System of the Brain in Health and Disease. Aging and Disease 2020; 11(1): 200–211

Shi, J., Zhao, Y., Wang, K., Shi, X., Wang, Y., Huang, H., Zhuang, Y., Cai, T., Wang, F., Shao, F. Cleavage of GSDMD by inflammatory caspases determines pyroptotic cell death. Nature 2015; 526(7575): 660–665

Shi, Y., Manis, M., Long, J., Wang, K., Sullivan, PM., Remolina Serrano, J., Hoyle, R., Holtzman, DM. Microglia drive APOE-dependent neurodegeneration in a tauopathy mouse model. The Journal of Experimental Medicine 2019; 216(11): 2546–2561

Shi, Y., Zhao, L., Wang, J., Liu, S., Zhang, Y., Qin, Q. The selective NLRP3 inflammasome inhibitor MCC950 improves isoproterenol-induced cardiac dysfunction by inhibiting cardiomyocyte senescence. European Journal of Pharmacology 2022; 937: 175364

Shibata, N., Yamamoto, T., Hiroi, A., Omi, Y., Kato, Y., Kobayashi, M. Activation of STAT3 and inhibitory effects of pioglitazone on STAT3 activity in a mouse model of SOD1-mutated amyotrophic lateral sclerosis. Neuropathology 2010; 30(4): 353–360

Shishodia, S., Aggarwal, BB. Nuclear Factor-κB Activation: A Question of Life or Death. BMB Reports 2002; 35(1): 28–40

Sidler, C., Kovalchuk, O., Kovalchuk, I. Epigenetic Regulation of Cellular Senescence and Aging. Frontiers in Genetics 2017; 8: 138

Sikora, E., Bielak-Zmijewska, A., Mosieniak, G. Cellular Senescence in Ageing, Age-Related Disease and Longevity. Current Vascular Pharmacology 2013; 12(5): 698–706

Soh, JEC., Shimizu, A., Molla, MR., Zankov, DP., Nguyen, LKC., Khan, MR., Tesega, W. W., Chen, S., Tojo, M., Ito, Y., Sato, A., Hitosugi, M., Miyagawa, S., Ogita, H. RhoA rescues cardiac senescence by regulating Parkin-mediated mitophagy. The Journal of Biological Chemistry 2023; 299(3): 102993

Spadaro, O., Goldberg, EL., Camell, CD., Youm, YH., Kopchick, JJ., Nguyen, KY., Bartke, A., Sun, LY., Dixit, VD. Growth Hormone Receptor Deficiency Protects against Age-Related NLRP3 Inflammasome Activation and Immune Senescence. Cell Reports 2016; 14(7): 1571–1580

Srinivas, US., Tan, BWQ., Vellayappan, BA., Jeyasekharan, AD. ROS and the DNA damage response in cancer. Redox Biology 2019; 25: 101084

Stancu, IC., Cremers, N., Vanrusselt, H., Couturier, J., Vanoosthuyse, A., Kessels, S., Lodder, C., Brône, B., Huaux, F., Octave, JN. Aggregated Tau activates NLRP3–ASC inflammasome exacerbating exogenously seeded and non-exogenously seeded Tau pathology in vivo. Acta Neuropathologica 2019; 137(4): 599–617

Stein, GH., Drullinger, LF., Soulard, A., Dulić, V. Differential roles for cyclin-dependent kinase inhibitors p21 and p16 in the mechanisms of senescence and differentiation in human fibroblasts. Molecular and Cellular Biology 1999; 19(3): 2109–2117

Storer, M., Mas, A., Robert-Moreno, A., Pecoraro, M., Ortells, MC., Di Giacomo, V., Yosef, R., Pilpel, N., Krizhanovsky, V., Sharpe, J., Keyes, WM. Senescence is a developmental mechanism that contributes to embryonic growth and patterning. Cell 2013; 155(5): 1119–1130

Streit, WJ. Microglial senescence: Does the brain's immune system have an expiration date? Trends in Neurosciences 2006; 29(9): 506–510

Streit, WJ., Braak, H., Xue, QS., Bechmann, I. Dystrophic (senescent) rather than activated microglial cells are associated with tau pathology and likely precede neurodegeneration in Alzheimer's disease. Acta Neuropathologica 2009; 118(4): 475–485

Strubbe-Rivera, JO., Schrad, JR., Pavlov, EV., Conway, JF., Parent, KN., Bazil, JN. The mitochondrial permeability transition phenomenon elucidated by cryo-EM reveals the genuine impact of calcium overload on mitochondrial structure and function. Scientific Reports 2021; 11(1): 1037

Su, L., Dong, Y., Wang, Y., Wang, Y., Guan, B., Lu, Y., Wu, J., Wang, X., Li, D., Meng, A., Fan, F. Potential role of senescent macrophages in radiation-induced pulmonary fibrosis. Cell Death & Disease 2012; 12(6): 527

Su, Y., Huang, X., Huang, Z., Huang, T., Xu, Y., Yi, C. STAT3 Localizes in Mitochondria-Associated ER Membranes Instead of in Mitochondria. Frontiers in Cell and Developmental Biology 2020; 8: 274

Sugimoto, K. Role of STAT3 in inflammatory bowel disease. World Journal of Gastroenterology 2008; 14(33): 5110–5114

Suzuki, M., Boothman, DA. Stress-induced premature senescence (SIPS)-influence of SIPS on radiotherapy. Journal of Radiation Research 2008; 49(2): 105–112

Swanson, KV., Deng, M., Ting, JPY. The NLRP3 inflammasome: Molecular activation and regulation to therapeutics. Nature Reviews Immunology 2019; 19(8): 477–489

Tai, GJ., Yu, QQ., Li, JP., Wei, W., Ji, XM., Zheng, RF., Li, XX., Wei, L., Xu, M. NLRP3 inflammasome links vascular senescence to diabetic vascular lesions. Pharmacological Research 2022; 178: 106143

Terzi, MY., Izmirli, M., Gogebakan, B. The cell fate: Senescence or quiescence. Molecular Biology Reports 2016; 43(11): 1213–1220

Tong, G., Krauss, A., Mochner, J., Wollersheim, S., Soltani, P., Berger, F., Schmitt, KRL. Deep hypothermia therapy attenuates LPS-induced microglia neuroinflammation via the STAT3 pathway. Neuroscience 2017; 358: 201–210

Toso, A., Revandkar, A., Di Mitri, D., Guccini, I., Proietti, M., Sarti, M., Pinton, S., Zhang, J., Kalathur, M., Civenni, G., Jarrossay, D., Montani, E., Marini, C., Garcia-Escudero, R., Scanziani, E., Grassi, F., Pandolfi, PP., Catapano, CV., Alimonti, A. Enhancing chemotherapy efficacy in Pten-deficient prostate tumors by activating the senescence-associated antitumor immunity. Cell Reports 2014; 9(1): 75–89

Trias, E., Beilby, PR., Kovacs, M., Ibarburu, S., Varela, V., Barreto-Núñez, R., Bradford, SC., Beckman, JS., Barbeito, L. Emergence of Microglia Bearing Senescence Markers During Paralysis Progression in a Rat Model of Inherited ALS. Frontiers in Aging Neuroscience 2019; 11: 42

Trudler, D., Nazor, KL., Eisele, YS., Grabauskas, T., Dolatabadi, N., Parker, J., Sultan, A., Zhong, Z., Goodwin, MS., Levites, Y., Golde, TE., Kelly, JW., Sierks, MR., Schork, NJ., Karin, M., Ambasudhan, R., Lipton, SA. Soluble α-synuclein-antibody

complexes activate the NLRP3 inflammasome in hiPSC-derived microglia. Proceedings of the National Academy of Sciences of the United States of America 2021; 118(15): e2025847118

Tsurumi, A., Li, W. Global heterochromatin loss. Epigenetics 2012; 7(7): 680–688

Utreras, E., Futatsugi, A., Rudrabhatla, P., Keller, J., Iadarola, MJ., Pant, HC., Kulkarni, AB. Tumor necrosis factor-alpha regulates cyclin-dependent kinase 5 activity during pain signaling through transcriptional activation of p35. The Journal of Biological Chemistry 2009; 284(4): 2275–2284

Van Deursen, JM. The role of senescent cells in ageing. Nature 2014; 509(7501): 439–446

van Olst, L., Verhaege, D., Franssen, M., Kamermans, A., Roucourt, B., Carmans, S., Ytebrouck, E., van der Pol, SMA., Wever, D., Popovic, M., Vandenbroucke, RE., Sobrino, T., Schouten, M., de Vries, HE. Microglial activation arises after aggregation of phosphorylated-tau in a neuron-specific P301S tauopathy mouse model. Neurobiology of Aging 2020; 89: 89–98

Vay, SU., Flitsch, LJ., Rabenstein, M., Rogall, R., Blaschke, S., Kleinhaus, J., Reinert, N., Bach, A., Fink, GR., Schroeter, M., Rueger, MA. The plasticity of primary microglia and their multifaceted effects on endogenous neural stem cells in vitro and in vivo. Journal of Neuroinflammation 2018; 15(1): 226

Velarde, MC., Menon, R. Positive and negative effects of cellular senescence during female reproductive aging and pregnancy. Journal of Endocrinology 2016; 230(2): R59–R76

Vergnes, L., Péterfy, M., Bergo, MO., Young, SG., Reue, K. Lamin B1 is required for mouse development and nuclear integrity. Proceedings of the National Academy of Sciences of the United States of America 2004; 101(28): 10428–10433

Vijayan, M., Alvir, RV., Alvir, RV., Bunquin, LE., Pradeepkiran, JA., Reddy, PH. A partial reduction of VDAC1 enhances mitophagy, autophagy, synaptic activities in a transgenic Tau mouse model. Aging Cell 2022; 21(8): e13663

von Bernhardi, R., Cornejo, F., Parada, GE., Eugenín, J. Role of TGFβ signaling in the pathogenesis of Alzheimer's disease. Frontiers in Cellular Neuroscience 2015; 9: 426

Waisman, A., Liblau, RS., Becher, B. Innate and adaptive immune responses in the CNS. The Lancet. Neurology 2015; 14(9): 945–955

Wallis, R., Milligan, D., Hughes, B., Mizen, H., López-Domínguez, JA., Eduputa, U., Tyler, EJ., Serrano, M., Bishop, CL. Senescence-associated morphological profiles (SAMPs): An image-based phenotypic profiling method for evaluating the inter and intra model heterogeneity of senescence. Aging 2002; 14(10): 4220–4246

Wang, E. Are cross-bridging structures involved in the bundle formation of intermediate filaments and the decrease in locomotion that accompany cell aging? Journal of Cell Biology 1985; 100(5): 1466–1473

Wang, Y., Mandelkow, E. Tau in physiology and pathology. Nature Reviews Neuroscience 2016; 17(1): 5–21

Wani, K., AlHarthi, H., Alghamdi, A., Sabico, S., Al-Daghri, NM. Role of NLRP3 Inflammasome Activation in Obesity-Mediated Metabolic Disorders. International Journal of Environmental Research and Public Health 2021; 18(2): 511

Waters, DW., Blokland, KEC., Pathinayake, PS., Wei, L., Schuliga, M., Jaffar, J., Westall, GP., Hansbro, PM., Prele, CM., Mutsaers, SE., Bartlett, NW., Burgess, JK., Grainge, CL., Knight, DA. STAT3 Regulates the Onset of Oxidant-induced Senescence in Lung Fibroblasts. American Journal of Respiratory Cell and Molecular Biology 2019; 61(1): 61–73

Wiel, C., Lallet-Daher, H., Gitenay, D., Gras, B., Le Calvé, B., Augert, A., Ferrand, M., Prevarskaya, N., Simonnet, H., Vindrieux, D., Bernard, D. Endoplasmic reticulum calcium release through ITPR2 channels leads to mitochondrial calcium accumulation and senescence. Nature Communications 2014; 5: 3792

Wiggins, KA., Clarke, MC. Senescence utilises inflammatory caspases to drive SASP. Aging 2019; 11(12): 3891–3892

Wiley, CD., Flynn, JM., Morrissey, C., Lebofsky, R., Shuga, J., Dong, X., Unger, MA., Vijg, J., Melov, S., Campisi, J. Analysis of individual cells identifies cell-to-cell variability following induction of cellular senescence. Aging Cell 2017; 16(5): 1043–1050

Wischhof, L., Adhikari, A., Mondal, M., Marsal-Cots, A., Biernat, J., Mandelkow, EM., Mandelkow, E., Ehninger, D., Nicotera, P., Bano, D. Unbiased proteomic profiling reveals the IP3R modulator AHCYL1/IRBIT as a novel interactor of microtubule-associated protein tau. The Journal of Biological Chemistry 2022; 298(4): 101774

Wood, JA., Wood, PL., Ryan, R., Graff-Radford, NR., Pilapil, C., Robitaille, Y., Quirion, R. Cytokine indices in Alzheimer's temporal cortex: No changes in mature IL-1 beta or IL-1RA but increases in the associated acute phase proteins IL-6, alpha 2-macroglobulin and C-reactive protein. Brain Research 1993; 629(2): 245–252

Wu, W., Fu, J., Gu, Y., Wei, Y., Ma, P., Wu, J. JAK2/STAT3 regulates estrogen-related senescence of bone marrow stem cells. The Journal of Endocrinology 2020; 245(1): 141–153

Yamada, K., Cirrito, JR., Stewart, FR., Jiang, H., Finn, MB., Holmes, BB., Binder, LI., Mandelkow, EM., Diamond, MI., Lee, VMY., Holtzman, DM. In vivo microdialysis reveals age-dependent decrease of brain interstitial fluid tau levels in P301S human tau transgenic mice. The Journal of Neuroscience: The Official Journal of the Society for Neuroscience 2011; 31(37): 13110–13117

Yan, Y., Jiang, W., Liu, L., Wang, X., Ding, C., Tian, Z., Zhou, R. Dopamine controls systemic inflammation through inhibition of NLRP3 inflammasome. Cell 2015; 160(1–2): 62–73

Yang, NC., Hu, ML. The limitations and validities of senescence associated-beta-galactosidase activity as an aging marker for human foreskin fibroblast Hs68 cells. Experimental Gerontology 2015; 40(10): 813–819

Ye, X., Sun, X., Starovoytov, V., Cai, Q. Parkin-mediated mitophagy in mutant hAPP neurons and Alzheimer's disease patient brains. Human Molecular Genetics 2015; 24(10): 2938–2951

Yoshiyama, Y., Higuchi, M., Zhang, B., Huang, SM., Iwata, N., Saido, TC., Maeda, J., Suhara, T., Trojanowski, JQ., Lee, VMY. Synapse Loss and Microglial Activation Precede Tangles in a P301S Tauopathy Mouse Model. Neuron 2007; 53(3): 337–351

Youm, YH., Kanneganti, TD., Vandanmagsar, B., Zhu, X., Ravussin, A., Adijiang, A., Owen, JS., Thomas, MJ., Francis, J., Parks, JS., & Dixit, VD. The Nlrp3 inflammasome promotes age-related thymic demise and immunosenescence. Cell Reports 2012; 1(1): 56–68

Yu, J., Nagasu, H., Murakami, T., Hoang, H., Broderick, L., Hoffman, HM., Horng, T. Inflammasome activation leads to Caspase-1–dependent mitochondrial damage

and block of mitophagy. Proceedings of the National Academy of Sciences 2014; 111(43): 15514–15519

Yun, JH., Lee, DH., Jeong, HS., Kim, HS., Ye, SK., Cho, CH. STAT3 activation in microglia exacerbates hippocampal neuronal apoptosis in diabetic brains. Journal of Cellular Physiology 2021; 236(10): 7058–7070

Zhang, F., Nance, E., Alnasser, Y., Kannan, R., Kannan, S. Microglial migration and interactions with dendrimer nanoparticles are altered in the presence of neuroinflammation. Journal of Neuroinflammation 2016; 13: 65

Zhang, X., Liu, X., Du, Z., Wei, L., Fang, H., Dong, Q., Niu, J., Li, Y., Gao, J., Zhang, M. Q., Xie, W., Wang, X. The loss of heterochromatin is associated with multiscale three-dimensional genome reorganization and aberrant transcription during cellular senescence. Genome Research 2021; 31(7): 1121–1135

Zhang, Y., Wu, KM., Yang, L., Dong, Q., Yu, JT. Tauopathies: New perspectives and challenges. Molecular Neurodegeneration 2022; 17(1): 28

Zhao, J., He, X., Zuo, M., Li, X., Sun, Z. Anagliptin prevented interleukin 1β (IL-1β)-induced cellular senescence in vascular smooth muscle cells through increasing the expression of sirtuin1 (SIRT1). Bioengineered 2021; 12(1): 3968–3977

Zheng, J., Li, HL., Tian, N., Liu, F., Wang, L., Yin, Y., Yue, L., Ma, L., Wan, Y., Wang, JZ. Interneuron Accumulation of Phosphorylated tau Impairs Adult Hippocampal Neurogenesis by Suppressing GABAergic Transmission. Cell Stem Cell 2020; 26(3): 331-345

Zheng, ZV., Chen, J., Lyu, H., Lam, SYE., Lu, G., Chan, WY., Wong, GKC.. Novel role of STAT3 in microglia-dependent neuroinflammation after experimental subarachnoid haemorrhage. Stroke and Vascular Neurology 2022; 7(1): 62–70

Zhou, R., Yazdi, AS., Menu, P., Tschopp, J. A role for mitochondria in NLRP3 inflammasome activation. Nature 2011; 469(7329): 221–225

Zhu, L., Wang, Z., Sun, X., Yu, J., Li, T., Zhao, H., Ji, Y., Peng, B., Du, M. STAT3/Mitophagy Axis Coordinates Macrophage NLRP3 Inflammasome Activation and Inflammatory Bone Loss. Journal of Bone and Mineral Research: The Official Journal of the American Society for Bone and Mineral Research 2023; 38(2): 335–353

Zhu, P., Duan, L., Chen, J., Xiong, A., Xu, Q., Zhang, H., Zheng, F., Tan, Z., Gong, F., Fang, M. Gene silencing of NALP3 protects against liver ischemia-reperfusion injury in mice. Human Gene Therapy 2011; 22(7): 853–864

Zhu, Y., Nwabuisi-Heath, E., Dumanis, SB., Tai, LM., Yu, C., Rebeck, GW., LaDu, MJ. APOE genotype alters glial activation and loss of synaptic markers in mice. Glia 2012; 60(4): 559–569

9 Acknowledgements

My life as a PhD student has come to an end. Firstly and foremost, words cannot express my gratitude to Prof. Michael Heneka and Dr. Christina Ising for hiring me as a PhD candidate in their lab. I could not have undertaken this journey without them, nor without my defence committee. Therefore, I would also sincerely like to thank all members of my defence committee, including Prof. Dr. Michael Heneka, Prof. Dr. Martin Korte, Prof. Dr. Jochen Walter and Prof. Dr. Elvira Mass. In addition, I am grateful for the help of Prof. Dr. Eicke Latz, for being affiliated to the Institute of Innate Immunity and continueing my PhD after the leave of Prof. Dr. Michael Heneka.

I want to give my deepest appreciaton to Dr. Christina Ising. It takes a lot of effort to raise a PhD student and without her I wouldn't be where I am. Dr. Christina Ising supported me since day one of my PhD journey and has offered excellent guidance and outstanding feedback. Due to her strong scientific, analytic and organizational skills, I have learned a lot, which definitely prepared me for the next step in my carreer. I also really appreciate the interesting scientific discussions we had.

Moreover, I would like to acknowledge Mr. Francesco Santarelli, Dr. Hannah Scheiblich, Ms. Angelika Griep, Ms. Sabine Opitz and Ms. Stephanie Schwarz for their technical support and help in taking care of the mice.

In addition, I want to say thank you to my friends (and colleagues) Mr. Kishore Aravind Ravichandran, Mr. Tao Li, Dr. Dilek Mercan, Mr. Max Komez and Ms. Charlotte Braatz for making the past years much more enjoyable and keeping me sane throughout the whole process. They were not only my safe haven at work, but also socially (e.g., our lovely diners, which will hopefully continue in the future).

Finally, I would like to highlight a few truly exceptional people who I love unconditionally. First of all my father and best friend, Mr. Cengiz Karabag, for his support throughout my entire life. Second, my mother, Ms. Anka Jacob (R.I.P.) who tragically passed away on the 5th of April 2021. I wish you were here to celebrate the end of an important life chapter

with me and I hope I have made you proud in heaven. Unfortunately, you did not get to know the love of my life, Ms. Duygu Cakil, who I met shortly after. She supported me unconditionally after your loss and during my PhD. Without her, I would feel lost. Therefore, I would like to say thank you, my love, for always being there for me. Lastly, a special thanks to my aunt Ms. Chantal Janssen-Jacob and uncle Mr. Ger Janssen for always having my back when I needed them and giving me important life lessons.

10 Most relevant publications

Karabag D, Scheiblich H, Griep A, Schwartz S, Heneka MT*, Ising C*. Characterizing microglial senescence: tau as a key player. J Neurochem (2023)

Karabag D, Griep A, Santarelli F, Schwartz S, Heneka MT*, Ising C*. Effects of the NLRP3 inflammasome on microglial senescence in tauopathies (in preparation)

*Co-corresponding authors.

11 Statistical details

Fig. 4B

Comparison	**Exact *P* value**
WT vs. Tau22	*P*=0.0079

Fig. 5 B

Comparison	**Exact *P* value**
WT vs. Tau22	*P*=0.0131

Fig. 6 B

Comparison	**Exact *P* value**
WT vs. Tau22	*P*=0.0068
WT vs. *Nlrp3*$^{-/-}$	*P*=0.8195
WT vs. Tau22/*Nlrp3*$^{-/-}$	*P*=0.8341
Tau22 vs. Tau22/*Nlrp3*$^{-/}$	*P*=0.0306
Tau22 vs. *Nlrp3*$^{-/-}$	*P*=0.0475
Nlrp3$^{-/-}$ vs. Tau22/*Nlrp3*$^{-/-}$	*P*=0.9998

Fig. 7 B

Comparison	**Exact *P* value**
WT vs. Tau22	*P*>0.9999
WT vs. *Nlrp3*$^{-/-}$	*P*>0.9999
WT vs. Tau22/*Nlrp3*$^{-/-}$	*P*>0.9999
Tau22 vs. Tau22/*Nlrp3*$^{-/}$	*P*>0.9999
Tau22 vs. *Nlrp3*$^{-/-}$	*P*>0.9999
Nlrp3$^{-/-}$ vs. Tau22/*Nlrp3*$^{-/-}$	*P*>0.9999

Fig. 7C

Comparison	**Exact *P* value**

WT vs. Tau22	*P*=0.0016
WT vs. *Nlrp3*$^{-/-}$	*P*=0.8385
WT vs. Tau22/*Nlrp3*$^{-/-}$	*P*=0.7066
Tau22 vs. Tau22/*Nlrp3*$^{-/}$	*P*=0.0135
Tau22 vs. *Nlrp3*$^{-/-}$	*P*=0.0139
Nlrp3$^{-/-}$ vs. Tau22/*Nlrp3*$^{-/-}$	*P*=0.9976

Fig. 7 D

Comparison	**Exact *P* value**
WT vs. Tau22	*P*=0.0011
WT vs. *Nlrp3*$^{-/-}$	*P*=0.9347
WT vs. Tau22/*Nlrp3*$^{-/-}$	*P*=0.8764
Tau22 vs. Tau22/*Nlrp3*$^{-/}$	*P*=0.0066
Tau22 vs. *Nlrp3*$^{-/-}$	*P*=0.0004
Nlrp3$^{-/-}$ vs. Tau22/*Nlrp3*$^{-/-}$	*P*=0.5781

Fig. 7 E

Comparison	**Exact *P* value**
WT vs. Tau22	*P*=0.0020
WT vs. *Nlrp3*$^{-/-}$	*P*=0.9917
WT vs. Tau22/*Nlrp3*$^{-/-}$	*P*=0.9204
Tau22 vs. Tau22/*Nlrp3*$^{-/}$	*P*=0.0069
Tau22 vs. *Nlrp3*$^{-/-}$	*P*=0.0019
Nlrp3$^{-/-}$ vs. Tau22/*Nlrp3*$^{-/-}$	*P*=0.8158

Fig. 7 F

Comparison	**Exact *P* value**
WT vs. Tau22	*P*=0.0061
WT vs. *Nlrp3*$^{-/-}$	*P*=0.9118
WT vs. Tau22/*Nlrp3*$^{-/-}$	*P*=0.9925
Tau22 vs. Tau22/*Nlrp3*$^{-/}$	*P*=0.0155

Tau22 vs. *Nlrp3*$^{-/-}$	*P*=0.0051
Nlrp3$^{-/-}$ vs. Tau22/*Nlrp3*$^{-/-}$	*P*=0.8216

Fig. 8 A

Comparison	**Exact *P* value**
control vs. tau 5 nM	*P*=0.2789
control vs. tau 15 nM	*P*=0.0333
tau 5 nM vs. tau 15 nM	*P*=0.2802

Fig. 8 B

Comparison	**Exact *P* value**
control vs. tau 5 nM	*P*=0.3652
control vs. tau 15 nM	*P*=0.8676
tau 5 nM vs. tau 15 nM	*P*=0.1953

Fig. 8 C

Comparison	**Exact *P* value**
control vs. tau 5 nM	*P*=0.2847
control vs. tau 15 nM	*P*=0.6850
tau 5 nM vs. tau 15 nM	*P*=0.6994

Fig. 8 E

Comparison	**Exact *P* value**
control vs. tau 5 nM	*P*=0.0213
control vs. tau 15 nM	*P*=0.0255
tau 5 nM vs. tau 15 nM	*P*=0.9865

Fig. 8 F

Comparison	**Exact *P* value**
control vs. tau 5 nM	*P*=0.0351
control vs. tau 15 nM	*P*=0.0053

tau 5 nM vs. tau 15 nM	*P*=0.2635

Fig. 8 G

Comparison	**Exact *P* value**
control vs. tau 5 nM	*P*=0.8649
control vs. tau 15 nM	*P*=0.0276
tau 5 nM vs. tau 15 nM	*P*=0.0153

Fig. 9 A

Comparison	**Exact *P* value**
control vs. tau 5 nM	*P*>0.9999
control vs. tau 15 nM	*P*<0.0001
tau 5 nM vs. tau 15 nM	*P*<0.0001

Fig. 9 B

Comparison	**Exact *P* value**
control vs. tau 5 nM	*P*>0.9999
control vs. tau 15 nM	*P*<0.0001
tau 5 nM vs. tau 15 nM	*P*=0.1484

Fig. 9 C

Comparison	**Exact *P* value**
control vs. tau 5 nM	*P*>0.4034
control vs. tau 15 nM	*P*<0.0001
tau 5 nM vs. tau 15 nM	*P*<0.0001

Fig. 9 D

Comparison	**Exact *P* value**
control vs. tau 5 nM	*P*>0.5391
control vs. tau 15 nM	*P*<0.0219
tau 5 nM vs. tau 15 nM	*P*<0.5391

Fig. 9 E

Comparison	**Exact *P* value**
control vs. tau 5 nM	*P*>0.7474
control vs. tau 15 nM	*P*<0.0035
tau 5 nM vs. tau 15 nM	*P*<0.0073

Fig. 9 F

Comparison	**Exact *P* value**
control vs. tau 5 nM	*P*=0.8902
control vs. tau 15 nM	*P*=0.0338
tau 5 nM vs. tau 15 nM	*P*=0.4081

Fig. 9 G

Comparison	**Exact *P* value**
control vs. tau 5 nM	*P*=0.0189
control vs. tau 15 nM	*P*=0.0002
tau 5 nM vs. tau 15 nM	*P*=0.0032

Fig. 9 H

Comparison	**Exact *P* value**
control vs. tau 5 nM	*P*=0.0396
control vs. tau 15 nM	*P*=0.0012
tau 5 nM vs. tau 15 nM	*P*=0.0269

Fig. 10 B

Comparison	**Exact *P* value**
control vs. PMA	*P*=0.0003

Fig. 10 C

Comparison	**Exact *P* value**

control vs. PMA	*P*=0.5262

Fig. 10 D

Comparison	**Exact *P* value**
control vs. PMA	*P*=0.0002

Fig. 10 E

Comparison	**Exact *P* value**
control vs. PMA	*P*<0.0001

Fig. 10 F

Comparison	**Exact *P* value**
control vs. PMA	*P*=0.0005

Fig. 11 B

Comparison	**Exact *P* value**
control vs. tau 5 nM	*P*=0.3797
control vs. tau 15 nM	*P*=0.0425
tau 5 nM vs. tau 15 nM	*P*=0.2606

Fig. 11 D

Comparison	**Exact *P* value**
control vs. tau 5 nM	*P*=0.9943
control vs. tau 15 nM	*P*=0.0024
tau 5 nM vs. tau 15 nM	*P*=0.0026

Fig. 12 E

Comparison	**Exact *P* value**	**Timepoint (in minutes)**
control vs. tau 5 nM	*P*=0.3556	30
control vs. tau 15 nM	*P*=0.6661	30
tau 5 nM vs. tau 15 nM	*P*=0.0124	30

control vs. tau 5 nM	*P*>0.9999	60
control vs. tau 15 nM	*P*=0.0005	60
tau 5 nM vs. tau 15 nM	*P*=0.0003	60

Fig. 12 F

Comparison	**Exact *P* value**	**Timepoint (in minutes)**
control vs. tau 5 nM	*P*=0.4227	30
control vs. tau 15 nM	*P*=0.8044	30
tau 5 nM vs. tau 15 nM	*P*=0.0268	30
control vs. tau 5 nM	*P*=0.9996	60
control vs. tau 15 nM	*P*=0.0002	60
tau 5 nM vs. tau 15 nM	*P*<0.0001	60

Fig. 13 B

Comparison	**Exact *P* value**
control vs. tau 5 nM	*P*=0.0520
control vs. tau 15 nM	*P*=0.0411
tau 5 nM vs. tau 15 nM	*P*=0.7811

Fig. 13 C

Comparison	**Exact *P* value**
control vs. tau 5 nM	*P*=0.0658
control vs. tau 15 nM	*P*=0.0359
tau 5 nM vs. tau 15 nM	*P*=0.9576

Fig. 14 C

Comparison	**Exact *P* value**
control vs. tau 5 nM	*P*=0.3256
control vs. tau 15 nM	*P*=0.3256
tau 5 nM vs. tau 15 nM	*P*<0.0001

Fig. 14 D

Comparison	**Exact *P* value**
control vs. tau 5 nM	*P*>0.9999
control vs. tau 15 nM	*P*<0.0003
tau 5 nM vs. tau 15 nM	*P*<0.0002

Fig. 14 E

Comparison	**Exact *P* value**
control vs. tau 5 nM	*P*=0.4526
control vs. tau 15 nM	*P*<0.0001
tau 5 nM vs. tau 15 nM	*P*<0.0001

Fig. 14 F

Comparison	**Exact *P* value**
control vs. tau 5 nM	*P*=0.5155
control vs. tau 15 nM	*P*=0.0207
tau 5 nM vs. tau 15 nM	*P*<0.0004

Fig. 14 G

Comparison	**Exact *P* value**
control vs. tau 5 nM	*P*>0.9999
control vs. tau 15 nM	*P*<0.0001
tau 5 nM vs. tau 15 nM	*P*<0.0001

Fig. 15 B

Comparison	**Exact *P* value**
control vs. tau 15 nM	*P*=0.0011
control vs. tau 15 nM + CRID3	*P*=0.9615
control vs. CRID3	*P*=0.7538
tau 15 nM vs. tau 15 nM + CRID3	*P*=0.0007
tau 15 nM vs. CRID3	*P*=0.0004

tau 15 nM + CRID3 vs. CRID3	*P*=0.9518

Fig. 15 C

Comparison	**Exact *P* value**
control vs. tau 15 nM	*P*<0.0001
control vs. tau 15 nM + CRID3	*P*<0.0001
control vs. CRID3	*P*>0.9999
tau 15 nM vs. tau 15 nM + CRID3	*P*<0.0001
tau 15 nM vs. CRID3	*P*<0.0001
tau 15 nM + CRID3 vs. CRID3	*P*<0.0001

Fig. 16 B

Comparison	**Exact *P* value**
control vs. tau 15 nM	*P*=0.0031
control vs. tau 15 nM + CRID3	*P*=0.8773
control vs. CRID3	*P*=0.9941
tau 15 nM vs. tau 15 nM + CRID3	*P*=0.0111
tau 15 nM vs. CRID3	*P*=0.9941
tau 15 nM + CRID3 vs. CRID3	*P*=0.0111

Fig. 16 C

Comparison	**Exact *P* value**
control vs. tau 15 nM	*P*=0.0099
control vs. tau 15 nM + CRID3	*P*=0.9118
control vs. CRID3	*P*=0.9927
tau 15 nM vs. tau 15 nM + CRID3	*P*=0.0310
tau 15 nM vs. CRID3	*P*=0.0062
tau 15 nM + CRID3 vs. CRID3	*P*=0.7918

Fig. 16 D

Comparison	**Exact *P* value**

control vs. tau 15 nM	*P*<0.0001
control vs. tau 15 nM + CRID3	*P*<0.0001
control vs. CRID3	*P*>0.9999
tau 15 nM vs. tau 15 nM + CRID3	*P*<0.0001
tau 15 nM vs. CRID3	*P*<0.0001
tau 15 nM + CRID3 vs. CRID3	*P*<0.0001

Fig. 16 E

Comparison	**Exact *P* value**
control vs. tau 15 nM	*P*<0.0001
control vs. tau 15 nM + CRID3	*P*<0.0001
control vs. CRID3	*P*=0.9827
tau 15 nM vs. tau 15 nM + CRID3	*P*<0.0001
tau 15 nM vs. CRID3	*P*<0.0001
tau 15 nM + CRID3 vs. CRID3	*P*<0.0001

Fig. 16 F

Comparison	**Exact *P* value**
control vs. tau 15 nM	*P*<0.0001
control vs. tau 15 nM + CRID3	*P*<0.0001
control vs. CRID3	*P*=0.9643
tau 15 nM vs. tau 15 nM + CRID3	*P*=0.0092
tau 15 nM vs. CRID3	*P*<0.0001
tau 15 nM + CRID3 vs. CRID3	*P*<0.0001

Fig. 16 G

Comparison	**Exact *P* value**
control vs. tau 15 nM	*P*<0.0001
control vs. tau 15 nM + CRID3	*P*<0.0001
control vs. CRID3	*P*>0.9999
tau 15 nM vs. tau 15 nM + CRID3	*P*=0.0002

tau 15 nM vs. CRID3	*P*<0.0001
tau 15 nM + CRID3 vs. CRID3	*P*<0.0001

Fig. 16 H

Comparison	**Exact *P* value**
control vs. tau 15 nM	*P*=0.0221
control vs. tau 15 nM + CRID3	*P*=0.0717
control vs. CRID3	*P*=0.9995
tau 15 nM vs. tau 15 nM + CRID3	*P*=0.8318
tau 15 nM vs. CRID3	*P*=0.0191
tau 15 nM + CRID3 vs. CRID3	*P*=0.0618

Fig. 16 I

Comparison	**Exact *P* value**
control vs. tau 15 nM	*P*=0.0217
control vs. tau 15 nM + CRID3	*P*= 0.0489
control vs. CRID3	*P*=0.9642
tau 15 nM vs. tau 15 nM + CRID3	*P*=0.9332
tau 15 nM vs. CRID3	*P*=0.0413
tau 15 nM + CRID3 vs. CRID3	*P*=0.0946

Fig. 16 J

Comparison	**Exact *P* value**
control vs. tau 15 nM	*P*<0.0001
control vs. tau 15 nM + CRID3	*P*=0.0001
control vs. CRID3	*P*=0.2022
tau 15 nM vs. tau 15 nM + CRID3	*P*=0.9791
tau 15 nM vs. CRID3	*P*<0.0001
tau 15 nM + CRID3 vs. CRID3	*P*<0.0001

Fig. 16 K

Comparison	**Exact *P* value**
control vs. tau 15 nM	*P*<0.0003
control vs. tau 15 nM + CRID3	*P*=0.0004
control vs. CRID3	*P*=0.3756
tau 15 nM vs. tau 15 nM + CRID3	*P*=0.9994
tau 15 nM vs. CRID3	*P*<0.0020
tau 15 nM + CRID3 vs. CRID3	*P*<0.0023

Fig. 17 B

Comparison	**Exact *P* value**
control (WT) vs. tau 15 nM (WT)	*P*=0.0007
control (WT) vs. control (*Nlrp3*$^{-/-}$)	*P*=0.1192
control (WT) vs. tau 15 nM (*Nlrp3*$^{-/-}$)	*P*=0.8237
tau 15 nM (WT) vs. control (*Nlrp3*$^{-/-}$)	*P*<0.0001
tau 15 nM (WT) vs. tau 15 nM (*Nlrp3*$^{-/-}$)	*P*=0.0002
control (*Nlrp3*$^{-/-}$) vs. tau 15 nM (*Nlrp3*$^{-/-}$)	P=0.4192

Fig. 17 C

Comparison	**Exact *P* value**
control (WT) vs. tau 15 nM (WT)	*P*=0.0003
control (WT) vs. control (*Nlrp3*$^{-/-}$)	*P*=0.0910
control (WT) vs. tau 15 nM (*Nlrp3*$^{-/-}$)	*P*=0.9281
tau 15 nM (WT) vs. control (*Nlrp3*$^{-/-}$)	*P*<0.0001
tau 15 nM (WT) vs. tau 15 nM (*Nlrp3*$^{-/-}$)	*P*<0.0001
control (*Nlrp3*$^{-/-}$) vs. tau 15 nM (*Nlrp3*$^{-/-}$)	*P*=0.2375

Fig. 17 D

Comparison	**Exact *P* value**
control (WT) vs. tau 15 nM (WT)	*P*=0.0007
control (WT) vs. control (*Nlrp3*$^{-/-}$)	*P*>0.9999
control (WT) vs. tau 15 nM (*Nlrp3*$^{-/-}$)	*P*=0.0009

tau 15 nM (WT) vs. control (*Nlrp3*$^{-/-}$)	*P*<0.0001
tau 15 nM (WT) vs. tau 15 nM (*Nlrp3*$^{-/-}$)	*P*<0.0001
control (*Nlrp3*$^{-/-}$) vs. tau 15 nM (*Nlrp3*$^{-/-}$)	*P*=0.0009

Fig. 17 E

Comparison	**Exact *P* value**
control (WT) vs. tau 15 nM (WT)	*P*<0.0001
control (WT) vs. control (*Nlrp3*$^{-/-}$)	*P*>0.9999
control (WT) vs. tau 15 nM (*Nlrp3*$^{-/-}$)	*P*<0.0001
tau 15 nM (WT) vs. control (*Nlrp3*$^{-/-}$)	*P*<0.0001
tau 15 nM (WT) vs. tau 15 nM (*Nlrp3*$^{-/-}$)	*P*<0.0001
control (*Nlrp3*$^{-/-}$) vs. tau 15 nM (*Nlrp3*$^{-/-}$)	*P*<0.0001

Fig. 17 F

Comparison	**Exact *P* value**
control (WT) vs. tau 15 nM (WT)	*P*<0.0001
control (WT) vs. control (*Nlrp3*$^{-/-}$)	*P*<0.0001
control (WT) vs. tau 15 nM (*Nlrp3*$^{-/-}$)	*P*<0.0001
tau 15 nM (WT) vs. control (*Nlrp3*$^{-/-}$)	*P*<0.0001
tau 15 nM (WT) vs. tau 15 nM (*Nlrp3*$^{-/-}$)	*P*<0.0001
control (*Nlrp3*$^{-/-}$) vs. tau 15 nM (*Nlrp3*$^{-/-}$)	*P*<0.0001

Fig. 18 B

Comparison	**Exact *P* value**
control vs. tau 15 nM	*P*=0.0043
control vs. tau 15 nM + CRID3	*P*=0.9165
control vs. CRID3	*P*=0.8694
tau 15 nM vs. tau 15 nM + CRID3	*P*=0.0020

Fig. 19 B

Comparison	**Exact *P* value**

control vs. CRID3	*P*=0.9775
control vs. tau 15 nM	*P*=0.9991
control vs. tau 15 nM + CRID3	*P*=0.9580
control vs. stattic + tau 15 nM	*P*=0.9198
tau 15 nM vs. tau 15 nM + CRID3	*P*=0.9989
tau 15 nM vs. stattic + tau 15 nM	*P*=0.9987
tau 15 nM + CRID3 vs. stattic + tau 15 nM + CRID3	*P*=0.9999
stattic vs. stattic + tau 15 nM	*P*=0.9972

Fig. 19 C

Comparison	**Exact *P* value**
control vs. CRID3	*P*=0.9998
control vs. tau 15 nM	*P*<0.0001
control vs. tau 15 nM + CRID3	*P*<0.0001
control vs. stattic + tau 15 nM	*P*=0.9799
tau 15 nM vs. tau 15 nM + CRID3	*P*>0.9999
tau 15 nM vs. stattic + tau 15 nM	*P*<0.0001
tau 15 nM + CRID3 vs. stattic + tau + CRID3	*P*<0.0001
stattic vs. stattic + tau 15 nM	*P*>0.9999

Fig. 20 A

Comparison	**Exact *P* value**
control vs. CRID3	*P*=0.9981
control vs. tau 15 nM	*P*<0.0001
control vs. tau 15 nM + CRID3	*P*<0.0001
control vs. stattic + tau 15 nM	*P*=0.9995
control vs. stattic + tau 15 nM + CRID3	*P*=0.9841
tau 15 nM vs. tau 15 nM + CRID3	*P*<0.0001
tau 15 nM vs. stattic + tau 15 nM	*P*<0.0001
tau 15 nM + CRID3 vs. stattic + tau + CRID3	*P*<0.0001

Fig. 20 B

Comparison	**Exact *P* value**
control vs. CRID3	*P*>0.9999
control vs. tau 15 nM	*P*<0.0001
control vs. tau 15 nM + CRID3	*P*<0.0001
control vs. stattic + tau 15 nM	*P*=0.9953
control vs. stattic + tau 15 nM + CRID3	*P*=0.9520
tau 15 nM vs. tau 15 nM + CRID3	*P*<0.0001
tau 15 nM vs. stattic + tau 15 nM	*P*<0.0001
tau 15 nM + CRID3 vs. stattic + tau + CRID3	*P*<0.0001

Fig. 20 C

Comparison	**Exact *P* value**
control vs. CRID3	*P*>0.9999
control vs. tau 15 nM	*P*<0.0001
control vs. tau 15 nM + CRID3	*P*=0.0001
control vs. stattic + tau 15 nM	*P*=0.9963
control vs. stattic + tau 15 nM + CRID3	*P*=0.9965
tau 15 nM vs. tau 15 nM + CRID3	*P*=0.0044
tau 15 nM vs. stattic + tau 15 nM	*P*<0.0001
tau 15 nM + CRID3 vs. stattic + tau + CRID3	*P*<0.0001

Fig. 20 D

Comparison	**Exact *P* value**
control vs. CRID3	*P*>0.9999
control vs. tau 15 nM	*P*<0.0001
control vs. tau 15 nM + CRID3	*P*=0.0001
control vs. stattic + tau 15 nM	*P*>0.9999
control vs. stattic + tau 15 nM + CRID3	*P*>0.9999
tau 15 nM vs. tau 15 nM + CRID3	*P*=0.0001

tau 15 nM vs. stattic + tau 15 nM	*P*<0.0001
tau 15 nM + CRID3 vs. stattic + tau + CRID3	*P*<0.0001

Fig. 20 E

Comparison	**Exact *P* value**
control vs. CRID3	*P*=0.9998
control vs. tau 15 nM	*P*=0.0112
control vs. tau 15 nM + CRID3	*P*=0.0121
control vs. stattic + tau 15 nM	*P*=0.9998
control vs. stattic + tau 15 nM + CRID3	*P*=0.9998
tau 15 nM vs. tau 15 nM + CRID3	*P*=0.9998
tau 15 nM vs. stattic + tau 15 nM	P=0.0036
tau 15 nM + CRID3 vs. stattic + tau + CRID3	*P*<0.0035

Fig. 20 F

Comparison	**Exact *P* value**
control vs. CRID3	*P*>0.9999
control vs. tau 15 nM	*P*<0.0001
control vs. tau 15 nM + CRID3	*P*=0.0030
control vs. stattic + tau 15 nM	*P*=0.8598
control vs. stattic + tau 15 nM + CRID3	*P*=0.6175
tau 15 nM vs. tau 15 nM + CRID3	*P*=0.7740
tau 15 nM vs. stattic + tau 15 nM	*P*<0.0001
tau 15 nM + CRID3 vs. stattic + tau + CRID3	*P*<0.0001

Fig. 20 G

Comparison	**Exact *P* value**
control vs. CRID3	*P*>0.9999
control vs. tau 15 nM	*P*=0.0005
control vs. tau 15 nM + CRID3	*P*=0.0003
control vs. stattic + tau 15 nM	*P*=0.9697

control vs. stattic + tau 15 nM + CRID3	*P*=0.9998
tau 15 nM vs. tau 15 nM + CRID3	*P*>0.9999
tau 15 nM vs. stattic + tau 15 nM	*P*=0.0053
tau 15 nM + CRID3 vs. stattic + tau + CRID3	*P*=0.0009

Fig. 20 H

Comparison	**Exact *P* value**
control vs. CRID3	*P*=0.8986
control vs. tau 15 nM	*P*=0.0261
control vs. tau 15 nM + CRID3	*P*=0.0768
control vs. stattic + tau 15 nM	*P*<0.0001
control vs. stattic + tau 15 nM + CRID3	*P*=0.0011
tau 15 nM vs. tau 15 nM + CRID3	*P*=0.8394
tau 15 nM vs. stattic + tau 15 nM	*P*<0.0001
tau 15 nM + CRID3 vs. stattic + tau + CRID3	*P*<0.0001

Fig. 21 B

Comparison	**Exact *P* value**
control vs. CRID3	*P*=0.0029
control vs. tau 15 nM	*P*=0.0052
control vs. tau 15 nM + CRID3	*P*=0.0108
control vs. stattic + tau 15 nM	*P=0.6079*
control vs. stattic + tau 15 nM + CRID3	*P*=0.0141
tau 15 nM vs. tau 15 nM + CRID3	*P*<0.0001
tau 15 nM vs. stattic + tau 15 nM	*P*=0.0002
tau 15 nM + CRID3 vs. stattic + tau + CRID3	*P*>0.9999